1995

Marcus Theory Applied To Acetal Cleavage And Aldol Reactions

Jonathan Arthur Barker

MARCUS THEORY APPLIED TO ACETAL CLEAVAGE AND ALDOL REACTIONS

by

Jonathan A. Barker

Department of Chemistry

Submitted in partial fulfilment
of the requirements for the degree of
Doctor of Phil/sophy

Faculty of Graduate Studies
University of Western Ontario
London, Ontario
February 1995

ISBN 0-315-99245-X

ABSTRACT

The acid catalyzed and uncatalyzed hydrolysis of the acetal 2,2-dimethoxypropane (DMOP) and the ortho ester trimethylorthoacetate (TMOA) have been studied in aqueous solution at 25 °C. Theoretical and experimental evidence have been found for a base catalyzed E2 mechanism of DMOP hydrolysis proceeding through an enol ether. This mechanism is neither predicted nor observed for TMOA hydrolysis. The specific acid catalyzed and uncatalyzed rate constants for hydrolysis are for DMOP $k_{H^+} = (2.5\pm0.3) \times 10^3\ M^{-1}s^{-1}$, $k_w = (3.6\pm0.2) \times 10^{-8}\ s^{-1}$, $k_{OH-E2} = (2.8\pm0.4) \times 10^{-8}\ M^{-1}s^{-1}$, and for TMOA k_{H^+} $(2.05\pm0.12) \times 10^4\ M^{-1}s^{-1}$, $k_w = (3.7\pm0.3) \times 10^{-6}\ s^{-1}$. General acid catalysis was observed for TMOA with four general acids. From the Bronsted plot, $\alpha = 0.76\pm0.05$. Evidence of general acid catalysis in the hydrolysis of DMOP with phenol as general acid was suggestive but inconclusive.

The rate and equilibrium constants for formation, dehydration and, when appropriate, isomerization, have been determined for four hydroxide catalyzed aldol condensations at 25.0 °C in aqueous solution. The four reactions studied were acetone, acting as carbon acid, with α,α,α-trifluoroacetophenone and with *p*-nitroacetophenone, and *p*-nitroacetophenone, acting as carbon acid, with *p*-nitroacetophenone and with acetone. The experimentally determined rate constants agree well with rate constants predicted by Marcus Theory, supporting the utility of Marcus theory in the prediction of rates of unstudied aldol reactions.

ACKNOWLEDGEMENTS

I wish to thank Dr. J. Peter Guthrie for his guidance and support for the past several years. It has been a privilege to work with someone whose knowledge of chemistry and the world around us is so remarkably vast as to be a local legend. His propensity for puns has likewise challenged the wit - and knowledge of history, politics, science, languages, literature....

I owe my greatest thanks to my wife Alexandra. The cost of an education is not only measured in dollars, but in time, energy, and commitment. These non-financial costs are often the most expensive and the most difficult to bear. Thank you for your patience, understanding, encouragement and love through a long and challenging time.

Thanks also to my and Alexandra's families for their support through the years. Their support has been most welcome and appreciated.

Many thanks to the members of the Guthrie group, past and present, who have enhanced my stay through the years. In "order of appearance": John Cossar, Dr. David Pike, Dr. Xiao Ping Wang, Dr. Jinqiao Lu, Junan Guo, Dr. Willis Lee, Bo Li, Dr. Tony Huntington, and Cuihua Liu. Special thanks also to Dr. Jeff Walker, Cam McPhail, Anton Dikmans, Dr. Jeff Cooke, Dr. Dave Hastings, Christina Tieszer, Ed Brecevic, and Robin Martin.

TABLE OF CONTENTS

LIST OF FIGURES

LIST OF TABLES

LIST OF SCHEMES

PART I:

THE HYDROLYSES OF 2,2-DIMETHOXYPROPANE AND TRIMETHYLORTHOACETATE

CHAPTER 1: INTRODUCTION

1.1 Background

Acetal hydrolysis reactions are of great biological importance. The polymers of N-acetylglucosamine and N-acetylmuramic acid which make up bacterial cell walls are held together by acetal linkages and these linkages can be cleaved by enzymes such as lysozyme. If we wish to better understand the mode of action of lysozyme - perhaps to help design antibacterial agents - we need to study acetal hydrolysis reactions.

Cellulose and starch are glucose polymers which are also held together by acetal linkages. If a commercially viable, catalytic method of cellulose hydrolysis could be found, then we would have an immense supply of glucose. This would be the feedstock for increased production of ethanol for use as a fuel. An estimated 40 percent of the 10^{11} tons of terrestrial biomass produced each year is cellulose.[1] Present use of this resource amounts to only 0.5 percent annually.

Saccharide linkages are unreactive acetals and lysozyme acts in neutral solution. It has been proposed that lysozyme acts by general acid catalysis (GAC) to facilitate acetal hydrolysis. Although there is much support for the GAC mechanism of lysozyme, non-enzymic examples of intermolecular general acid catalysis of analogous acetals using other general acids (such as acetic acid or dihydrogen phosphate) have been difficult to find.

1.2 Definitions of specific- and general-acid catalysis.

Specific acid catalysis in aqueous solution is catalysis due to the hydronium ion and involves the conjugate acid of the reactant, formed in a rapid equilibrium prior to the rate determining step. The rate depends only on the pH and is independent of the concentration of any general acid. This mechanism is depicted in Scheme 1.

Scheme 1. Mechanism of specific acid catalysis of acetal hydrolysis.

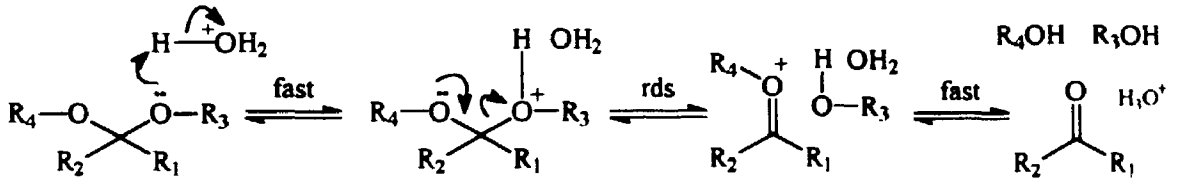

General acid catalysis employs other acids such as buffer components, which are weaker acids than the hydronium ion, to catalyze a reaction without fully forming the conjugate acid of the reactant. The formation of a generally unstable intermediate is thus avoided; instead there is concerted bond breakage and proton transfer along a preformed hydrogen bond. This is shown in Scheme 2.

Scheme 2. Mechanism of general acid catalysis of acetal hydrolysis.

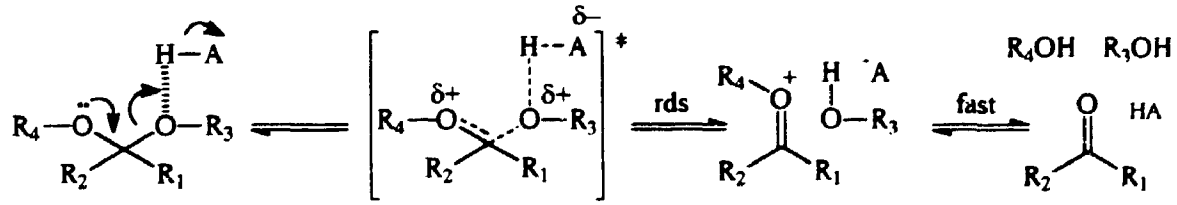

1.3 Examples of general-acid catalysis in acetal hydrolysis and an explanation of acetal reactivity.

General acid catalysis was sought for acetals and the structurally similar ortho esters as early as 1929 when Bronsted found buffer catalysis for ortho esters but not for acetals.[2] This difference between similar functional groups has led to attempts to find examples of GAC in acetal hydrolysis.

General acid catalyzed hydrolysis of acetals has been observed but the acetals are not the unreactive sort found in sugar linkages. The acetals for which catalysis has been observed have properties which predispose them to GAC. These include electron withdrawing substituents in the leaving groups, electron donating non-leaving groups which stabilize the intermediate carbocation, or ground state strain which is relieved on forming the intermediate carbocation.

Examples of the use of better leaving groups include the hydrolyses of methyl phenyl ketals of acetone and acetaldehyde,[3,4] and the hydrolysis of aryloxytetrahydropyrans.[5,6]

Generation of stabilized carbocations from tropone diethyl ketal,[7] benzophenone ketals,[8] and *p*-(dimethylamino)benzaldehyde acetals[9] have been used. As shown for tropone diethyl ketal in Scheme 3, the expulsion of the etLoxy group leaves a stable tropylium ion.

Better leaving groups and stabilized carbocations are sometimes combined as shown by the work on benzaldehyde aryl alkyl acetals.[10,11]

Scheme 3. Hydrolysis of tropone diethyl ketal.

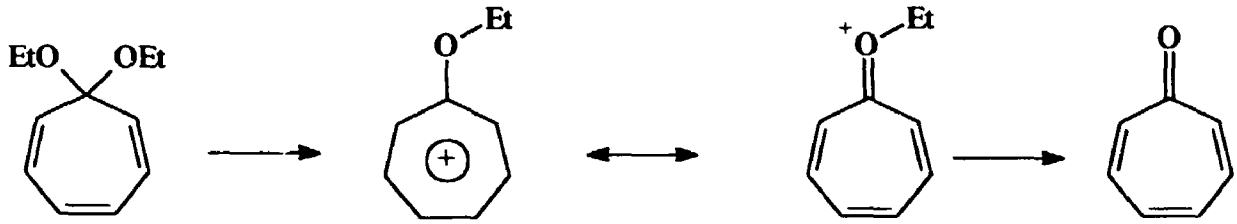

A strained benzaldehyde dialkyl acetal has also shown general acid catalyzed hydrolysis.[12] Benzaldehyde di-*tert*-butyl acetal benefits from the aryl stabilization of the carbocation as well as relief of steric strain on the loss of one of the *tert*-butyl groups.

The reasons that these factors promote general acid catalysis have been examined.[13-15] The acetals with better leaving groups (such as aryloxy) will have less basic oxygens. That is, the conjugate acid of the acetal will have a higher energy than that of a more basic acetal, and GAC would avoid generation of this high energy intermediate. Acetals leading to stabilized carbocations and those where strain is relieved on going to the carbocation do not require as good a leaving group. General acid catalysis allows an improvement in leaving group ability which is less than the strong activation provided by full protonation of the leaving group oxygen but does not impose the energetic cost of protonation.

The effect of different substituents and general acids on the transition state has been discussed:[11] one observation is that the hydrogen to be transferred is positioned closer to the general acid in the transition state when acids of higher pKa are used. A second observation is the roughly opposite hydrogen motion in the presence of electron withdrawing non-leaving groups. Qualitatively then, for more basic acetals, we would

need a general acid with a higher pKa to bring the position of the hydrogen to a more intermediate position in the transition state, when GAC would be observable.

1.4 Predictions for observability of general acid catalysis in acetal and orthoester hydrolysis and definition of the scope of this work.

The relationship between general acid pKa and transition state structure has been analyzed and predictions have been made of the pKa ranges where general acid catalysis should be observable.[13] For simple acetals such as 2,2-dimethoxypropane (DMOP) the lower general acid pKa limit for observable catalysis should be about 10. This suggests that general acid catalysis has not been observed for simple acetals because we have not been studying appropriate pH and general acid pKa ranges.

Key to the predictions is the determination or estimation of the specific acid catalyzed and the water (uncatalyzed) rate constants for hydrolysis of the acetal of interest. These are used to determine the activation free energies for the extreme steps, which allow limits to be placed on a general acid catalyzed mechanism. The limits result from the assumption that reaction will proceed along the reaction path corresponding to the uncatalyzed reaction until the pKa of the developing carbonium ion matches that of the general acid. At that point the proton is transferred along the preformed hydrogen bond and reaction proceeds along the specific acid catalyzed path, having avoided the extrema of both steps. The predicted general acid pKa lower limit for acetophenone dimethyl acetal hydrolysis based on estimated rate constants was 10. and DMOP is expected to be comparable. In addition to looking for general acid catalysis then, this project seeks to determine the specific acid catalyzed and uncatalyzed rates for DMOP hydrolysis in

aqueous solution so that pKa range predictions can be based on determined, not estimated, rate constants. A pH rate profile for DMOP hydrolysis is then one of the goals of this work to determine properly the uncatalyzed and specific acid catalyzed hydrolysis rate constants.

The second part of this project was the study of the hydrolysis of an analogous ortho ester, trimethyl orthoacetate (TMOA), so that comparisons could be made between acetal and ortho ester reactivities. As stated previously, GAC has long been known for ortho esters.[2] This is consistent with Guthrie's prediction of the lower limit of general acid pKa to be about 6.5 for trimethylorthobenzoate which is expected to behave similarly as TMOA.[13]

Notice also in Scheme 1, that if we replace $-R_1$ with $-OR_1$ we have an ortho ester, and this would lead to a resonance stabilized carbocation intermediate. Thus an ortho ester could be considered an acetal with an electron donating non-leaving group.

Scheme 4. The hydrolyses of 2,2-dimethoxypropane and trimethylorthoacetate.

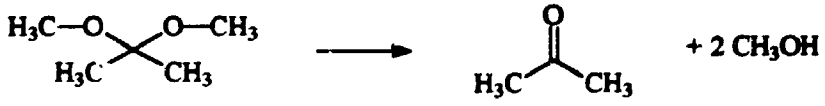

DMOP

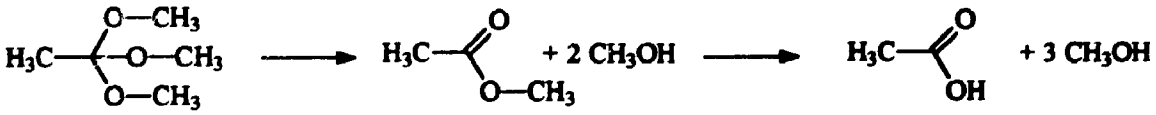

TMOA

With specific acid catalyzed and uncatalyzed rate constants in hand, we can better estimate the range of allowable general acid pKa for observable catalysis. We will also be

able to apply Marcus Theory to refine our predictions. Measured specific acid catalyzed and uncatalyzed rate constants will allow comparison of actual experimental rate constants with rate constants predicted from the assumed mechanisms.

The specific reactions studied are depicted in Scheme 4.

1.5 Marcus Theory

Marcus Theory began as an relationship derived for activation free energies in weak-overlap electron transfer reactions.[16] The theory predicts the free energy of activation for a reaction as a function of the free energy change for the reaction and the **intrinsic barrier** of the reaction. The intrinsic barrier of a reaction in simple cases may be interpreted as the activation energy for the identity reaction where the products are the same as reactants, and in which the overall free energy change is zero.

Marcus Theory applies to reaction occurring within an **encounter complex**. That is, the work terms for bringing reactants together from solution to form the encounter complex and for diffusional separation after reaction must have already been taken into account. After applying Marcus Theory, the rate constants for reaction within the encounter complex must be converted to macroscopic rate constants by incorporating the work terms previously used to isolate the reaction within the encounter complex. Marcus applied this relation, in a slightly modified form, to atom and proton transfers[17-19] and Guthrie has since applied Marcus Theory to many reactions including acetal and orthoester hydrolysis, and aldol condensations.[20]

A simple example for visualization is methyl group transfer. Equation 1 shows the equilibrium for bringing reactants together from solution to form an encounter complex

complex with an equilibrium constant K_{enc}, reaction within the encounter complex, and then diffusional separation of products after reaction, with an equilibrium constant K_{diff} which equals $1/K_{enc}$. In the simple case where X equals Y we have an identity reaction for which the free energy change must be zero and hence the activation energy must be equal to the intrinsic barrier.

$$Y: + CH_3X \overset{K_{enc}}{\rightleftharpoons} \underbrace{Y:CH_3X \rightleftharpoons YCH_3:X}_{\text{reaction within encounter complex}} \overset{K_{diff}}{\rightleftharpoons} YCH_3 + :X \qquad [1]$$

The free energy for reaction within the encounter complex is approximated by two intersecting parabolas of equal curvature, with their minima at $x = 0$ and $x = 1$ corresponding to starting materials and products respectively. The intersection of the parabolas is the transition state. As reaction proceeds from $x = 0$, the free energy will increase up the first parabola. When the energy of the first parabola matches that of the second, reaction will then proceed along the second (now lower energy) parabola and on to products. This is shown in Figure 1 for the identity reaction ($\Delta G^\circ = 0$) and for a general reaction ($\Delta G^\circ \neq 0$).

If we define the energy at x=0 to be zero, then we can derive an expression for the energy at the point of intersection of the two parabolas. The two parabolas are given by:

$$\Delta G_1 = b\,x^2$$

$$\Delta G_2 = \Delta G^\circ + b\,(1-x)^2$$

The transition state is located at $x = x^\ddagger$ at the intersection of the two parabolas. The energy at the transition state is defined as $\Delta G^\ddagger$ and at this point the energy of the two parabolas is the same so that:

$$b\,x^{\ddagger 2} = \Delta G^\circ + b\,(1-2x^{\ddagger}+x^{\ddagger 2})$$

or $$x^{\ddagger} = (\Delta G^\circ + b) / 2b = 1/2 + \Delta G^\circ / 2b$$

then the energy at the transition state is given by:

$$\Delta G^{\ddagger} = b\,(1/2 + \Delta G^\circ / 2b)^2$$

when $\Delta G^\circ = 0$, $\Delta G^{\ddagger} = b / 4$; therefore $b = 4\,\Delta\widetilde{G}$

$$\Delta G^{\ddagger} = \Delta\widetilde{G}\,(1 + \Delta G^\circ / 4\Delta\widetilde{G})^2$$

This is the form of the Marcus equation as we use it.

Figure 1. Two parabola model for reaction energy used by Marcus Theory.

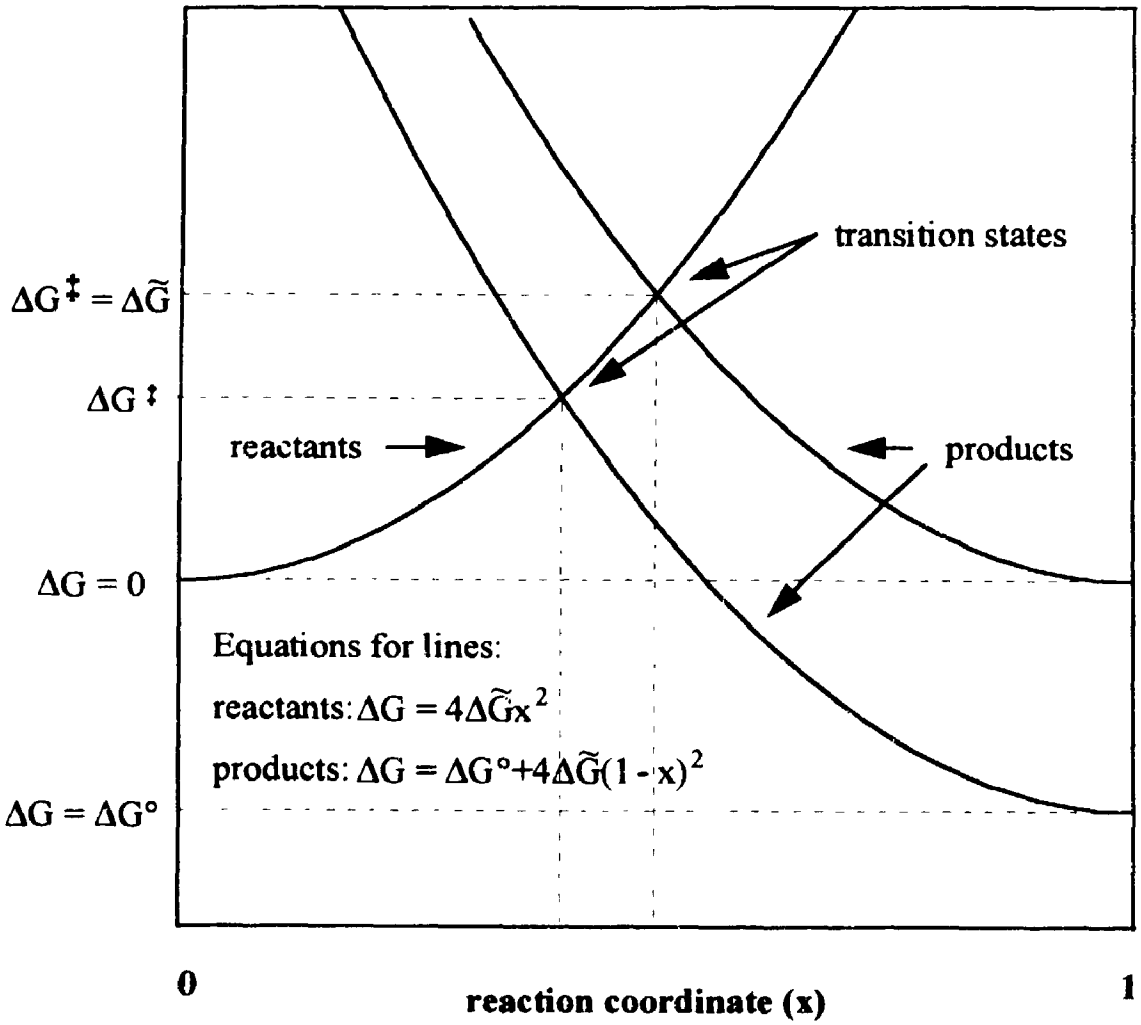

The above derivation is a one-dimensional treatment of Marcus Theory. In a reaction involving more than one reaction coordinate, such as concerted bond formation and breakage, we need to consider energy barriers in more than one dimension. For multidimensional cases, the derivation follows from four postulates:

1. Reactants are in equilibrium with starting material or product at each point along each reaction coordinate. This is a starting assumption of Transition State Theory.

2. At each section through the reaction hypersurface for which only one reaction coordinate changes, Marcus Theory will apply and will be determined by the initial and final energies, and the intrinsic barrier for that coordinate. This follows from postulate 1 for reaction along a perpendicular coordinate.

3. The intrinsic barrier for any reaction coordinate is independent of the values of the other reaction coordinates. This is required to keep the equations relatively simple and to keep the amount of input manageable.

4. For any reaction coordinate chosen as a progress variable, at fixed values of the other coordinates, the free energy will be a quartic function of the progress variable.

A quartic function will better approximate the shape of the reaction surface at the transition state.

The first task in Marcus Theory analysis is to estimate the **corner energies** where each corner will have a value for each reaction coordinate of 0 or 1. These energies will include the free energy relative to starting material, hydrogen bonding energies, ion pairing energies and encounter complex formation energies.

Treatment of well characterized systems allows calculation of intrinsic barriers for various bond formation and breakage processes. This has been performed for many

reactions. With the corner energies and the intrinsic barrier for each dimension, the reaction energy surface can be calculated and searched for the lowest energy path between starting materials and products. This allows for the determination of the transition state as a function of the progress along each of the reaction coordinates. Determination of a mechanism as either stepwise or concerted is then possible.

CHAPTER 2: OVERALL KINETICS AND RESULTS OF DMOP HYDROLYSIS

2.1 Overall kinetics

The hydrolyses of DMOP and TMOA are both pseudo-first order processes which are subject to specific acid catalysis by analogy with 2,2-diethoxypropane and triethyl-orthoacetate.[2] TMOA hydrolysis is similarly known to be general acid catalyzed.[2] A specific acid catalyzed and uncatalyzed (water) rate for each were determined in this work. Unless otherwise noted, experiments were run at 25.0 °C in aqueous solution with ionic strength 1.0 M. Kinetics data were fitted to a single exponential by non-linear least squares. For reactions run in buffers, the rate extrapolated to zero buffer concentration is called the zero-buffer rate, and will equal the sum of the water rate and specific acid catalyzed rate at that pH. Zero-buffer rate and water rate are used interchangeably to describe the observed rate for unbuffered hydroxide solutions.

For experiments followed by proton NMR, the amount of DMOP or TMOA was expressed as a fraction of the initial concentration, allowing ratios of peak integrals to be used, thereby avoiding the need for an internal standard and the determination of actual concentrations. To improve the fit of the data and because hydrolysis proceeds essentially 100%, points were often added to the set of observed data to force the fraction of DMOP or TMOA at infinite time to approach zero during least-squares fitting.

For experiments followed by UV spectrophotometry, 10 cm cells were used to give a sufficiently large absorbance from the weak acetone and methyl acetate chromophores. DMOP or TMOA was injected directly via syringe to initiate reaction.

The saponification of methyl acetate produced by hydrolysis of TMOA was also observed. Its rate of alkaline saponification was previously determined[21] as $k_{OH^-} = 0.151$ $M^{-1}s^{-1}$, and was not studied here.

In all tables, values have been rounded to an appropriate number of significant figures for presentation. Calculations were performed on unrounded data using appropriate weightings. Small discrepancies may appear if table values are used to repeat calculations.

2.2 Kinetics of hydrolysis of DMOP in pH 4-8 buffers

The kinetics of hydrolysis of DMOP were studied by UV spectrophotometry in aqueous buffers at pH 4.7, 6.5, and 7.8. Acetic acid / sodium acetate buffers were used for the pH 4.7 experiments and potassium dihydrogen phosphate / disodium hydrogen phosphate buffers were used for the pH 6.5 and 7.8 experiments. In each set of experiments the total buffer concentration was varied but the buffer ratio, and hence the pH, was kept constant; the ionic strength was maintained at 1 M by the addition of potassium chloride.

The observed rate constants for the appearance of acetone are listed in Tables 1, 2, and 3 for experiments at pH 4.7, 6.5 and 7.8 respectively. Plots (not shown) were made of the observed rate constants versus the concentration of the acidic buffer component. Early results with phosphate buffers suggested the presence of general acid catalysis, but experimental scatter necessitated improved technique. Scrupulous drying of salts, and improvements to the temperature control of the spectrophotometer caused the apparent catalytic effect to vanish. Because there was no evidence of GAC, the zero-buffer rate at

each pH was taken as the weighted average of the observed rate constants divide 'by the average hydronium ion concentration.

A sample plot of the kinetics obtained for DMOP hydrolysis in pH 6.5 phosphate buffer is shown in Figure 2.

Table 1. Rate constants for the hydrolysis of DMOP in pH 4.8 buffers.[a]

[AcOH][b] (M)	pH[c]	α	β	$10^2 \lambda_{obs}$ (s^{-1})
0.50	4.78	0.292	-0.202	5.63±0.07
0.50	4.77	0.310	-0.199	4.23±0.09
0.50	4.76	0.594	-0.230	4.06±0.04
0.50	4.76	0.389	-0.237	4.18±0.05
0.50	4.76	0.660	-0.510	4.33±0.02
0.50	4.78	0.603	-0.490	4.48±0.02
0.40	4.76	0.403	-0.280	4.51±0.03
0.40	4.76	0.374	-0.240	4.97±0.04
0.40	4.75	0.430	-0.280	4.44±0.03
			av	4.44±0.10

[a] In aqueous acetic acid / sodium acetate buffer (1:1) at 25.0 °C; ionic strength maintained at 1.0 M with KCl. Following acetone chromophore at 265 nm by UV spectrophotometry. Absorbance-time data fitted to $A = \alpha + \beta \exp(-\lambda t)$. Cell length 2.000 cm. [DMOP]$_i \approx 0.04$ M.

[b] concentration of undissociated acetic acid

[c] pH of cell contents measured after reaction.

Table 2. Rate constants for the hydrolysis of DMOP in pH 6.5 buffers.[a]

$[H_2PO_4^-]$[b] (M)	pH[c]	α	β	$10^4 \lambda$ (s^{-1})
0.450	6.51	0.989	-0.535	7.14± 0.02
0.360	6.51	0.858	-0.558	7.26± 0.02
0.360	6.51	0.848	-0.557	7.21± 0.01
0.270	6.48	0.770	-0.542	6.92± 0.01
0.270	6.48	0.751	-0.557	7.15± 0.02
0.180	6.46	0.658	-0.550	7.23± 0.01
0.180	6.50	0.682	-0.566	7.08± 0.01
			av	7.15± 0.04

[a] In aqueous potassium dihydrogen phosphate / disodium hydrogen phosphate buffer (1:1) at 25.0 °C; ionic strength maintained at 1.0 M with KCl. Following acetone chromophore at 265 nm by UV spectrophotometry. Absorbance-time data fitted to $A = \alpha + \beta \exp(-\lambda t)$. Cell length 1.000 cm. $[DMOP]_i = 0.003$ M

[b] concentration of dihydrogen orthophosphate monoanion

[c] pH of cell contents measured after reaction.

Table 3. Rate constants for the hydrolysis of DMOP in pH 7.9 buffers.[a]

$[H_2PO_4^-]$[b] (M)	pH[c]	α	β	$10^5 \lambda$ (s^{-1})
0.0692[d]	7.96	1.869	-1.636	4.728± 0.004
0.0692[d]	7.96	1.847	-1.612	4.837± 0.003
0.0554[d]	7.88	1.820	-1.609	5.083± 0.004
0.0554[d]	7.88	1.807	-1.632	5.388± 0.005
0.0692[e]	7.96	0.950	-0.570	5.059± 0.004
0.0692[e]	7.96	0.991	-0.520	5.265± 0.007
0.0692[e]	7.96	0.720	-0.554	4.818± 0.013
0.0692[e]	7.96	0.735	-0.565	4.855± 0.007
0.0554[e]	7.88	0.726	-0.571	5.363± 0.008
0.0554[e]	7.88	0.719	-0.561	5.365± 0.010
0.0415[e]	7.87	0.682	-0.564	5.896± 0.003
0.0415[e]	7.87	0.689	-0.574	5.839± 0.003
			av	5.29± 0.13

[a] In aqueous potassium dihydrogen phosphate / disodium hydrogen phosphate buffer (1:1C) at 25.0 °C; ionic strength maintained at 1.0 M with KCl. Following acetone chromophore at 265 nm by UV spectrophotometry. Absorbance-time data fitted to $A = \alpha + \beta \exp(-\lambda t)$. Cell length 10.000 cm.

[b] concentration of dihydrogen orthophosphate monoanion

[c] pH of cell contents measured after reaction.

[d] $[DMOP]_i = 0.006$ M

[e] $[DMOP]_i = 0.003$ M

Figure 2 . Absorbance vs. time plot for DMOP in pH 6.5 phosphate buffer; $[H_2PO_4^-] = 0.36$ M

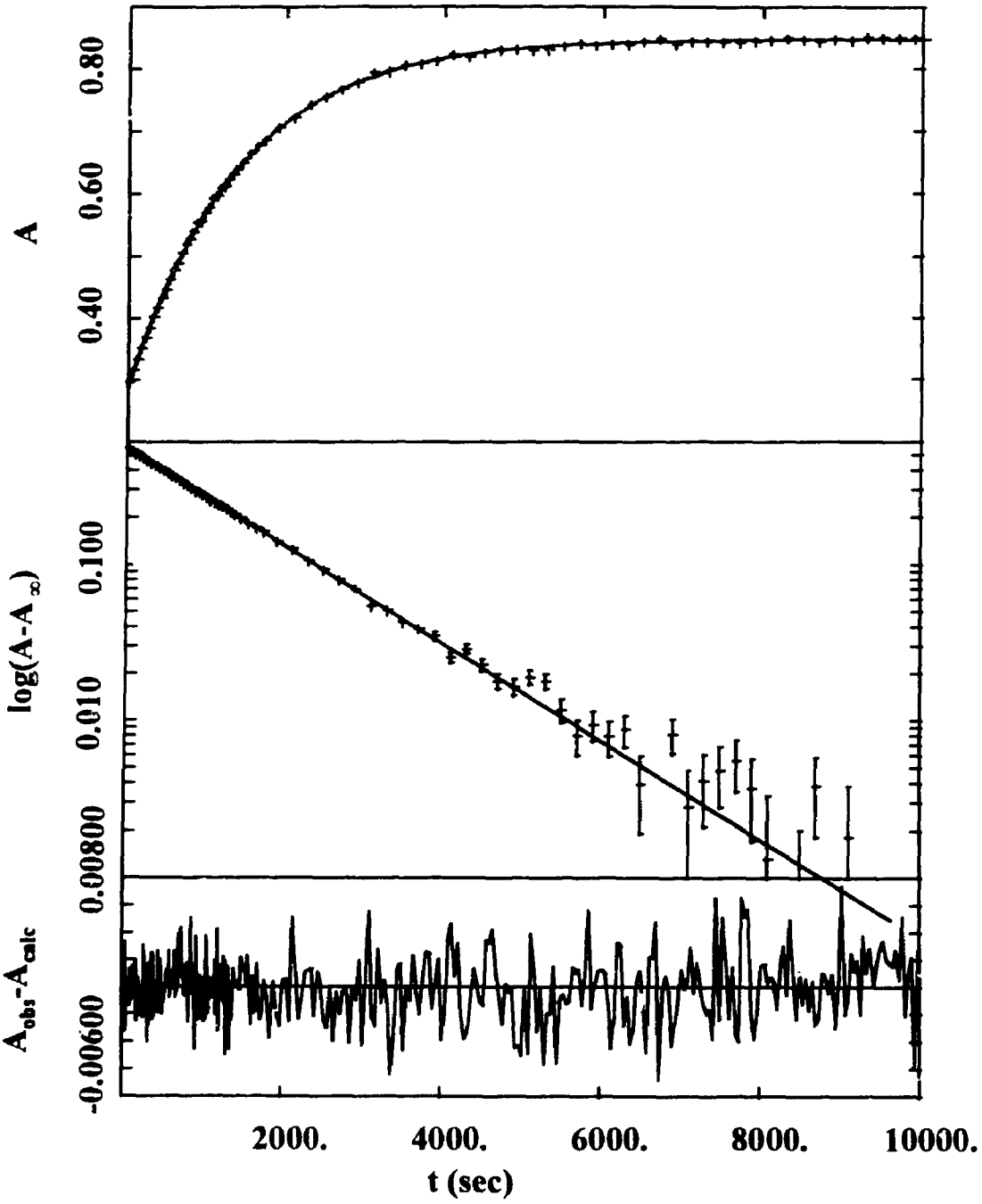

Table 4. Rate constants for the hydrolysis of DMOP in pH 9.2 buffers.[a]

[PhOH][b] (M)	pH[c]	α[d]	β[e]	$10^6 \lambda$ (s^{-1})
0.45[f]	9.21	0.00	0.86	1.79± 0.24
0.36[f]	9.20	0.00	0.87	1.80± 0.17
0.27[f]	9.19	0.00	0.97	2.14± 0.15
0.18[f]	9.21	0.00	0.93	2.18± 0.24
0.09[f]	9.14	0.00	0.86	2.16± 0.26
0.45[g]	9.20	0.00	0.93	2.10± 0.11
0.36[g]	9.20	0.00	0.97	2.28± 0.11
0.27[g]	9.19	0.00	0.89	2.01± 0.02
0.18[g]	9.22	0.00	0.86	2.08± 0.15
0.09[g]	9.21	0.00	0.88	2.09± 0.19
			av	2.02± 0.02

[a] In aqueous phenol / sodium phenoxide buffers (9:1) at 25.0 °C; ionic strength and aromatic ring concentration maintained at 1.0 M with KCl and sodium benzoate. Followed by ^{1}H NMR using methoxy peak integrations to determine the fraction of DMOP (f_{DMOP}) remaining. f_{DMOP}-time data were fitted to $f_{DMOP} = \alpha + \beta\exp(-\lambda t)$.

[b] concentration of undissociated phenol.

[c] pH of pure buffer solution.

[d] α constrained to be close to zero by using a synthetic data point, $f_{DMOP} = 0.0$ at $t = 10^9$ s.

[e] standard deviations of β values are in the range 0.02-0.07

[f] $[DMOP]_i = 0.10$ M

[g] $[DMOP]_i = 0.05$ M

2.3 Kinetics of hydrolysis of DMOP in pH 9.2 buffers

The kinetics of hydrolysis of DMOP in phenol / sodium phenoxide (9:1) buffers at pH 9.2 were studied at 25.0 °C by NMR analysis of hydroxide quenched samples. The

results of two sets of buffer runs are shown in Table 4. No general acid catalysis was observed. A sample kinetics plot is shown in Figure 2.

2.4 Kinetics of hydrolysis of DMOP in pH 10.1 buffers

The kinetics of hydrolysis of DMOP were studied in 1:1 phenol / phenoxide buffers at pH 10.1 and 65 °C by NMR analysis of thermally quenched samples. The observed rate constants for 65 °C are listed in Table 5 and a summary of this and the previous work[22] is presented in Table 6. Combination of these results with previous work[22] at 40 and 56 °C allowed determination of the water and general acid catalyzed rates at 25 °C as $k_{H2O} = (2.1\pm3.2) \times 10^{-7}$ ($\log k_{H2O} = -6.67\pm0.65$) and $k_{PhOH} = (3.5\pm22.) \times 10^{-7}$ ($\log k_{PhOH} = -6.45\pm2.65$) respectively, by extrapolation from the linear least squares fit of $\log k_{H2O}$ vs 1/T and $\log k_{PhOH}$ vs 1/T. Neither the water nor general acid catalyzed rates are well defined. The general acid catalyzed rate, in particular, is not distinguishable from zero. Arrhenius plots for zero-buffer and general acid catalyzed rate constants are shown in Figures 5 and 6 respectively.

The earlier work also included experiments at 65 °C, using samples sealed in NMR tubes and kept in a drying pistol heated by refluxing methanol. The slow heat transfer between the drying pistol and NMR tubes, aggravated by repeated sampling, resulted in depressed observed rate constants. This work used reaction solution sealed in ampoules which were kept in a 65 °C water bath. Each ampoule was used only once so that thermal equilibration problems from repeated sampling were avoided.

Figure 3. Fraction of DMOP remaining vs. time for hydrolysis at pH 9.2; [PhOH] = 0.27 M; analysis by NMR

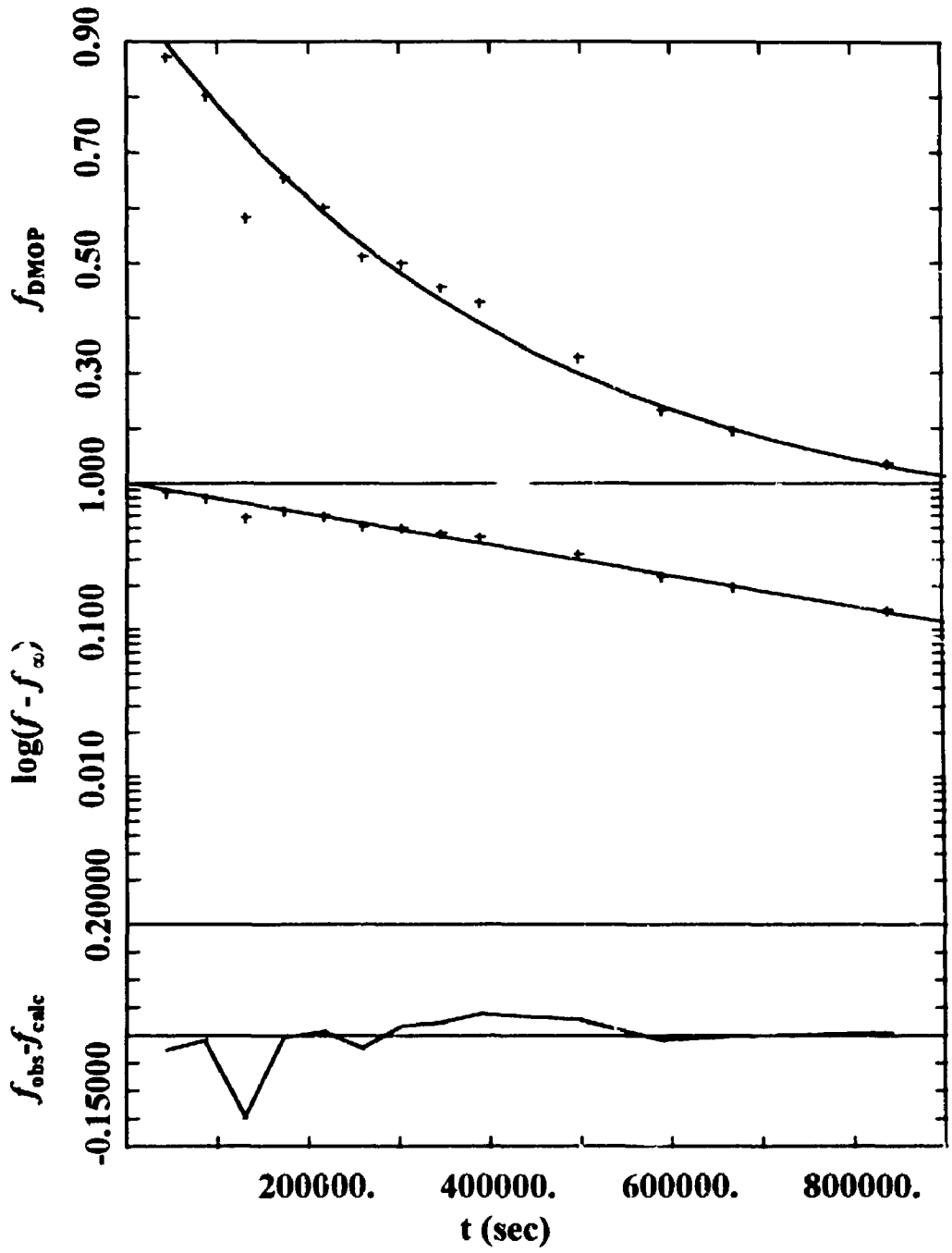

Table 5. Rate constants for the hydrolysis of DMOP in pH 10.1 buffers at 65 °C.

[PhOH][b] (M)	pH[c]	α^d	β	$10^6 \lambda$ (s^{-1})
0.50	10.12	0.00	1.02	3.00±0.10
0.40	10.12	0.00	1.00	2.49±0.06
0.30	10.12	0.00	0.95	2.36±0.10
0.20	10.12	0.00	1.00	2.30±0.02
0 10	10.12	0.00	0.96	2.17±0.05
			av	2.32±0.06

[a] Reaction carried out at 65.0 °C. Buffers 1:1 phenol : sodium phenoxide; ionic strength and aromatic ring concentration each maintained at 1.0 M with KCl and sodium benzoate. Followed by ^{1}H NMR using methoxy peak integrations to determine the fraction of DMOP (f_{DMOP}) remaining. f_{DMOP}-time data were fitted to $f_{DMOP} = \alpha + \beta\exp(-\lambda t)$. $[DMOP]_i = 0.10$ M

[b] concentration of undissociated phenol.

[c] pH of pure buffer solution at room temperature.

[d] α constrained to be close to zero by using a synthetic data point, $f_{DMOP} = 0.0$ at $t = 10^9$ s

[e] deviations in β are 0.01-0.02

Figure 4 . Dependence of DMOP hydrolysis rate on phenol concentration in pH 10.1 buffers at 65 °C.

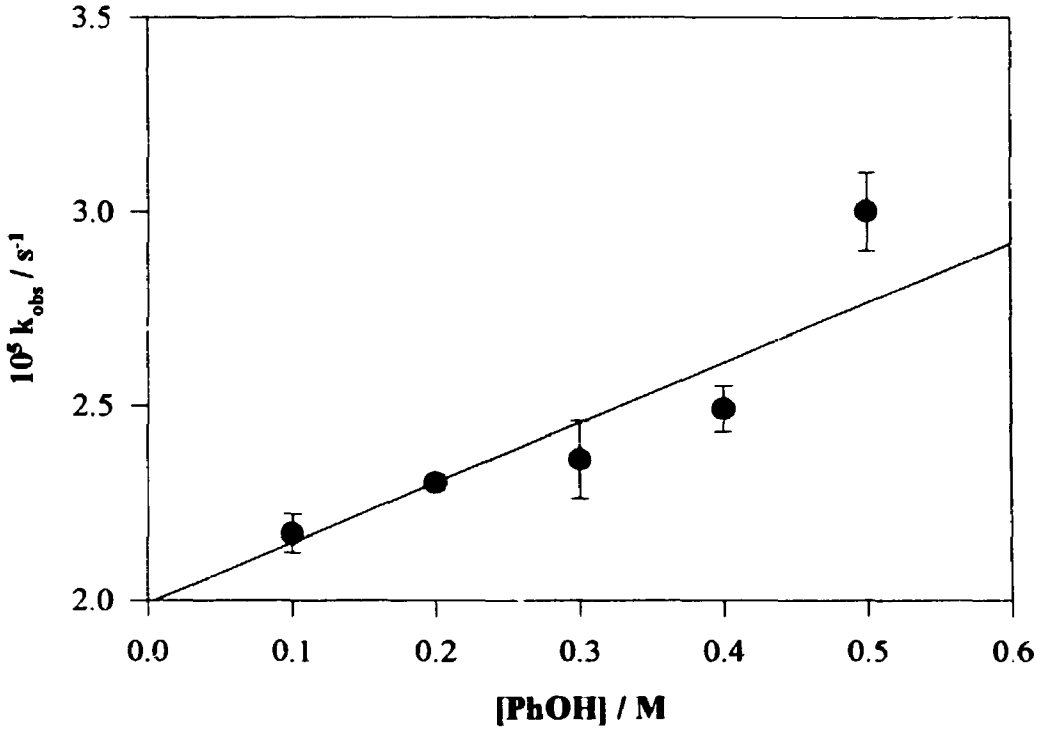

Table 6. Summary of Rate Constants for DMOP hydrolysis at pH 10.1

T (°C)	10^3/T (K^{-1})	$10^6 k_{zero\text{-}buffer}$ (s^{-1})	log ($k_{zero\text{-}buffer}$ / s^{-1})	$10^6 k_{gac}$ ($M^{-1}.s^{-1}$)	log (k_{gac} / $M^{-1}s^{-1}$)
40.0 [a]	3.193	1.34 ± 0.08	-5.87±0.03	1.6± 0.3	-5.78±0.09
56.0 [a]	3.038	6.5 ±1.1	-5.18±0.07	10.7± 3.4	-4.97±0.14
65.0 [b]	2.957	19.9± 0.9	-4.70±0.02	15.4± 3.8	-4.81±0.11

[a] Ref. 22

[b] this work, see Table 5.

Figure 5. Arrhenius plot of second-order rate constants for DMOP hydrolysis in phenol buffers.

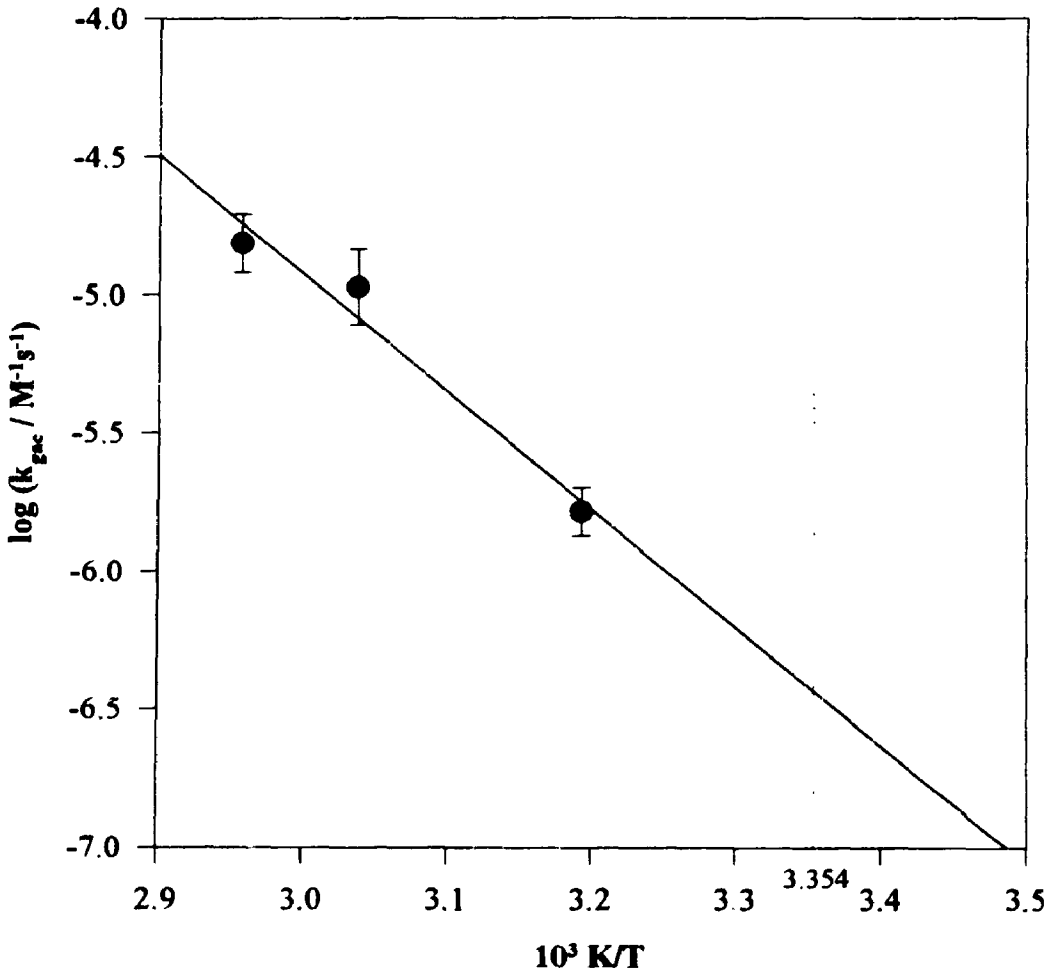

Figure 6. Arrhenius plot of DMOP hydrolysis zero-buffer rate constants at pH 10.1

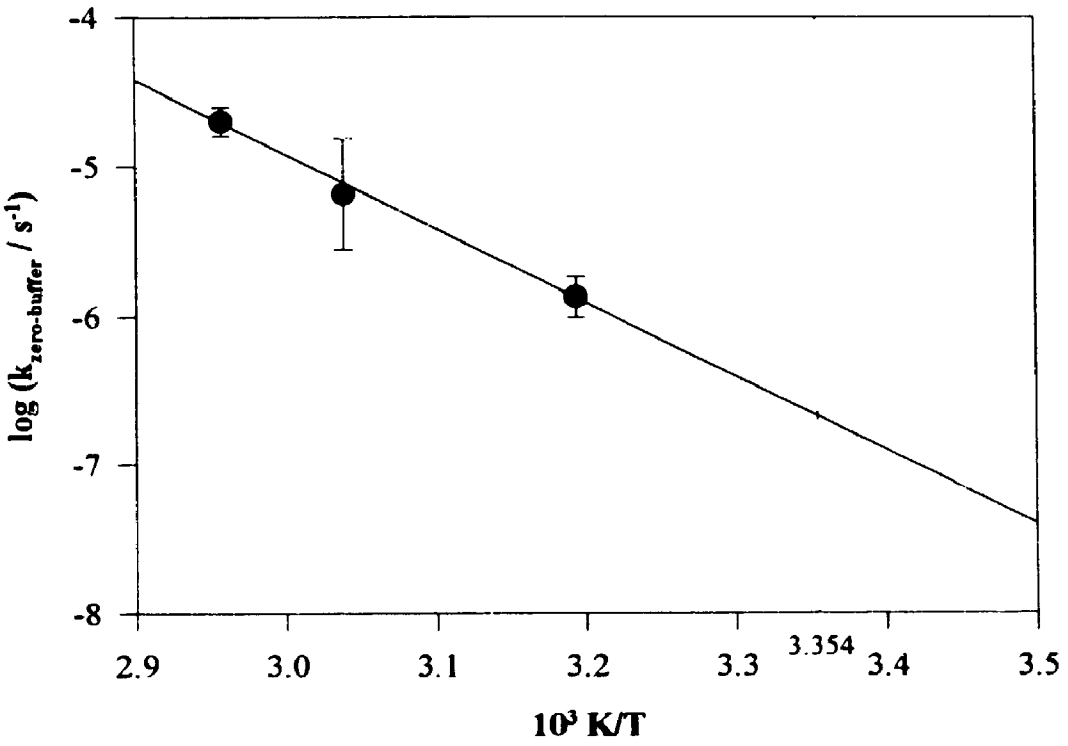

2.5 Kinetics of hydrolysis of DMOP in aqueous hydroxide

The kinetics of hydrolysis of DMOP were studied in dilute aqueous base at 25.0, 35.0, 56.0 and 65.0 °C by NMR spectroscopy to determine the water (uncatalyzed) rate for DMOP hydrolysis. Leblanc[23] found ill-behaved kinetics and extensive etching of the glass NMR tubes by hydroxide while studying the hydrolysis of DMOP in dilute hydroxide solution at elevated temperatures. This study avoided the problems of glass etching by using teflon liners, used much like ampoules, to contain the samples within the NMR tubes. The rate constants were found to be significantly higher, with excellent

evidence for pH-independent (uncatalyzed) hydrolysis of DMOP at high pH.

The results of kinetics at all temperatures are summarized in Table 7. Extrapolation from high temperature experiments back to room temperature lead to large uncertainties in the 25 °C rate. Therefore, initial rate kinetics were used at 25° (and 35 °C) to determine a more reliable value.

Initial rate kinetics, following the first 15% of reaction, were used to measure the hydrolysis rate directly at 25.0 (and 35.0) °C for 0.1 M and 1.0 M hydroxide solutions. Teflon bottles containing 25 mL of aqueous hydroxide solution of DMOP periodically had samples removed for analysis by NMR, which was performed in locked mode following addition of deuterium oxide to the sample. The uncertainties arising from initial rate kinetics are markedly smaller than those arising from extrapolation. The rate constants from 25 °C initial rate studies were used for the pH rate profile.

The rate in 1.0 M hydroxide is considerably faster than that in 0.1 M hydroxide. This is attributed to the involvement of a hydroxide catalyzed E2 mechanism which will be discussed in further detail during Marcus theory analysis.

Table 7. Rate constants for hydrolysis of DMOP in aqueous hydroxide at 25, 35, 56, and 65 °C.[a]

T (°C)	$10^3/T$ (K^{-1})	k^b_{water} (s^{-1})	log (k_{water} / s^{-1})
(a) [NaOH] = 1.00 M			
65[c]	2.957	$9.5\pm0.5 \times 10^{-6}$	-5.02± 0.13
56[c]	3.038	$4.9\pm0.3 \times 10^{-6}$	-5.31± 0.16
35[d]	3.245	$1.0\pm0.1 \times 10^{-7}$	-6.99± 0.30
25[d]	3.354	$6.4\pm0.3 \times 10^{-8}$	-7.20± 0.12
(b) [NaOH] = 0.10 M; [KCl] = 0.90 M			
65[c]	2.957	$1.4\pm0.1 \times 10^{-5}$	-4.86± 0.20
56[c]	3.038	$4.7\pm0.4 \times 10^{-6}$	-5.33± 0.20
35[d]	3.245	$8.5\pm0.5 \times 10^{-8}$	-7.07± 0.14
25[d]	3.354	$3.9\pm0.2 \times 10^{-8}$	-7.41± 0.12
(c) [NaOH] = 0.01 M; [KCl] = 0.99 M			
65[c]	2.957	$1.5\pm0.1 \times 10^{-5}$	-4.82± 0.13
56[c]	3.038	$1.2\pm0.4 \times 10^{-5}$	-4.91± 0.71

[a] Reactions performed under varying conditions according to temperature: 56, 65 °C: samples sealed in groups of teflon NMR tube liners, used as ampoules, which were inserted into NMR tubes for analysis; 25, 35 °C: 25 mL of reaction solution was contained in a screw capped teflon bottle, which was periodically opened for withdrawal of 0.6 mL of solution for NMR analysis. Followed by ^1H NMR using methoxy peak integrations to determine the fraction of DMOP (f_{DMOP}) remaining. For 56, 65 °C: f_{DMOP}-time data were fitted to $f_{DMOP} = \alpha + \beta\exp(-\lambda t)$; For 25, 35 °C: f_{MeOH} fitted to $f_{MeOH} = \alpha + \beta t$.

[b] T = 56, 65 °C: $k = \lambda$; T = 25, 35 °C: $k = \beta$

[c] $[DMOP]_i = 0.10$ M

[d] $[DMOP]_i = 0.30$ M

Figure 7. Arrhenius plot of DMOP hydrolysis rate constants in aqueous base. Data are for ○ 1.0 M NaOH; □ 0.10 M NaOH; Δ 0.01 M NaOH. Line shown is the best fit to both 1.0 and 0.10 M NaOH data sets taken together.

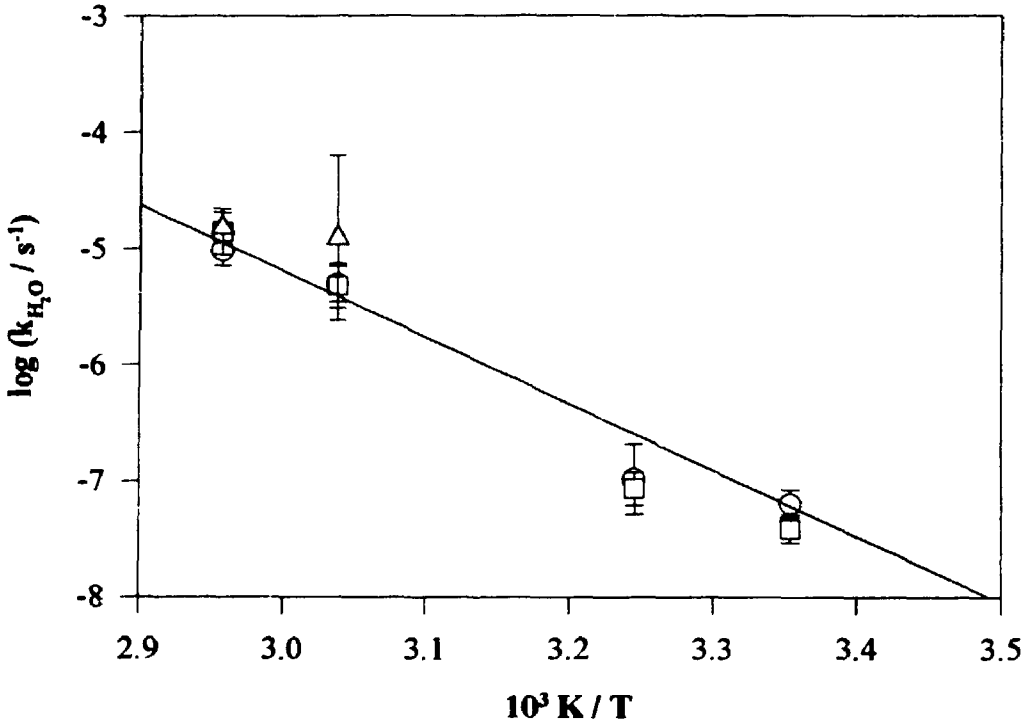

CHAPTER 3: RESULTS OF TMOA HYDROLYSIS

3.1 Kinetics of hydrolysis of TMOA in pH 6.5 and 7.9 buffers

The hydrolysis of TMOA was studied in aqueous phosphate buffers at pH 6.5 and 7.9 by UV spectrophotometry, following the appearance of methyl acetate. The rate constants for the two series of buffer concentrations are given in Tables 8 and 9 and are plotted in Figure 8. The linear dependence of rate on buffer concentration clearly shows GAC. The slight curvature of the plots is consistent with the change in the specific acid catalyzed rate caused by changing buffer pH. Least squares fitting of the observed rate constants to the equation $\lambda = k_{HA}[HA] + k_{H+}[H^+]$, where HA is the general acid dihydrogen phosphate, gave for pH 6.5 and 7.9 respectively: $k_{HA} = (5.9\pm0.1) \times 10^{-2}$ $M^{-1}s^{-1}$, $(4.0\pm0.1) \times 10^{-2}$ $M^{-1}s^{-1}$ and $k_{H+} = (2.02\pm0.02) \times 10^{4}$ $M^{-1}s^{-1}$, $(4.1\pm0.2) \times 10^{4}$ $M^{-1}s^{-1}$. Simultaneous fitting of both sets of data to the same equation gave $k_{HA} = (4.7\pm0.1) \times 10^{-2}$ $M^{-1}s^{-1}$ and $k_{H+} = (2.22\pm0.06) \times 10^{4}$ $M^{-1}s^{-1}$. These latter values can be taken as the best overall fit. The individual lines shown in Figure 8 are simple linear fits and are shown for reference only. Simultaneous fitting gives a poorer fit to each of the sets of experiments, but should give better overall values for the specific acid catalyzed and general acid catalyzed rate constants.

The discrepancy between the second order rate constants at pH 6.5 and 7.9, and the change in pH with changing buffer concentration indicate that the non-ideality of the solutions resulting from high salt concentrations was not negligible. Nonetheless, without investiging specific salt effects, the non-ideality of the buffers must be ignored.

Table 8. Rate constants for hydrolysis of TMOA in pH 6.5 buffers.[a]

$[H_2PO_4^-]^b$ (M)	pH[c]	α	β	$10^2 \lambda$ (s^{-1})
0.100	6.51	1.383	-0.795	1.219± 0.005
0.100	6.51	1.414	-0.812	1.204± 0.002
0.080	6.50	1.410	-0.820	1.127± 0.002
0.080	6.50	1.438	-0.849	1.099± 0.002
0.060	6.49	1.409	-0.827	0.999± 0.002
0.060	6.49	1.399	-0.806	0.996± 0.002
0.040	6.49	1.376	-0.807	0.893± 0.002
0.040	6.49	1.415	-0.824	0.895± 0.002
0.020	6.49	1.407	-0.829	0.775± 0.002
0.020	6.49	1.409	-0.826	0.779± 0.003
0.010	6.49	1.427	-0.833	0.714± 0.002
0.010	6.49	1.441	-0.851	0.708± 0.002

[a] In aqueous potassium dihydrogen phosphate / disodium hydrogen phosphate buffer (1:1) at 25.0 °C; ionic strength maintained at 1.0 M with KCl. $[TMOA]_i$ = 0.02 M. Following methyl acetate chromophore at 210 nm by UV spectrophotometry. Absorbance-time data fitted to $A = \alpha + \beta \exp(-\lambda t)$. Cell length 1.000 cm.

[b] concentration of dihydrogen phosphate monoanion

[c] pH of pure buffer

Table 9. Rate constants for hydrolysis of TMOA in pH 7.9 buffers.[a]

$[H_2PO_4^-]^b$ (M)	pH[c]	α	β	$10^3 \lambda$ (s^{-1})
0.069	7.96	2.599	-2.186	3.124± 0.012
0.069	7.96	2.648	-2.267	3.169± 0.007
0.055	7.88	2.553	-2.212	2.798± 0.007
0.055	7.88	2.607	-2.289	2.731± 0.007
0.042	7.87	2.558	-2.252	2.332± 0.006
0.042	7.87	2.496	-2.171	2.317± 0.007
0.028	7.80	2.558	-2.321	1.799± 0.006
0.028	7.80	2.634	-2.344	1.807± 0.006
0.014	7.76	2.656	-2.438	1.238± 0.003
0.014	7.76	2.516	-2.288	1.292± 0.004

[a] In aqueous potassium dihydrogen phosphate / disodium hydrogen phosphate buffer (1:1) at 25.0 °C; ionic strength maintained at 1.0 M with KCl. [TMOA]$_i$ = 0.02 M. Following methyl acetate chromophore at 210 nm by UV spectrophotometry. Absorbance-time data fitted to $A = \alpha + \beta \exp(-\lambda t)$. Cell length 1.000 cm.

[b] concentration of dihydrogen phosphate monoanion

[c] pH of pure buffer

3.2 Kinetics of hydrolysis of TMOA in pH 9.4 buffers

The hydrolysis of TMOA was studied in aqueous 1,1,1,3,3,3-hexafluoro-2-propanol (HFIP) buffers at pH 9.4. NMR analysis of base quenched samples allowed determination of the fraction of TMOA remaining. The basic quench not only slowed the TMOA hydrolysis, but also saponified any methyl acetate to methanol and acetate ion.

This simplified the NMR analysis because only two methoxy peaks needed to be quantified.

Figure 8. Dependence of TMOA hydrolysis rate on dihydrogen phosphate concentration at pH 6.5 and 7.9

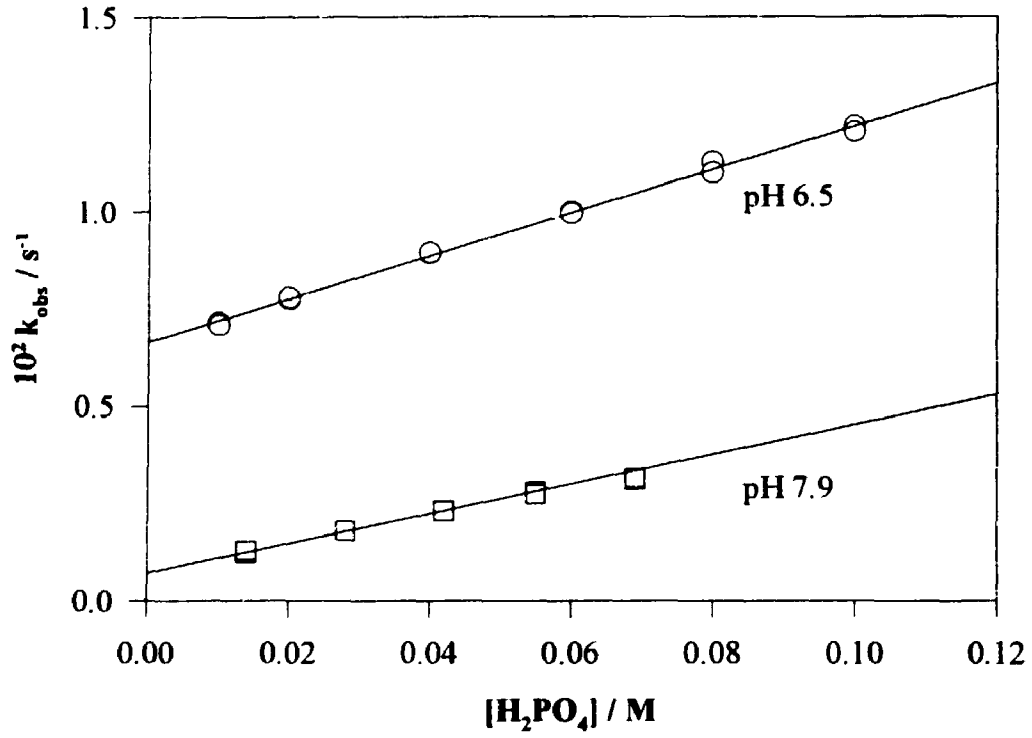

The rate constants for reaction in a series of buffers are listed in Table 10 and are plotted in Figure 9. The dependence of rate on buffer concentration is clearly not linear. A plot (not shown) of observed rate constants versus the square of the buffer concentration is surprisingly linear, but there is no apparent mechanistic reason for this. It is reasonable that solvent effects from the large hexafluoro-2-propanol and 2-propanol concentrations are responsible. Omitting the 2-propanol gives very poor buffer pH

control on dilution, but 2-propanol has a lower molar volume than the hexafluoro analog (76.4 mL / mol vs. 105 mL / mol). The lower molar volume would result in the more concentrated buffers being more organic and this should promote general acid catalysis by making generation of carbocations less favorable and hence make concerted pathways relatively more favorable.

Table 10. Rate constants for hydrolysis of TMOA in pH 9.4 buffers.[a]

[HFIP][b] (M)	pH[c]	α[d]	β	$10^4 \lambda$ (s^{-1})
0.5	9.55	0.00	0.757	25.7± 1.1
0.4	9.51	0.00	0.839	19.0± 0.7
0.3	9.49	0.00	0.892	11.3± 0.3
0.3	9.49	0.00	0.879	12.1± 0.3
0.2	9.45	0.00	0.942	6.9± 0.2
0.2	9.45	0.00	0.957	7.2± 0.1
0.1	9.43	0.00	1.066	5.2± 0.2

[a] In aqueous hexafluoro-2-propanol (HFIP)/ sodium hexafluoro-2-propoxide buffers at 25.0 °C. Ionic strength maintained at 1.0 M with KCl; organic content maintained at 1.0 M with 2-propanol. [TMOA]i = 0.1 × [HFIP]. Reaction followed by NMR analysis of base quenched samples to determine fraction of TMOA (f_{TMOA}) remaining. f_{TMOA}-time data fitted to $f_{TMOA} = \alpha + \beta \exp(-\lambda t)$.

[b] concentration of acidic buffer component

[c] measured for pure buffer

[d] constrained to be close to zero by using $f_{TMOA} = 0.0$ at $t = 10^7$ s.

To extract meaningful rate constants requires some assumptions. The best water rate extrapolated to zero buffer should be the intercept from the k vs $[HFIP]^2$. This is

assumed because the effects, whatever they are, leading to this unusual behavior should cancel themselves out to give a reasonable zero-buffer rate. The best value for the general acid catalyzed rate constant should come from the two lowest buffer concentrations. Here the perturbation of solvent by the buffer would be at a minimum so we can assume that there should be a linear dependence of rate on buffer concentration. Both of these assumptions will be imperfect but should be adequate.

The derived rate constants are then $k_{zero\text{-}buffer} = (3.8\pm0.3) \times 10^{-5}\ s^{-1}$ and $k_{GAC} = (1.9\pm0.3) \times 10^{-5}\ M^{-1}s^{-1}$.

Figure 9. Dependence of TMOA hydrolysis rate on hexafluoro-2-propanol concentration at pH 9.4

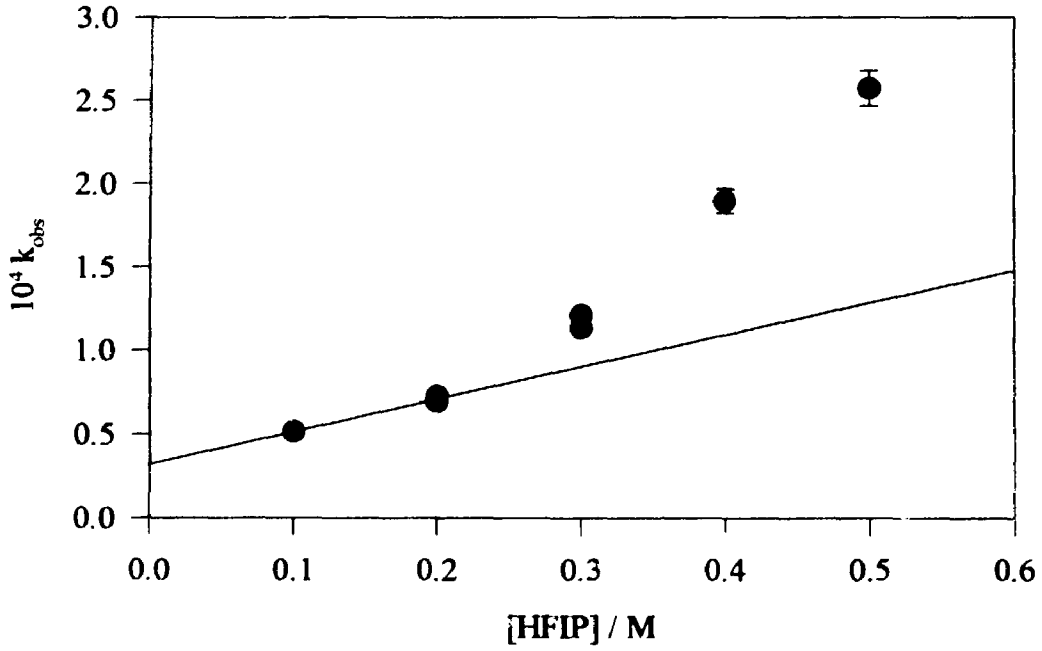

3.3 Kinetics of hydrolysis of TMOA in pH 10 buffers.

The hydrolysis of TMOA was studied in pH 10 phenol buffers by thermostatted NMR. Saponification of the product methyl acetate was on a time scale comparable[21] to the hydrolysis of the TMOA, requiring that the buffer concentration be kept much higher than that of TMOA to ensure pseudo-first order kinetics. Further, both the methyl acetate and saponification products acetate and methanol required quantitation. In practice, the integration for the methoxy peak for methyl acetate was added to that for the methanol peak to give a total methoxy integration for products. The integration for the methoxy peak of TMOA was used as the starting material integration. The remaining starting material was compared to the total for starting materials and products.

Table 11. Rate constants for hydrolysis of TMOA in pH 10.2 buffers.[a]

[PhOH][b] (M)	pH[c]	α[d]	β	$10^5 \lambda$ (s^{-1})
0.5	10.17	0.00	0.99	8.11± 0.12
0.4	10.17	0.00	1.05	6.77± 0.12
0.3	10.18	0.00	1.03	4.94± 0.10
0.2	10.17	0.00	1.03	3.47± 0.13

[a] In aqueous phenol / sodium phenoxide (1:1) buffers at 25.0 °C. Ionic strength and aromatic ring concentration maintained at 1.0 M by addition of KCl and sodium benzoate. [TMOA]$_i$ = 0.1 × [PhOH]. Reaction followed by thermostatted (25.0 °C) NMR using integration of methoxy peaks from TMOA, methyl acetate and methanol. Fraction TMOA remaining (f_{TMOA}) calculated as $f_{TMOA} = i_{TMOA\text{-}OCH_3} / (i_{TMOA\text{-}OCH_3} + i_{MeCO\text{-}OCH_3} + i_{H\text{-}OCH_3})$ and fitted to $f_{TMOA} = \alpha + \beta\exp(-\lambda t)$ by least squares.

[b] undissociated phenol

[c] for pure buffer

[d] constrained to be close to zero by using $f_{TMOA} = 0.0$ at $t = 10^7$ s.

Keeping the TMOA concentration well below the buffer concentration prevented the study of buffer concentrations lower than 0.2 M phenol. Therefore, the percentage uncertainty for the zero-buffer rate is large because of extrapolation errors but the general-acid catalyzed rate constant is well defined. The observed rate constants are listed in Table 11 and are plotted against phenol concentration in Figure 10.

Figure 10. Dependence of TMOA hydrolysis rate on phenol concentration at pH 10.2

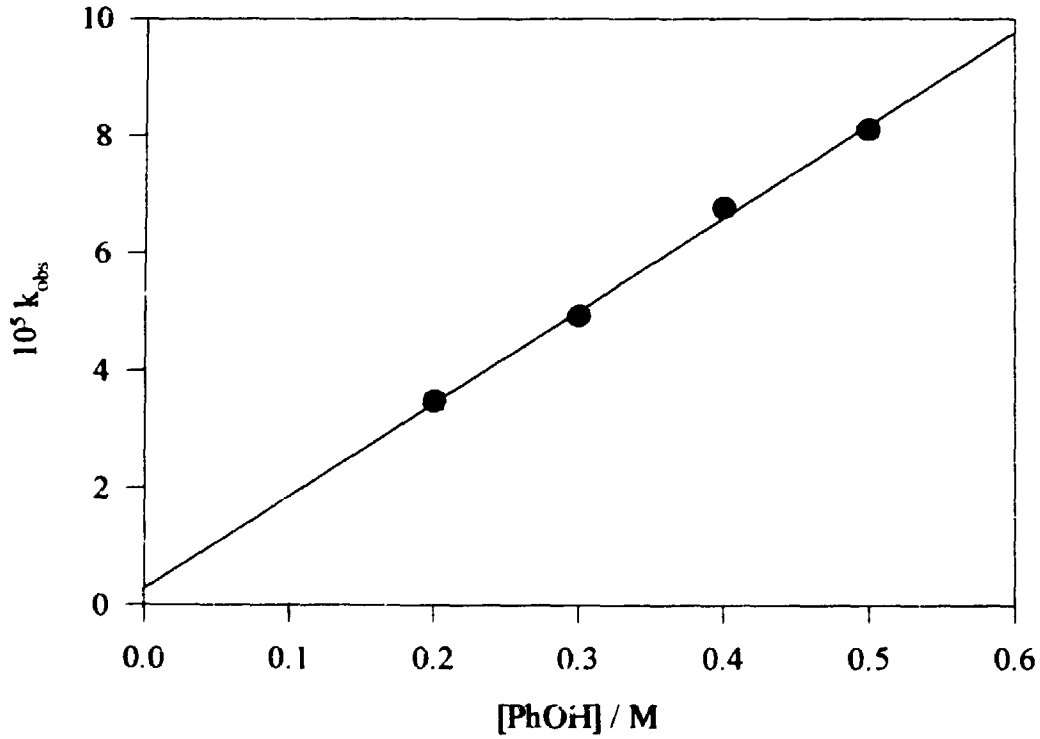

3.4 Kinetics of hydrolysis of TMOA in pH 12.4 buffers

The hydrolysis of TMOA was studied in pH 12.4 trifluoroethanol buffers at 25.0 °C by titration with aqueous hydrochloride. The saponification of methyl acetate at pH 12.4 is fast relative to its production by hydrolysis of TMOA. Thus the observed products of TMOA hydrolysis will be the saponification products of methyl acetate: acetate ion and methanol. Titration of the buffer remaining in the basic form allows calculation of the amount of buffer consumed in saponification, and therefore the extent of TMOA hydrolysis. This method relies on: rapid saponification of methyl acetate in basic solution, slow hydrolysis of TMOA during the titration until saponification slows enough that further hydrolysis will not be detected as saponification products; negligible changes in apparent buffer concentration from carbonate production; hydrolysis being slow relative to the time required for titration; TMOA concentration such that changes in buffer concentration are easily measured but do not greatly affect the rate of reaction by significantly changing the pH or general acid concentration. These conditions were satisfied. The observed rate constants for a series of buffers are listed in Table 12 and are plotted against trifluoroethanol concentration in Figure 11. The rate depends linearly on the general acid concentration. The zero-buffer and GAC rates are, respectively, $(3.28\pm0.18) \times 10^{-6}$ s^{-1} and $(6.7\pm0.6) \times 10^{-6}$ $M^{-1}s^{-1}$.

Table 12. Rate constants for hydrolysis of TMOA in pH 12.4 buffers.[a]

$[CF_3CH_2OH]$[b] (M)	pH[c]	α	β	$10^6 \lambda$ (s^{-1})
0.5	12.4	1.637	0.321	6.7± 0.8
0.4	12.4	1.182	0.360	5.8± 0.5
0.3	12.4	0.797	0.361	5.5± 0.5
0.2	12.4	0.405	0.361	4.6± 0.4
0.1[d]	12.4	0.215	0.169	3.9± 0.6

[a] In aqueous trifluoroethanol / sodium trifluoroethoxide (1:1) buffers at 25.0 °C. Reaction followed by titration of buffer remaining after saponification. Volume-time data for the volume of 0.125 M HCl used to titrate 0.5 mL of solution fit to $V = \alpha + \beta exp(-\lambda t)$. $[TMOA]_i = 0.10$ M unless otherwise noted.

[b] for acidic buffer component

[c] for pure buffer

[d] $[TMOA]_i = 0.05$ M

3.5 Kinetics of hydrolysis of TMOA in 0.1 M NaOH

The kinetics of hydrolysis of TMOA were studied in 0.1 M NaOH by titration of base not consumed by saponification. The factors affecting this method have been discussed in Section 3.4 for hydrolysis in pH 12.4 trifluoroethanol buffers. The observed rate constant was $(3.73 \pm 0.04) \times 10^{-6}$ s^{-1}.

Figure 11. Dependence of TMOA hydrolysis rate on trifluoroethanol concentration at pH 12.4

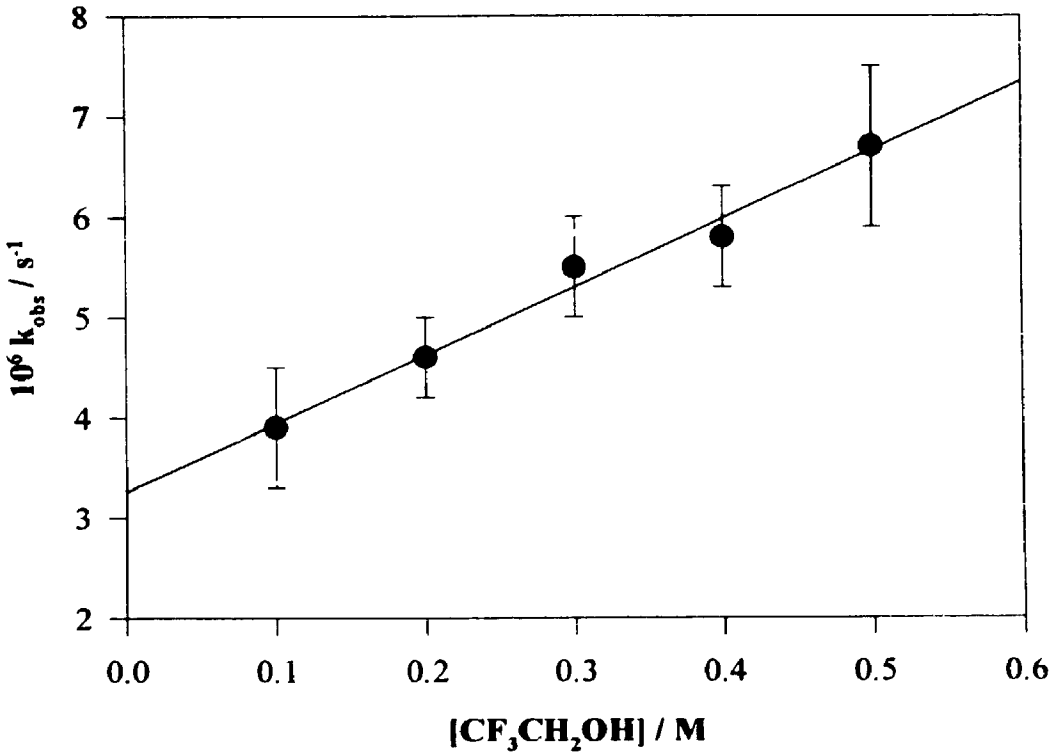

CHAPTER 4: RESULTS SUMMARY, MARCUS THEORY ANALYSIS, AND CONCLUSIONS FOR DMOP AND TMOA HYDROLYSES

4.1 Kinetics summary for the hydrolyses of DMOP and TMOA

The first order zero-buffer and second order general-acid catalyzed rate constants for hydrolysis of DMOP and TMOA are summarized in Tables 13 and 14 respectively. The pH rate profiles for both are plotted in Figure 12.

The second order specific acid catalyzed and first order uncatalyzed (water) rate constants for both DMOP and TMOA are summarized in Table 15. The specific acid catalyzed rate constants for both TMOA and DMOP, and the uncatalyzed rate constant for TMOA were calculated by weighted least squares fitting of the pseudo-first order rate constants to the equation $k_{zero\text{-}buffer} = k_w + k_{H^+}[H^+]$, where the $[H^+]$ was determined from the pH. The k_w determined for DMOP was not considered to be accurate because of the presence of a base catalyzed process, and was calculated only as a correction for the points below pH 13. The experimental observation of an increase in rate from pH 13 to pH 14, and the theoretical justification for a hydroxide catalyzed mechanism at high pH (see the Marcus theory analysis of DMOP and TMOA hydrolysis) necessitated a different treatment.

The rates at pH 13 and 14 were first corrected by subtracting the acid catalyzed component. The resulting rate constants were treated as two points defining a line from which can be calculated a slope and an intercept. The equations are familiar:

k_{OH^-} = slope = $(k_2 - k_1) / ([OH^-]_2 - [OH^-]_1)$

k_{H2O} = intercept = $([OH^-]_1 k_2 - k_1 [OH^-]_2) / ([OH^-]_2 - [OH^-]_1)$

The water rate and hydroxide catalyzed rates and their corresponding errors were calculated in this way. The water rate is listed in Table 15. The hydroxide catalyzed rate is $(2.8\pm0.4) \times 10^{-8}\ M^{-1}s^{-1}$.

The GAC rate constants for TMOA hydrolysis are summarized in Table 16 and the corresponding Bronsted plot is shown in Figure 13. The α value calculated from the data is 0.76±0.05

Table 13. Summary of zero-buffer rate constants for DMOP hydrolysis

pH	$k_{zero\text{-}buffer}$ (s^{-1})	$\log (k_{zero\text{-}buffer} / s^{-1})$
4.76	$(4.44\pm0.10)\times10^{-2}$	-1.352 ± 0.009
7.15	$(7.15\pm0.04)\times10^{-4}$	-3.146 ± 0.003
7.92	$(5.29\pm0.13)\times10^{-5}$	-4.276 ± 0.011
9.20	$(5.69\pm0.02)\times10^{-6}$	-5.694 ± 0.004
10.12	$(2.1\pm1.5)\times10^{-7}$	-6.67 ± 0.31
13.0	$(3.9\pm0.2)\times10^{-8}$	-7.41 ± 0.02
14.0	$(6.4\pm0.3)\times10^{-8}$	-7.20 ± 0.02

Table 14. Summary of zero-buffer rate constants for TMOA hydrolysis

pH	$k_{zero\text{-}buffer}$ (s^{-1})	log ($k_{zero\text{-}buffer}$ / s^{-1})
6.50	$(6.4\pm0.6)\times10^{-3}$	-2.194 ± 0.004
7.90	$(5.2\pm0.2)\times10^{-4}$	-3.28 ± 0.02
9.20	$(3.8\pm0.3)\times10^{-5}$	-4.42 ± 0.03
10.12	$(2.87\pm2.44)\times10^{-4}$	-5.54 ± 0.37
12.4	$(3.28\pm0.18)\times10^{-6}$	-5.48 ± 0.02
13.0	$(3.73\pm0.04)\times10^{-6}$	-5.429 ± 0.005

Table 15. Summary of specific acid catalyzed and uncatalyzed rate constants for hydrolyses of DMOP and TMOA

	k_{H+} ($M^{-1}s^{-1}$)	k_{H2O} (s^{-1})	log k_{H+}	log k_{H2O}
DMOP	$(2.5\pm0.3)\times10^{3}$	$(3.6\pm0.2)\times10^{-8}$	3.39 ± 0.05	-7.45 ± 0.03
TMOA	$(2.05\pm0.12)\times10^{4}$	$(3.7\pm0.3)\times10^{-6}$	4.31 ± 0.03	-5.43 ± 0.03

Table 16. Summary of general acid catalyzed rate constants for the hydrolysis of TMOA

pH	pKa[a]	k (s^{-1})	log (k / s^{-1})
6.50	6.74	$(5.87\pm0.10)\times10^{-2}$	-1.23 ± 0.10
7.90	6.74	$(4.04\pm0.08)\times10^{-2}$	-1.39 ± 0.05
9.20	9.24	$(1.9\pm0.3)\times10^{-4}$	-3.71 ± 0.41
10.12	9.84	$(1.58\pm0.07)\times10^{-4}$	-3.80 ± 0.10
12.4	12.24	$(6.7\pm0.6)\times10^{-6}$	-5.18 ± 0.20

[a] corrected for ionic strength by Davies equation.

Figure 12. pH rate profiles for DMOP and TMOA hydrolyses

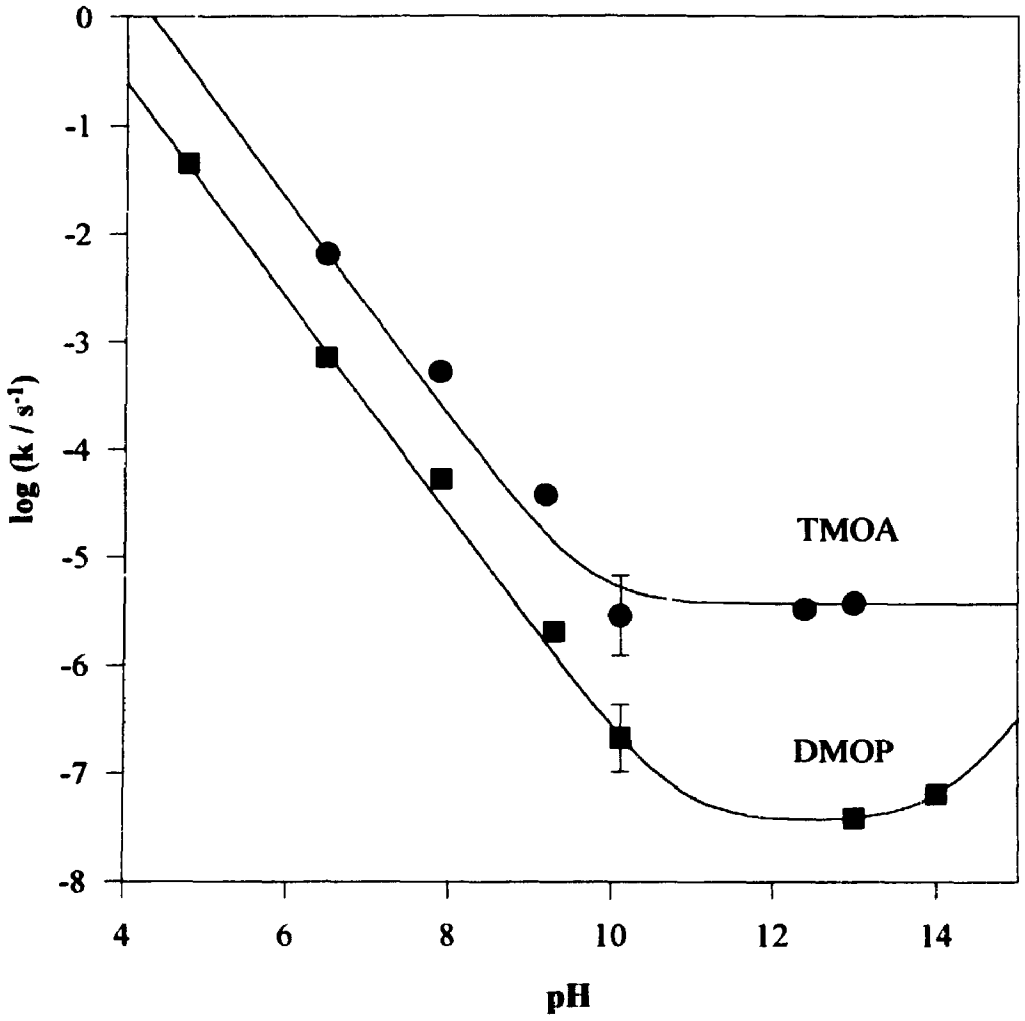

Figure 13. Bronsted plot for general acid catalyzed hydrolysis of TMOA

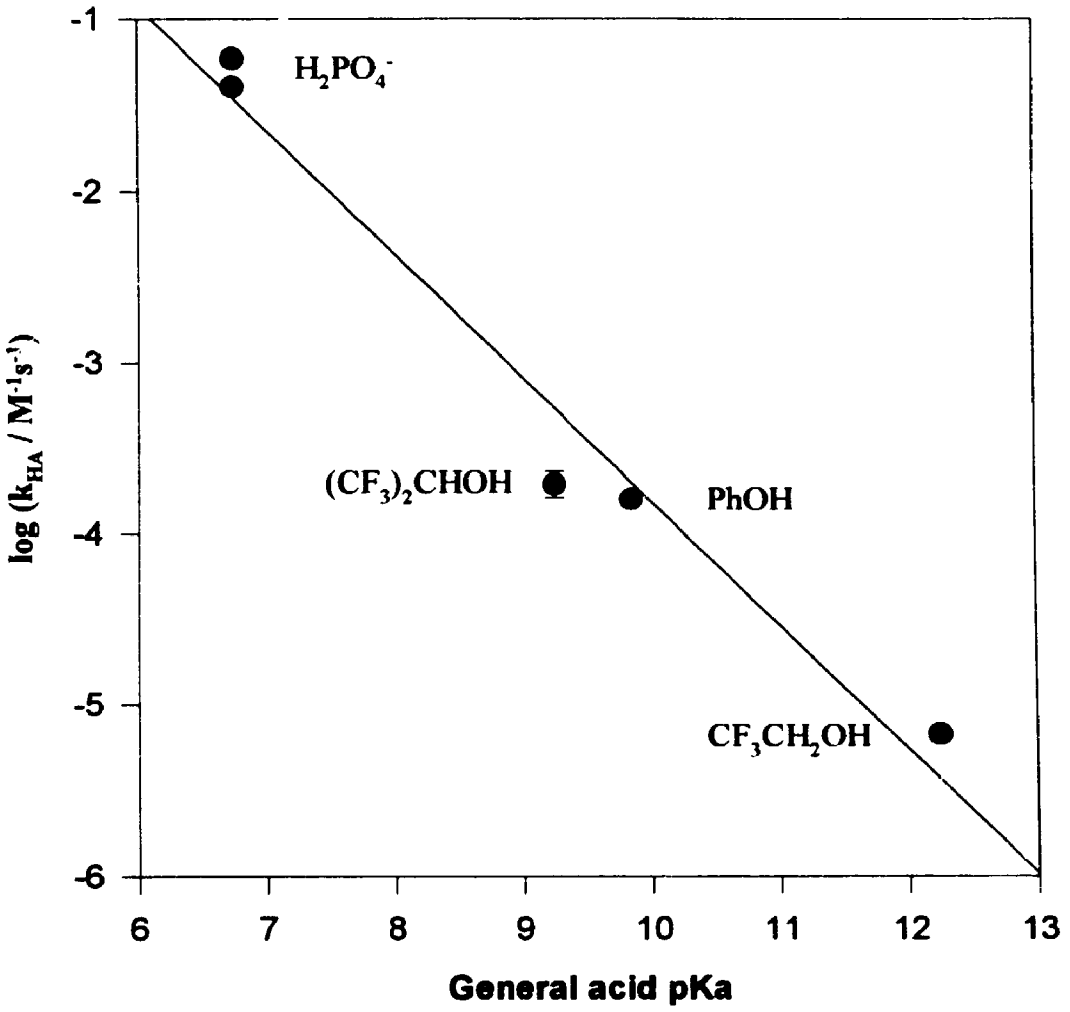

4.2 Application of Marcus Theory to the hydrolysis of DMOP and TMOA

The hydrolysis of both DMOP and TMOA were examined using multidimensional Marcus Theory. The uncatalyzed, acid catalyzed, and general acid catalyzed mechanisms were examined for each. A novel hydroxide catalyzed hydrolysis mechanism was also

investigated. These reactions are summarized in Scheme 5. The general acid catalyzed mechanism, for the purpose of calculations, is equivalent to the specific acid catalyzed mechanism with a general acid HA in the place of H_3O^+.

Scheme 5. Summary of catalyzed and uncatalyzed reactions of DMOP and TMOA analyzed by Marcus Theory.

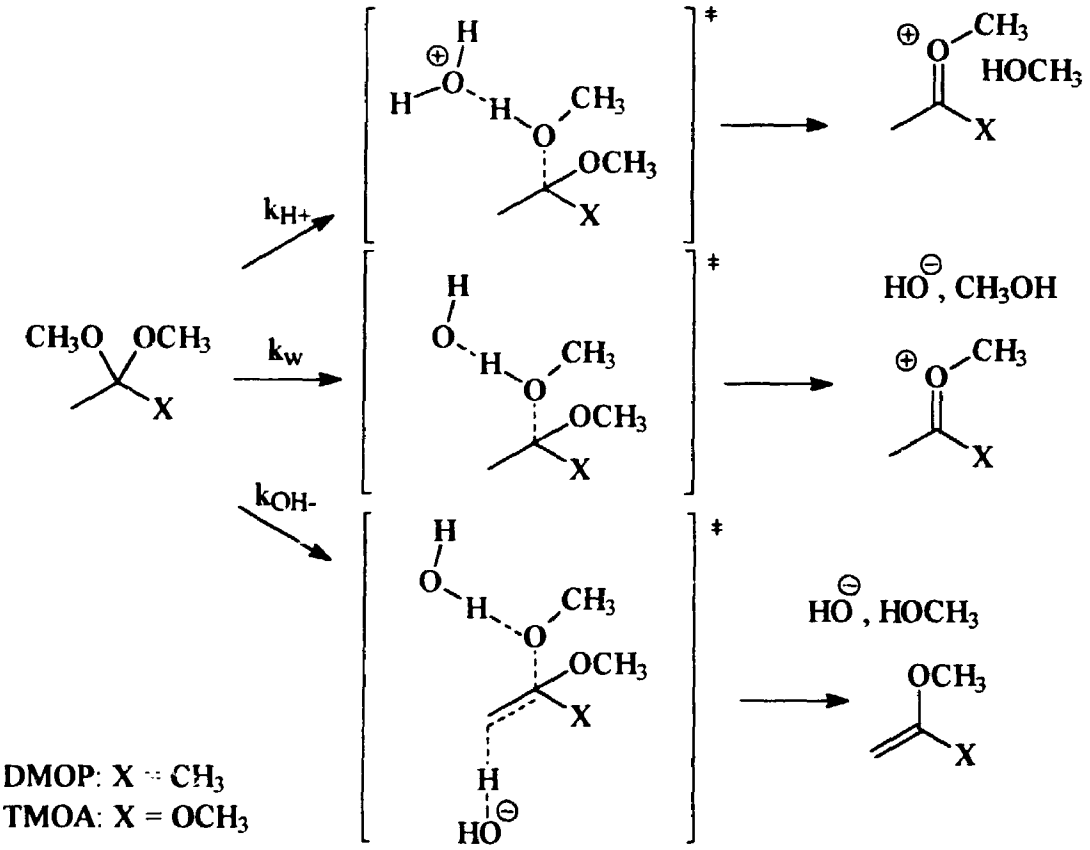

An example of a reaction square is shown in Figure 14 for the acid catalyzed expulsion of a methoxy group from DMOP. The coordinates of the corners of the square are reaction coordinates, essentially bond order coordinates, for each of the bonds undergoing reaction. They are defined to be 0 for no bond and 1 for a full bond, but recalculated to make 00 the origin and 11 the end. To treat DMOP and TMOA hydrolysis

with Marcus Theory, the corner energies of all of the reaction squares were estimated. The corner energies for the reactions studied are listed in Table 17 and their detailed calculation is listed in Appendix I. Table 18 contains the results of fitting to the Marcus equation for each of the reaction mechanisms.

Figure 14. Reaction square for the acid catalyzed loss of methoxide from DMOP.

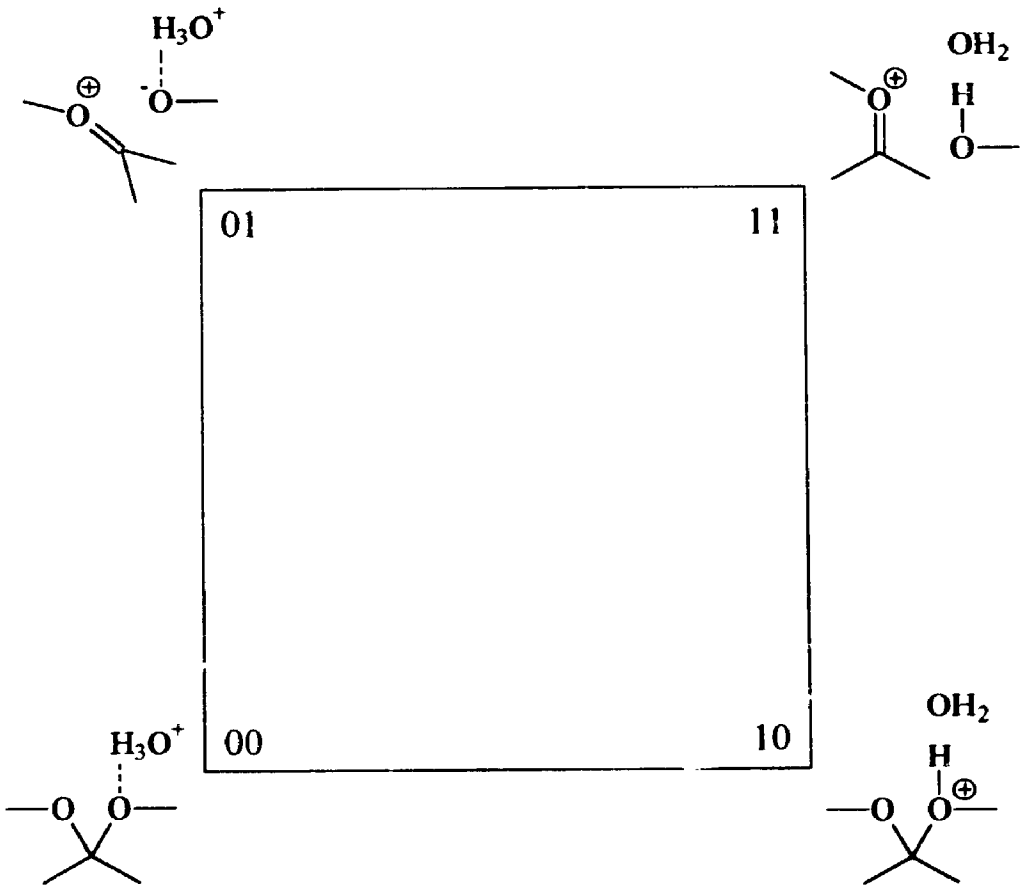

Table 17. Summary of calculated corner energies for Marcus Theory analysis. [a]

Reaction Corner Composition	Corner [b] Coordinates	ΔG_{corner} [c] (kcal.mole^{-1})	$\Delta G_{rezeroed}$ [d] (kcal.mole^{-1})
A. Reaction square for acid catalyzed hydrolysis of DMOP - Step 1			
$Me_2C(OMe)(OMe,H_3O^+)$	00	3.13	0.00
$Me_2C(OMe)(O^+(H)Me)$	10	7.59	4.46
$Me_2C^+(OMe),^-OMe,H_3O^+$	01	27.14	24.01
$Me_2C^+(OMe),HOMe$	11	6.02	2.89
B. Reaction square for uncatalyzed hydrolysis of DMOP - Step 1			
$Me_2C(OMe)(OMe),H_2O$	00	0.00	0.00
$Me_2C(OMe)(O^+(H)Me),^-OH$	10	20.86	20.86
$Me_2C(O^+Me),MeO^-,H_2O$	01	31.09	31.09
$Me_2C(O^+Me),MeOH,^-OH$	11	26.79	26.79
C. Reaction square for hydroxide catalyzed E2 hydrolysis of DMOP - Step 1			
$MeC(OMe)(OMe)(CH_3,OH^-)$	00	8.86	0.00
$MeC(OMe)(OMe)(CH_2^-,H_2O)$	10	35.52	26.65
$MeC^+(OMe)(CH_3,OH^-),MeO^-$	01	33.63	24.77
$MeC(OMe)=CH_2,MeO^-,H_2O$	11	13.81	4.94

D. Reaction square for hydroxide catalyzed E2 hydrolysis of DMOP - Step 2

$MeC(OMe)=CH_2,OH^-, H_2O$	00	9.52	0.00
$MeC^+(OMe)(CH_3,OH^-),OH^-$	10	28.38	18.86
$MeC(OH)(OMe)(CH_2^-,H_2O),H_2O$	01	29.77	20.25
$MeC(OH)(OMe)(CH_3,OH^-)$	11	3.11	-6.40

E. Reaction square for phenol catalyzed DMOP reaction - Step 1

$Me_2C(OMe)(OMe,HOPh)$	00	2.86	0.00
$Me_2C(OMe)(O^+(H)Me,^-OPh)$	10	17.34	14.47
$Me_2C^+(OMe),(^-OMe,HOPh)$	01	32.06	29.19
$Me_2C^+(OMe),HOMe,^-OPh$	11	20.97	18.10

F. Reaction square for trifluoroethanol catalyzed DMOP hydrolysis - Step 1

$Me_2C(OMe)(OMe,HOR)$	00	2.67	0.00
$Me_2C(OMe)(O^+(H)Me,^-OR)$	10	19.68	17.01
$Me_2C^+(OMe),(^-OMe,HOR)$	01	32.77	30.11
$Me_2C^+(OMe),HOMe,^-OR$	11	24.64	21 97

G. Reaction square for acid catalyzed reaction of TMOA - Step 1

$MeC(OMe)(OMe)(OMe.H_3O^+)$	00	3.89	0.00
$MeC(OMe)(OMe)(O^+(H)Me)$	10	11.80	7.91
$MeC^+(OMe)(OMe),(^-OMe,H_3O^+)$	01	25.78	21.89
$MeC^+(OMe)(OMe),HOMe$	11	3.27	-0.63

H. Reaction square for uncatalyzed hydrolysis of TMOA -Step 1

$MeC(OMe)(OMe)(OMe),H_2O$	00	0.00	0.00
$MeC(OMe)(OMe)(O^+HMe),^-OH$	10	24.07	24.07
$MeC^+(OMe)(OMe),MeO^-,H_2O$	01	26.18	26.18
$MeC(OMe)(O^+Me),MeOH,^-OH$	11	22.13	22.13

I. Reaction square for hydroxide catalyzed E2 hydrolysis of TMOA - Step 1

$(MeO)_2C(OMe)(CH_3,OH^-)$	00	8.62	0.00
$(MeO)_2C(OMe)(CH_2^-,H_2O)$	10	32.78	24.16
$(MeO)_2C^+(CH_3,OH^-),MeO^-$	01	30.86	22.23
$(MeO)_2C{=}CH_2,MeO^-,H_2O$	11	21.88	13.25

J. Reaction square for phenol catalyzed TMOA hydrolysis - Step 1

MeC(OMe)(OMe)(OMe.HOPh)	00	2.92	0.00
$MeC(OMe)(OMe)(O^+(H)Me,^-OPh)$	10	20.89	17.97
$MeC^+(OMe)(OMe),(^-OMe,HOPh)$	01	30.13	27.20
$MeC^+(OMe)(OMe),HOMe,^-OPh$	11	18.20	15.28

K. Reaction square for TFE catalyzed TMOA hydrolysis - Step 1

MeC(OMe)(OMe)(OMe.HOR)	00	2.61	0.00
$MeC(OMe)(OMe)(O^+(H)Me,^-OR)$	10	23.51	20.90
$MeC^+(OMe)(OMe),(^-OMe,HOR)$	01	30.84	28.23
$MeC^+(OMe)(OMe),HOMe,^-OR$	11	21.87	19.26

[a] detailed calculations in Appendix I

[b] corners are defined by the extent of reaction along each reaction coordinate and

can have values of 0 or 1 along each coordinate; the first coordinate is for proton transfer and the second for C-O bond formation / cleavage

[c] free energy of encounter complex relative to reactants in solution

[d] free energy of encounter complex relative to corner "00", taken as $\Delta G = 0$

Table 18. Transition state energies and positions determined by Marcus Theory for DMOP and TMOA hydrolyses. [a]

Mechanism	ΔG_{00} [b]	$\Delta G^{\ddagger}_{calc}$ [c]	$\Delta G^{\ddagger}_{pred}$ [d]	$\Delta G^{\ddagger}_{obs}$ [e]	$\Delta G^{\ddagger}_{obs}-\Delta G^{\ddagger}_{calc}$	$x^{\ddagger}_{(C/O)-H}$ [f]	$x^{\ddagger}_{C-O}$ [g]
A	3.13	7.62	10.75	12.82	2.07	1.00	0.46
B	0.00	28.35	28.35	27.61	-0.74	1.00	0.64
C	8.86	19.03	27.89	27.76	-0.13	0.50	0.55
D	9.52	13.24	22.76	-	-	0.47	0.47
E	2.86	20.42	23.28	26.56	3.28	1.00	0.59
F	2.67	23.83	26.50	-	-	1.00	0.62
G	3.89	8.82	12.71	11.57	-1.14	1.00	0.30
H	0.00	25.46	25.46	24.86	-0.60	0.55	0.74
I	8.62	20.37	28.99	-	-	0.48	0.67
J	2.92	20.61	23.53	22.63	-0.90	0.83	0.50
K	2.61	23.77	26.38	24.80	-1.58	0.76	0.58

[a] calculations were performed using a program developed by J.P. Guthrie to search the reaction surface for the transition state; input values are the corner energies for the reaction and the intrinsic barrier for motion along each reaction coordinate; intrinsic barriers are taken as 1.0 kcal.mole^{-1} for proton transfers to/from carbon or oxygen, and 3.9 kcal.mole^{-1} for methoxide addition to carbonyls.[24]

[b] free energy of initial encounter complex relative to reagents in solution

[c] calculated free energy of activation for reaction within the encounter complex

[d] predicted observable free energy of activation: $\Delta G^{\ddagger}_{calc} + \Delta G^{\ddagger}_{(O)}$

ϵ observed free energy of activation: $\Delta G^{\ddagger}_{obs} = (12.79 - \log k_{obs}) \times 2.303 / 1.688$
f position of transition state along proton transfer coordinate
g position of transition state along C-O bond coordinate

The activation free energies for acid catalyzed and uncatalyzed hydrolysis of DMOP and TMOA agree within reasonable error limits with the predicted values. Based on the position of the transition state, both reactions proceed as expected with initial protonation of the leaving group oxygen, followed by rate-limiting C-O bond cleavage.

The uncatalyzed hydrolysis reaction for DMOP begins with protonation of the leaving group oxygen by water, giving protonated substrate plus hydroxide, and this is then followed by rate-limiting C-O bond cleavage. This mechanism is, in effect, acid catalysis with water acting as the general acid, but would be observed as a pH independent reaction. Marcus Theory analysis shows that the observed water rate is actually an acid catalyzed rate.

The uncatalyzed hydrolysis reaction of TMOA is similar to that of DMOP. In this case, however, the position of the transition state indicates that the proton transfer from water is concerted with C-O bond cleavage. Once again, the water rate is actually an acid catalyzed rate with water acting as the acid.

The alternative one dimensional reactions for DMOP and TMOA hydrolysis, proceeding without protonation by water, were several kilocalories too high in energy to be observable. The difficulty is that the reaction must proceed through the oxocation-methoxide ion pair corner if the one dimensional model is used and consequently the free energy of this corner is the lower limit on the predicted $\Delta G^{\ddagger}$: 31.09 kcal for DMOP and 28.62 kcal for TMOA. The actual predicted $\Delta G^{\ddagger}$'s from this model are 34.93 kcal and

31.34 respectively - far too high to be observed given the alternative reaction paths available.

An early error in the calculation of the energy for the uncatalyzed path led to attempts to find alternative mechanisms which would match the experimental value and possibly account for the increase in rate of DMOP hydrolysis from 0.1 M hydroxide to 1.0 M hydroxide. Because of this search, an unlikely mechanism was investigated. Marcus Theory was used to predict the rate of hydrolysis of DMOP and TMOA by a hydroxide catalyzed E2 route proceeding through the enol ethers corresponding to the elimination of methanol. The mechanism is depicted for DMOP in Scheme 5. This was considered unlikely because enol ethers are considered to be base-stable. A mechanism which required that an enol ether be an intermediate which did not accumulate in sufficient quantities to be detected was unlikely.

Surprisingly, the Marcus Theory analysis of the E2 mechanism predicted a rate constant for DMOP hydrolysis which was very close to the observed values at high pH. The mechanism is expected to be concerted based on the predicted position of the transition state. The free energy of activation for the second step, attack of hydroxide on the enol ether with concerted protonation of the developing carbanion by water, is predicted to be significantly lower than for formation of the enol ether. This is fortunate because there was no observable accumulation of any intermediate in the any of the experiments.

For DMOP there is a two-fold increase in rate between 0.1 and 1.0 M hydroxide. A pH independent mechanism giving way to a hydroxide dependent mechanism would be

required to truly account for only a two-fold increase in rate. This would be the case with a water rate and hydroxide catalyzed E2 rate with comparable energies as is predicted here. The existence of the E2 mechanism has not been proven, but the evidence is suggestive. If the rate of hydrolysis of the enol ether 2-methoxypropene was found to depend on hydroxide concentration and follow the Marcus prediction for Step 2 of the E2 mechanism of DMOP hydrolysis, then Step 1 would likely be correct as well.

The general acid catalyzed hydrolysis of TMOA was also studied with Marcus Theory. The results in Table 18 show that theoretical and measured $\Delta G^{\ddagger}$'s agree very well. The position of the transition state in each case shows that this is a classic case of general acid catalysis with the proton of the general acid in flight in the transition state, and concerted with C-O bond cleavage.

Marcus Theory was also used to predict the observable $\Delta G^{\ddagger}$ for general acid catalyzed acetal hydrolysis. The specific acid catalyzed reaction's observable activation energy at pH 10 would be 26.46 kcal.mole^{-1}. General acid catalysis should be observable with general acids of pKa near 10 as originally predicted. If the Marcus Theory estimate of the activation energy for the phenol catalyzed reaction is accurate, it should actually be possible to see catalysis slightly below pH 10. If the experimental value is to be believed, then pH 10 is a realistic lower limit.

The unusual feature of general acid catalysis for DMOP is that proton transfer will be complete at the transition state. This is counter to the usual mechanistic definition of general acid catalysis where proton transfer is concerted with C-O bond cleavage. Figure 14a is an energy diagram for the phenol catalyzed hydrolysis of DMOP (Step 1).

Diffusion of phenoxide from the encounter complex will be slower than C-O bond cleavage so that the transition state will contain phenol, and the rate will therefore be phenol concentration dependent and general acid catalyzed by the kinetic definition.

Figure 14a. Energy diagram for the phenol catalyzed hydrolysis of DMOP.

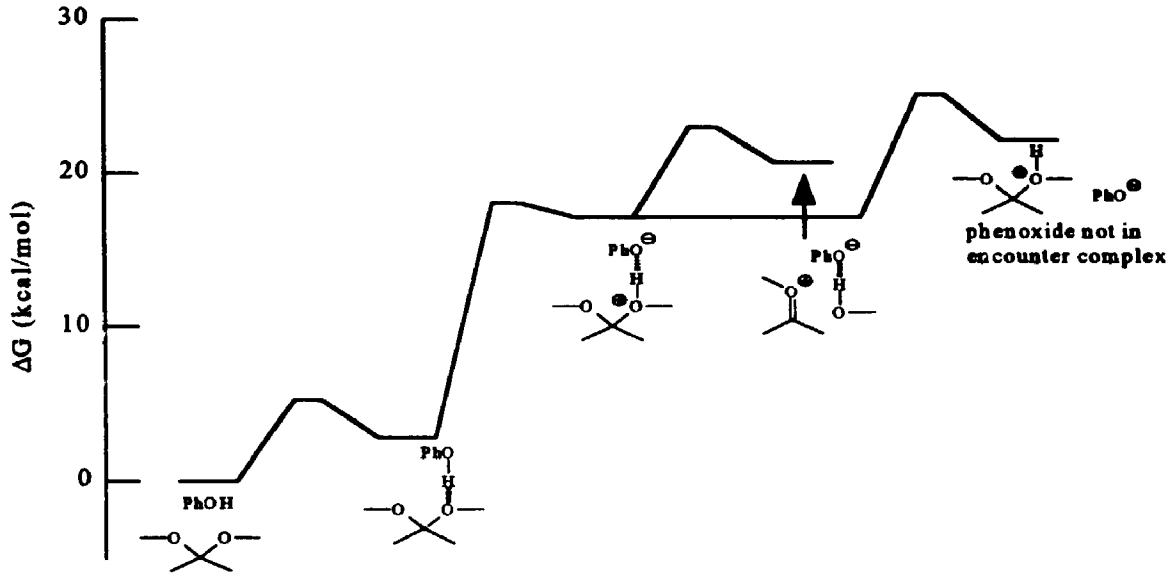

4.3 Conclusions

The pH rate profiles for the hydrolysis of DMOP and TMOA have been determined, with the specific acid catalyzed and uncatalyzed rate constants well defined, given the experimental conditions. The uncatalyzed hydrolysis of acetals like DMOP has not traditionally attracted much attention because of the inherently slow rate. As such, this determination is a significant contribution in an area with a dearth of information.

The most surprising result is the experimental and theoretical evidence for a hydroxide catalyzed mechanism of DMOP hydrolysis proceeding by an E2 elimination of methanol to give an enol ether. Subsequent hydrolysis of the enol ether proceeds by the

reverse mechanism: a concerted attack of hydroxide on the enol ether and protonation of the developing carbanion by water.

This finding is contrary to the conventional thinking of the reactivity of acetals and enol ether and was not envisioned as a part of the original project. It is important to view this result in the proper perspective: The E2 mechanism in strong base becomes competitive with a reaction which is painfully slow. The appearance of the E2 mechanism merely shows the crossover of "bad" and "worse".

Marcus Theory predicts that this mechanism will not be observed in TMOA hydrolysis. The E2 mechanism is expected to be several orders of magnitude slower than the uncatalyzed mechanism and therefore be unobservable. There is currently no experimental evidence to evaluate that prediction.

TMOA has shown general acid catalysis, as expected by analogy with triethylorthoacetate.[2] A good Bronsted plot with a slope ($\alpha = 0.76$) was obtained for the general acids studied: this is in reasonable agreement with Marcus theory predictions.

The experimental evidence in support of general acid catalysis in DMOP hydrolysis was encouraging, but not conclusive. Although the experiments at elevated temperatures are strongly suggestive of general acid catalysis, extrapolation to room temperature results in a significant uncertainty. Further, the non-ideality of the solutions employed cannot be discounted and any conclusive evidence of GAC would necessarily require several general acids to be used, and several salts used to maintain ionic strength.

Marcus Theory does predict that we will begin to see general acid catalysis with DMOP at higher pH's and pKa's and the prediction for catalysis by phenol agrees with

experiment within experimental error, which is admittedly large.

Marcus Theory has proven to be a valuable tool in the elucidation of the mechanism of acetal and orthoester hydrolysis. It has shown that the water rates for these two hydrolyses are actually the result of an acid catalyzed mechanism. A new base catalyzed mechanism of acetal hydrolysis proceeding by an E2 elimination has been suggested on the basis of experimental evidence and Marcus Theory analysis. Without the theory, this mechanism would have been overlooked and the increase in rate of DMOP hydrolysis at high pH would have merely been attributed to salt effects. Further experimental evidence will be required before this mechanism can be fully accepted.

General acid catalysis is still predicted to be observable for DMOP. Marcus Theory analysis states this catalysis will not fit the conventional model with proton transfer concerted with C-O bond cleavage. Instead, proton transfer will be complete at the transition state. This is required because the two extrema in aqueous solution are proton transfer from hydronium ion and proton transfer from water. Both the specific acid catalyzed and water reaction show complete proton transfer at the transition state.

4.4 Future Work

Confirmation of the presence of the E2 mechanism of hydrolysis should be sought. For DMOP as substrate, this will require hydroxide concentrations in excess of 1 M and a correspondingly high ionic strength. The non-ideality of such solutions would pose a problem but useful results should still be possible. Alternatively, it may be possible to find a substrate which would show the mechanism at a lower pH. Marcus Theory should be able to predict which substrates would be good candidates. Ideally the activation free

energy for the E2 mechanism should be slightly less than the activation energy for the uncatalyzed mechanism.

The hydroxide catalyzed hydrolysis of 2-methoxypropene should also be studied. Based on Marcus Theory, there should be a hydroxide catalyzed hydrolysis path which would be expected to be faster than that found for the hydrolysis of DMOP. The presence of this reaction would further support the hydroxide catalyzed E2 mechanism for DMOP hydrolysis. If, on the other hand, the hydrolysis of 2-methoxypropene is found to be slower than that of DMOP in one molar hydroxide, then this would discount this mechanism.

The results of the elevated temperature phenol buffer experiments are encouraging in the search for general acid catalysis in DMOP hydrolysis. Experimental difficulties with high temperature runs and uncertainty introduced by extrapolation should be avoided by using initial rate kinetics at 25 °C. General acids in the pKa range 10-13 such as trifluoroethanol should be tried. The specific salt effects observed in this work caution that several salts will have to be used if evidence of GAC is to be confirmed. The presence of a concerted hydroxide catalyzed mechanism also suggests that it is important to distinguish between general acid and general base catalyzed mechanisms in any such studies.

NMR analysis methods are labor and time intensive and may be replaceable by high pH reversed phase HPLC. Postchromatographic derivatization of the DMOP and hydrolysis products or the choice of a different substrate with a suitable chromophore would be desired to enhance the sensitivity of the HPLC method.

CHAPTER 5 EXPERIMENTAL

5.1 General

Unless otherwise indicated, organic compounds were obtained from the Aldrich Chemical Company Inc.. Inorganic salts were obtained from BDH Chemicals. Anhydrous nitrogen was obtained from Canox Limited. pH measurements were made with an Orion 701 pH meter equipped with a Fisher combination glass electrode (13-620-92, pH range 0 to 14, temperature range -5 °C to 110 °C). Water used in solution preparation was doubly distilled and nitrogen degassed. NMR spectra were taken on a Varian XL-200 or Gemini 200 spectrometers. UV spectra were taken a Shimadzu UV-160 UV/Vis spectrophotometer. UV kinetics are described in Section 5.6. Neslab Exacal EX-300 baths were used for 25.0 °C work, and Lauda B-1 and Julabo bath heaters were used for elevated temperatures. Glass ampoules were hand-made from borosilicate glass tubing. Teflon ampoules / NMR tube liners were made from 5/32" o.d. teflon tubing which was formed to the bottom of an NMR tube with gentle heating.

5.2 Purification of materials

Phenol was sublimed at 0.5 mm Hg prior to use.

DMOP was purified in a two step procedure. Catalytic hydrogenation for four hours at room temperature and pressure using 5% palladium on barium sulphate[25] dramatically reduced the absorbance of a UV absorbing impurity (possibly 2-methoxypropene). Fractional distillation was then performed, taking three cuts: bp < 78 °C; bp 78-

9 °C; bp > 79 °C . Only the middle cut was used. No trace of the strongly UV absorbing impurity remained as determined by a UV spectrum of pure DMOP in a 1 cm cell.

5.3 Aqueous sodium hydroxide and hydrochloride solutions

Hydrochloric acid solution was prepared by dilution of concentrated hydrochloric acid in nitrogen degassed doubly distilled water. The concentration was determined by triplicate titrations against Trizma base to a Methyl Red endpoint.

Sodium hydroxide solution was prepared by dissolving sodium hydroxide (BDH) in nitrogen degassed doubly distilled water. The concentration was determined by titration with standardized hydrochloride solution to phenolphthalein and Methyl Red endpoints, and then correcting for carbonate.

5.4 Buffer preparation

pH 4.7 acetic acid / sodium acetate buffers

Glacial acetic acid (6.005 g, 0.1000 moles) and potassium chloride (3.7275 g, 0.0500 moles) were weighed into a 100 mL volumetric flask. Aqueous sodium hydroxide (50.00 mL x 1.00 M, 0.05 moles) was added by pipette and doubly distilled water was added to the mark. This gave [AcOH] = [AcONa] = [KCl] = 0.5 M for a pH 4.7 buffer with 1.0 M ionic strength

A second buffer was prepared by pipetting 20.00 mL of the above buffer into a 25 mL volumetric flask. Aqueous potassium chloride (2.5 mL x 2.00 M, 0.05 moles) to make 0.1 M ionic strength was pipetted into the flask and doubly distilled water was added to the mark.

pH 6.5, 7.9 potassium dihydrogen phosphate / disodium hydrogen phosphate buffers

Set 1: for DMOP hydrolysis

Potassium dihydrogen phosphate (15.2942 g, 0.1124 moles) and disodium hydrogen phosphate (15.9510, 0.1124 mole) were weighed into a 250 mL volumetric flask and doubly distilled water was added to the mark.

Other buffers with 4/5, 3/5, 2/5, and 1/5 the concentration of this buffer were prepared by pipetting aliquots of the above buffer into volumetric flasks, adding 2.00 M aqueous potassium chloride to maintain the ionic strength and diluting to the mark with doubly distilled water.

Set 2: for TMOA hydrolysis

Potassium dihydrogen phosphate (3.4024 g, 0.0250 moles) and disodium hydrogen phosphate (3.5510 g, 0.1124 mole) were weighed into a 250 mL volumetric flask and doubly distilled water was added to the mark.

Other buffers with 4/5, 3/5, 2/5, and 1/5 the concentration of this buffer were prepared by pipetting aliquots of the above buffer into volumetric flasks, adding 2.00 M aqueous potassium chloride to maintain the ionic strength and diluting to the mark with doubly distilled water.

pH 9.0 phenol buffers

Phenol (4.705 g, 0.0500 moles), sodium benzoate (7.2055 g, 0.0500 moles) and potassium chloride (3.3542 g, 0.0450 moles) were weighed into a 100 mL volumetric flask. Aqueous sodium hydroxide (5.00 mL x 1.00 M, 0.005 moles) was added to the

flask and nitrogen degassed, doubly distilled water was added to the mark. This gave a phenol / phenoxide (9:1) buffer with [PhOH] = 0.45 M, [PhONa] = 0.05 M, [KCl] = 0.45 M, [PhCOONa] = 0 50 M for a buffer with 1.0 M ionic strength and 1.0 M aromatic ring concentration.

Buffers with 4/5, 3/5 and 2/5 this concentration were prepared by pipetting aliquots into 25 mL volumetric flasks, aoding sufficient 2.00 M sodium benzoate to maintain aromatic ring concentration and ionic strength, and diluting with nitrogen degassed doubly Jistilled water to the mark.

pH 9.4 hexafluoro-2-propanol buffers

1,1,1,3,3,3-Hexafluoro-2-propanol (HFIP) (16.8130 g, 0.1000 moles) and potassium chloride (3 7275 g, 0.0500 moles) were weighed into a 100 mL volumetric flask. Aqueous sodium hydroxide (49.00 mL x 1.02 M, 0.0500 moles) was added by burette and doubly distilled water was added to the mark.

Buffers with 4/5, 3/5, 2/5, and 1/5 the original concentration were prepared by pipetting aliquots into 25 mL volumetric flasks, adding 2.00 M potasium chloride to maintain the ionic strength at 1.0 M and 2-propanol to maintain the organic content at 1.0 M. Doubly distilled water was then added to the mark.

pH 10 phenol buffers

Phenol (9.412 g, 0 2612 moles) and potassium chloride (3.7262 g, 0.0500 moles) were weighed into a 100 mL volumetric flask. Aqueous sodium hydroxide (50 mL x

1.00 M, 0.0500 moles) was added by pipette and nitrogen degassed doubly distilled water was added to the mark.

Other buffers with 4/5, 3/5, 2/5 and 1/5 this phenol concentration were prepared in 25 mL volumetric flasks by dispensing aliquots of the above buffer, adding sodium benzoate to maintain ionic strength and aromatic ring concentration at 1.0 M, and then diluting to the mark with nitrogen degassed doubly distilled water.

pH 11.4 trifluoroethanol buffers

1,1,1-Trifluoroethanol (10.007 g, 0.1000 moles) and potassium chloride (3.7278 g, 0.0500 moles) were weighed into a 100 mL volumetric flask. Aqueous sodium hydroxide (50.00 mL x 1.00 M, 0.0500 moles) was added by pipette and degassed doubly distilled water was added to the mark.

Other buffers with 4/5, 3/5, 2/5 and 1/5 this trifluoroethanol concentration were prepared in 25 mL volumetric flasks by dispensing aliquots of the above buffer, adding 2.00 M potassium chloride to maintain ionic strength at 1.0 M, and adding ethanol to maintain organic content at 1.0 M, and diluting with water.

5.5. Kinetics - ^{1}H NMR

Reactions followed by ^{1}H NMR used ratios of integrals to determine the extent of reaction. The fraction of DMOP remaining was taken as $f_{DMOP} = i_{DMOP\text{-}OC\underline{H}_3} / (i_{MeOH\text{-}OC\underline{H}_3} + i_{DMOP\text{-}OC\underline{H}_3})$ or $f_{DMOP} = i_{DMOP\text{-}CC\underline{H}_3} / (i_{(C\underline{H}_3)_2CO} + i_{DMOP\text{-}CC\underline{H}_3})$, where i is the integral for the indicated peak . The value based on the methoxy peaks was usually more reliable because of spectrum phasing problems between the C-C$\underline{H}_3$ of DMOP and acetone.

The fraction of TMOA remaining was likewise calculated as: $f_{TMOA} = i_{TMOA\text{-}OC\underline{H}_3} / (i_{CH_3COOC\underline{H}_3} + i_{C\underline{H}_3OH} + i_{TMOA\text{-}OC\underline{H}_3})$.

Shimming of the spectrometer was performed on a deuterium oxide sample with a volume and height equal to those of the samples to be run. The spectrum was then acquired in unlocked mode.

The NMR shifts for the reactants and products are listed in Table 19.

Table 19. NMR shifts of diagnostic signals used in DMOP and TMOA reactions followed by NMR[a]

Compound	δ (C-C$\underline{H}_3$) (ppm)	δ (O-C$\underline{H}_3$) (ppm)
DMOP	1.37	3.22
TMOA	1.47	3.26
acetone[b]	2.21	
methyl acetate[c]	2.09	3.68
acetate ion	1.89	
methanol		3.27

[a] Samples taken in D_2O with 0.04 M NaOD unless otherwise noted. Shifts recorded relative to DSS which was added as an internal standard.
[b] Run without NaOD to avoid exchange.
[c] Run without NaOD to avoid saponification.

5.5.1 Thermostatted NMR

The NMR tube containing reaction solution was inserted in the probe of the Varian XL-200 which was thermostatted to 25.0 °C. Queued experiments with varying pre-acquisition delays allowed unattended collection of spectra over several hours. No

internal NMR lock was used.

5.5.2 Thermaliy and chemically quenched samples

Reactions at elevated temperatures were temporarily quenched by quickly cooling in cold water. Reactions run in ampoules had samples refrigerated and analyzed in groups; reactions run in NMR tubes were analyzed immediately and returned to the thermostatted bath. Reactions quenched chemically used excess base to consume the buffer and reduce the hydrolysis rate to the uncatalyzed rate. No internal lock was used.

5.5.3 Initial rate samples

Reactions in aqueous hydroxide at 25 °C for DMOP were analyzed by withdrawing 0.5 mL samples from the reaction vessel, and adding to 0.1 mL of deuterium oxide in an NMR tube. The NMR analysis was performed with a deuterium lock allowing more transients to be collected for much better sensitivity and signal to noise ratio.

5.6 Kinetics - UV

Kinetics followed by UV spectrophotometry were carried out using a Cary 210 spectrophotometer equipped with a thermostatted cell holder and thermal isolator plates. A Neslab Exacal EX-300 circulating bath at 24.8 °C maintained the cell temperature at 25.0±0.1 °C as monitored by a thermistor in the cell holder. Cells were Far-UV Spectrosil.

Reactions were initiated by direct injection of the substrate (DMOP or TMOA) from a microsyringe into a UV cell containing all other reactants, which had been in the

thermostatted cell holder for at least 15 min. Mixing was accomplished for most reactions by repeatedly rapidly inverting the cell and then returning it to the cell holder.

Digital absorbance data were taken from the Digital Interface Port of the Cary 210 by a Dynabyte BC_2 controller board which provided time values and stored absorbance-time data until the completion of a run. Data were then transferred to an IBM-compatible microcomputer for processing and permanent storage.

All reactions were carried out under pseudo-first order conditions and data were collected for several half-lives.

Data were fitted to a single exponential equation using previously developed computer programs employing weighted least squares. Direct, semi-log, and residual plots of the experimental data and calculated lines were made as appropriate.

PART II:

SUBSTITUENT EFFECTS IN

SELECTED ALDOL REACTIONS

CHAPTER 6: INTRODUCTION

6.1 General

Aldol reactions are a class of carbon - carbon bond forming reactions in which the α-carbon of one aldehyde or ketone adds to the carbonyl carbon of another. This is shown in Scheme 6. The immediate product is a β-hydroxy aldehyde or ketone which may then dehydrate to give α,β-unsaturated aldehydes or ketones, or undergo further aldol reactions. The entire reaction including dehydration is an equilibrium which is typically catalyzed oy a base such as hydroxide. The equilibrium for the reaction of two unhindered aldehydes lies far to the right whereas that for two ketones lies far to the left. The α,β-unsaturated and β-hydroxy aldehydes or ketones produced can likewise be cleaved by treatment with hydroxide in a *retroaldol* reaction.

Scheme 6. General aldol condensation

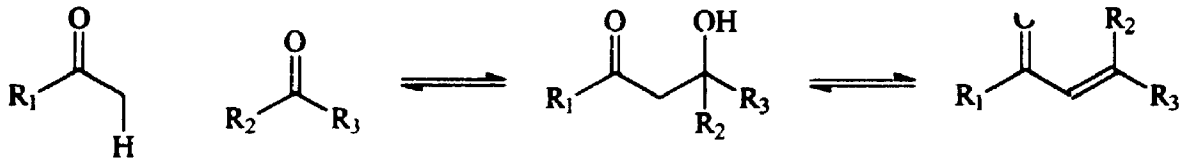

R_{1-3}: H, alkyl, aryl

The aldol reaction is an exceptionally important synthetic reaction. A full volume of Organic Reactions is required to review it,[26] and recent years have seen an explosion in the number of variants on the aldol using various metals and auxiliaries to achieve specific stereochemistry or selectivity.[27] With the aldol reaction being so important, it is surprising that a theory for the quantitative prediction of aldol reaction rates has not existed until

very recently.[20]

6.2 Application of Marcus Theory to aldol reactions

Guthrie has used Marcus Theory to analyze the relationship between rate and equilibrium constants for several previously studied aldol reactions.[20] Following this method, Marcus Theory has been used to predict rate constants for selected aldol reactions based on estimated equilibrium constants. Equilibrium constants can either be measured or estimated from Linear Free Energy Relationships. The latter is often the more convenient and useful method because the aldol reaction itself does not have to have been studied.

The use of Marcus Theory to predict reaction rates for unstudied reactions has two great potential benefits: (1) Experimental design for the study of novel reactions would be improved by knowing the approximate rate and equilibrium constants before starting, and; (2) Estimation of rate constants for reactions which are exceedingly difficult or impossible to study directly would extend our abilities to characterize complex chemical systems.

One potential application of Marcus Theory is the estimation of rate constants for acid catalyzed aldol and retroaldol reactions. Acidic conditions are often used to study the hydration-dehydration equilibrium of aldol products without interference from retroaldol reaction, [28-31] but not all acid catalyzed retroaldol rates are negligible.[32] Marcus Theory could be used to predict when acid-catalyzed retroaldol reaction would interfere.

6.3 Project goals and scope

The specific aldol reactions studied are the reaction of acetone, acting as carbon acid, with α,α,α-trifluoroacetophenone and with *p*-nitroacetophenone, and the reaction of *p*-nitroacetophenone, acting as carbon acid, with acetone and with *p*-nitroacetophenone. The reactions are summarized in Scheme 7.

Scheme 7. Aldol reactions investigated in this study

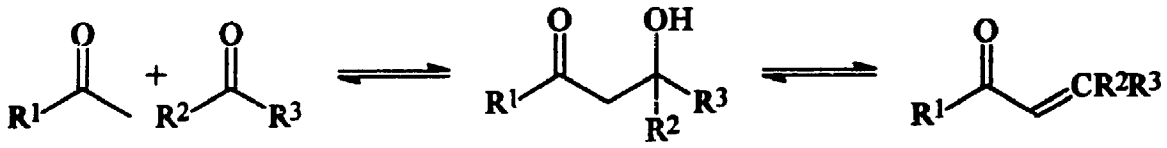

R^1	R^2	R^3
CH_3	Ph	CF_3
CH_3	p-NO_2-Ph	CH_3
p-NO_2-Ph	CH_3	CH_3
p-NO_2-Ph	p-NO_2-Ph	CH_3

The goal of this study was the characterization of the hydroxide catalyzed kinetics and equilibria of all four reactions including both aldol formation and dehydration. This adds four fully characterized aldol condensations to those which have already been studied.[29,31,33-41] Marcus Theory predictions of the aldol reactions' rates based on the previously studied reactions are compared to the experimentally determined values. Conclusions are drawn about the ability of Marcus Theory to make such predictions.

Some acid catalyzed enone isomerization and hydration equilibria were also studied to avoid the complications associated with their study in base using aldol formation reactions. In these experiments, the principal goal was the determination of the

equilibrium constants. The determination of the actual acid catalyzed rates was of secondary importance.

Several of the ketols and enones involved in the condensations of interest had not previously been synthesized so that the preparation and characterization of several new compounds was also required.

6.4 Marcus Theory analysis of the aldol reactions

Marcus Theory was applied to the four aldol reactions by the established method.[20] This required the pKa's of acetone, *p*-nitroacetophenone, and the four ketols of interest. The pKa's of both acetone and of *p*-nitroacetophenone are available from the literature.[42,43] The pKa's for the four ketols were estimated by treating them as simple carbinols and using the linear free energy relationship found in the literature for tertiary alcohols.[44,45] The pKa's for all compounds are listed in Table 20 and detailed calculations of ketol pKa's can be found in Appendix II.

The equilibrium constants for aldol formation are predicted by the standard method[20] using the γ and Δ values of Sanders and Jencks[46] which are, respectively, a measure of the tendency of a nucleophile to add to a carbonyl and a measure of the sensitivity of a carbonyl to γ. The γ and Δ values used are listed in Table 20. Calculation of the equilibrium constants is detailed in Appendix II and the results are summarized in Table 21.

Table 20. pKa's, γ and Δ values required for Marcus theory analysis

Compound	pKa[a]	γ[b]	Δ[c]
acetone	19.16[d]	0.16[e]	0.92[f]
TFA			0.24[f]
PNAC	16.6[g]	0.05[h]	1.02[f]
2	11 78		
12	14.55		
15	15.68		
9	14.02		

[a] pKa's for ketones were from the literature. pKa's for ketols are estimated in Appendix II

[b] γ is a measure of the tendency of a nucleophile to add to a carbonyl[46]

[c] Δ is the sensitivity of a carbonyl to nucleophile γ values for additions[46]

[d] Ref. 42

[e] Ref. 20

[f] Ref. 35

[g] Ref. 43 using values obtained from ref. 47 and corrected using ref. 48

[h] taken as the same as acetophenone in Ref. 35

For an aldol reaction, we consider the reaction of a ketone enolate with a second ketone to give a ketolate: the deprotonated form of a β-hydroxy ketone. To consider only this reaction, we must allow for the generation of the enolate using the ketone pKa, and also for the protonation of the ketolate to give ketol by using the ketol pKa. The aldol formation and retroaldol rates can be predicted with these two pKa's, an estimated equilibrium constant, an estimated encounter complex formation energy and an intrinsic barrier.

Scheme 8 shows how the observable aldol equilibrium constant K and the

macroscopic rate constants k+ and k- are related to the constant K_2 and the microscopic rate constants k_{2+} and k_{2-} which are for reaction within the encounter complex and which are treated by Marcus Theory.

Scheme 8. Thermodynamic cycle used to derive the equilibrium constant required for Marcus Theory analysis of aldol reactions

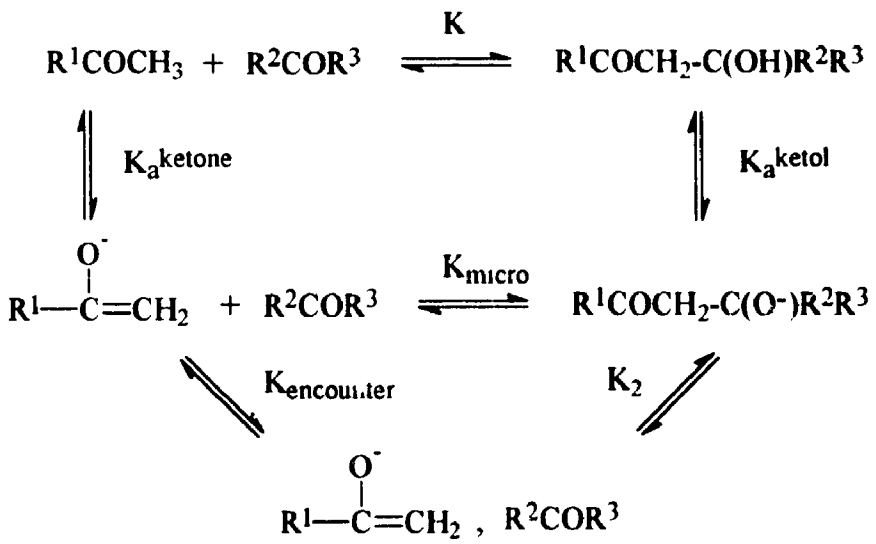

Table 21. Predicted aldol equilibrium constants and reaction rates.[a]

Nucleophile	Electrophile	log (K_{aldol} / M^{-1})	log (k^+ / $M^{-2}s^{-1}$)	log (k^- / $M^{-1}s^{-1}$)
acetone	TFA	2.47	-2.01	-4.48
PNAC	PNAC	-2.41	0.16	2.57
acetone	PNAC	-2.30	-2.24	0.059
PNAC	acetone	-1.26	0.097	1.36

[a] detailed calculations in Appendix II; K_{aldol} is the equilibrium constant for aldol reaction relative to neutral starting materials and products; k^+ is the forward macroscopic rate constant for aldol reaction; k^- is the macroscopic retroaldol rate constant; $K_{aldol} = k^+ / k^-$

Table 21 lists the predicted hydroxide catalyzed aldol rates using Guthrie's conventions. [20] The intrinsic barrier used for the calculations was 13.89 kcal.mol^{-1} and the log ($K_{encounter}$) was taken as -1.77.

CHAPTER 7: OVERALL RESULTS AND KINETIC METHODOLOGY

7.1 Preparation and characterization of ketols and enones

Of the four ketols and seven enones in the four aldol condensations studied, four enones had previously been synthesized: Z-2-phenyl-1,1,1-trifluoro-2-pentene-4-one (**3**),[49] E- and Z-1,3-bis-(4-nitrophenyl)-2-butene-1-one (**10**, **11**)[50], and 1-(4-nitrophenyl)-2-butene-1-one (**16**)[51]. Each of these was prepared by the literature method. The synthesis of only one of the ketols (**2**) has been reported in the literature,[52] though too late to be of use and using a different method than found herein.

The synthesis and characterization of 1,1,1-trifluoro-2-hydroxy-2-phenyl-4-pentanone (**2**), 4-hydroxy-4-(4-nitrophenyl)-2-pentanone (**12**), E-2-phenyl-1,1,1-trifluoro-2-pentene-4-one (**4**), E-4-(4-nitrophenyl)-3-pentene-2-one (**13**), Z-4-(4-nitrophenyl)-3-pentene-2-one (**14**), 3-hydroxy-1,3-bis-(4-nitrophenyl)-1-butanone (**9**), and 3-hydroxy-3-methyl-1-(4-nitrophenyl)-1-butanone (**15**) was required.

The ketols **2** and **12** were synthesized by directed aldol reactions employing preformed lithium enolates as shown in Scheme 9. Attempts to prepare the ketols **9** and **15** using analogous procedures failed. The procedure of Mukaiyama[53] was then employed, using the titanium tetrachloride promoted reaction of the trimethylsilyl enol ether of *p*-nitroacetophenone with *p*-nitroacetophenone and acetone respectively. These reactions are depicted in Schemes 10 and 11.

The E-enone **13** was prepared by dehydration of ketol **12** with methanolic hydrochloric acid on silica gel as depicted in Scheme 12. The Z-isomer **14** was prepared

by photoisomerization of 13 s shown in Scheme 13 followed by separation of the mixture of isomers by Low Pressure Column Chromatography.

Scheme 9.

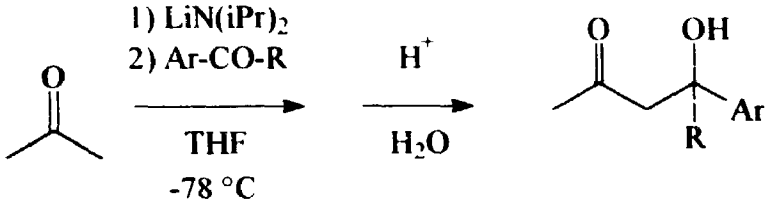

2: Ar = C_6H_5- ; R = CF_3
12: Ar = p-NO_2-C_6H_4- ; R = CH_3

Scheme 10.

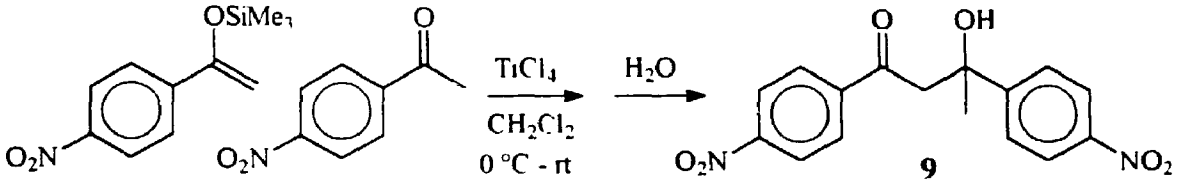

Scheme 11.

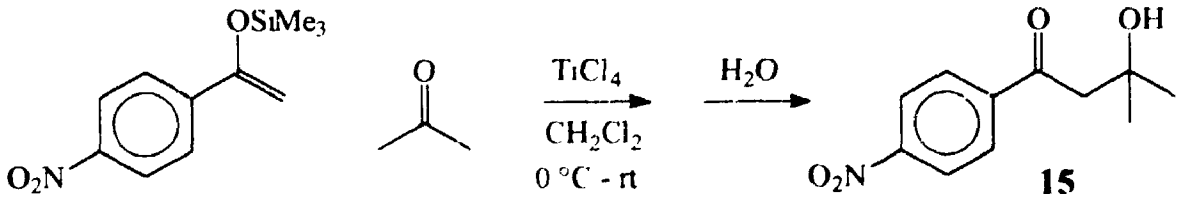

Scheme 12.

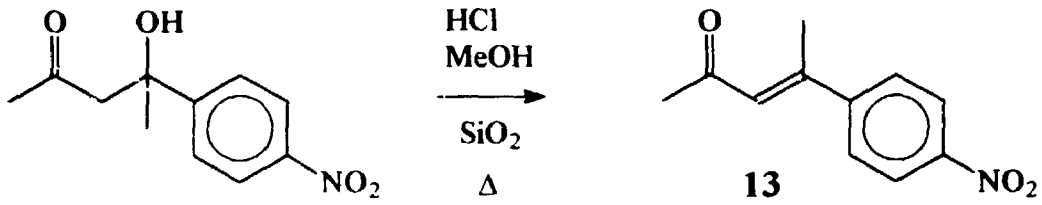

Scheme 13.

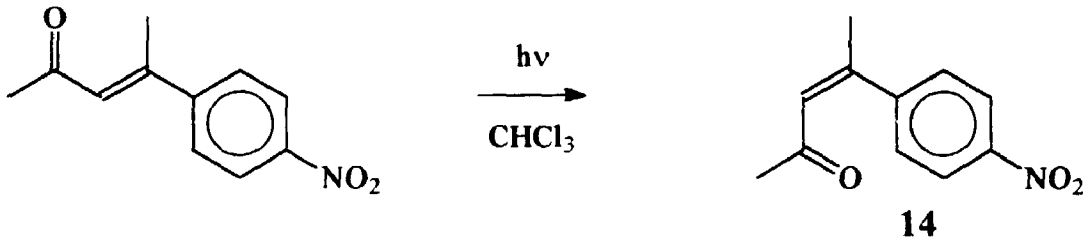

7.2 Overall kinetics and methodology

The condensations studied can be summarized in the two reaction Schemes 14 and 15 which reflect the natural divisions of the experiments.

Scheme 14. The aldol condensation of acetone with trifluoroacetophenone.

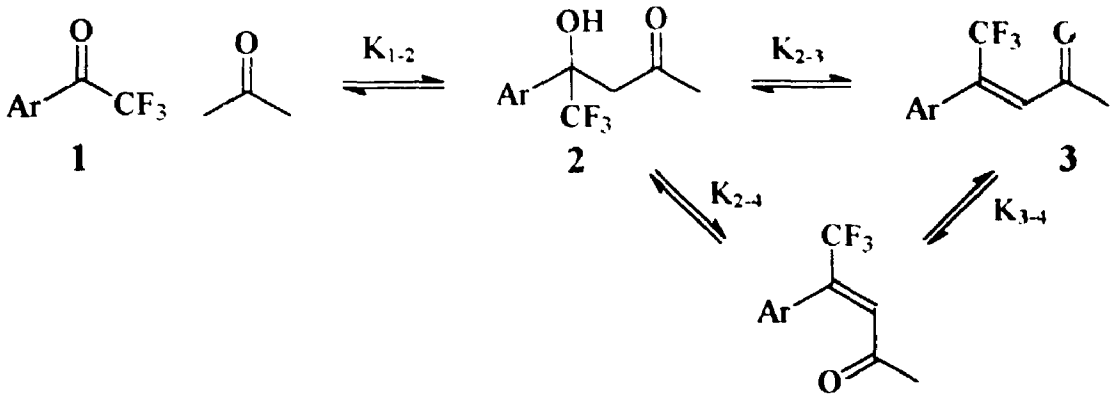

$Ar = C_6H_5$-

Because the aldol equilibria lie well to the side of starting materials, the kinetics of the reactions are most easily studied in the retroaldol sense which results in much cleaner kinetics. The kinetics were followed by either UV spectrophotometry or HPLC analysis of quenched samples and fitted to single or double exponential equations as appropriate. When HPLC analysis was used, and the data supported it, simultaneous fitting of peak integrations of multiple species from multiple experiments was used to obtain the best fit to all of the available data.

In aqueous base, isomerization of enones was observable as a kinetic phase faster than hydration. Isomerization equilibrium constants could be determined by analysis of HPLC data.

Isomerization being fast relative to hydration is a striking feature of the kinetics requiring that the ketol not be an intermediate on the reaction path from E-enone to Z-enone. This observation was also made for the corresponding condensation of acetone with acetophenone.[31] The suggested mechanism is shown in Scheme 16 where attack of hydroxide on enone gives the enolate corresponding to the ketol. Most often this is

followed by reversal: expulsion of hydroxide ion to give one or the other enone. Protonation at carbon to give ketol proceeds at a slower rate. A second, kinetically equivalent isomerization mechanism with γ-proton removal followed by isomerization was also presented.[31] There is no γ-proton for the aldol product of acetone with trifluoroacetophenone which rules out the second mechanism and suggests that the first is likely to be the mechanism in this and earlier studies.

Scheme 15. The aldol condensations involving *p*-nitroacetophenone.

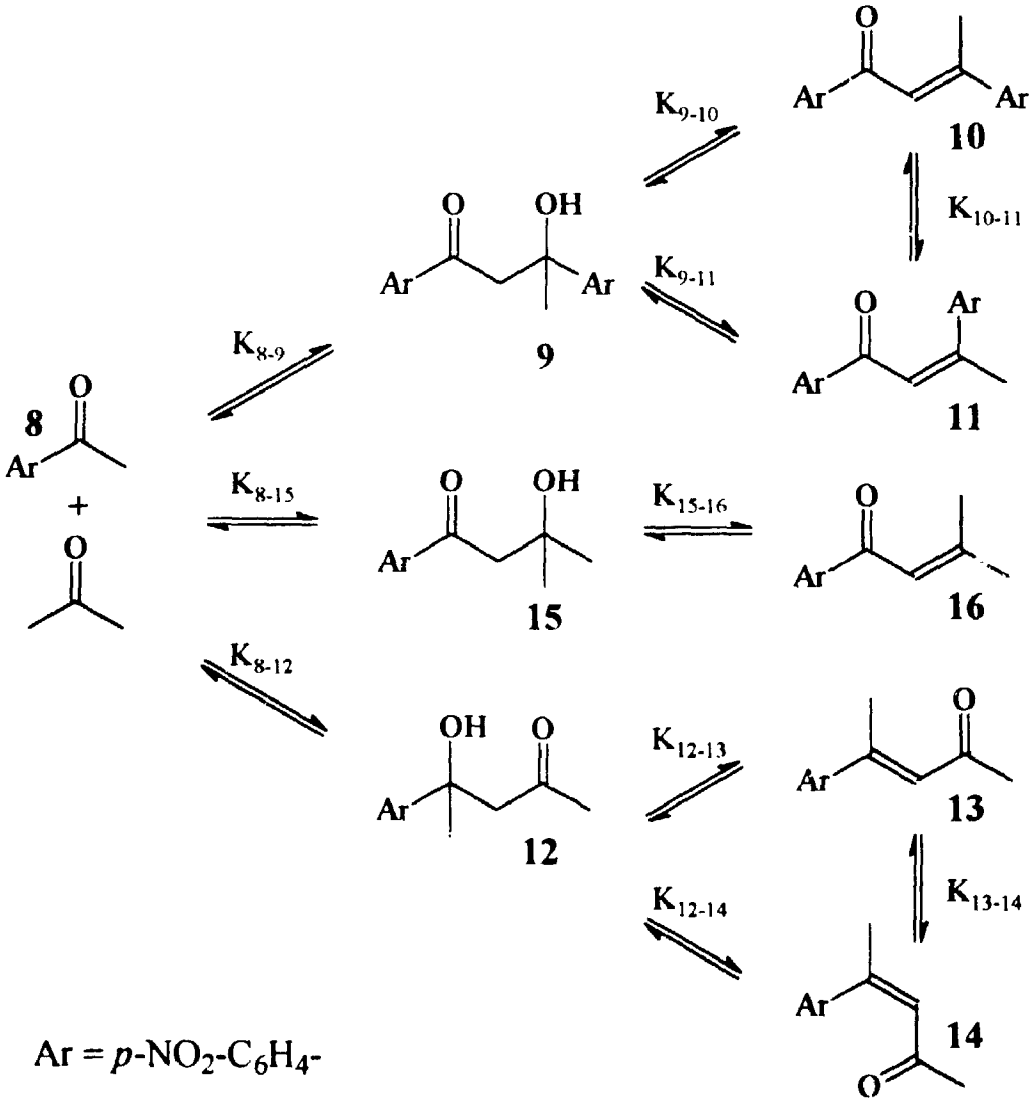

Scheme 16. Base catalyzed enone hydration and retroaldol mechanism

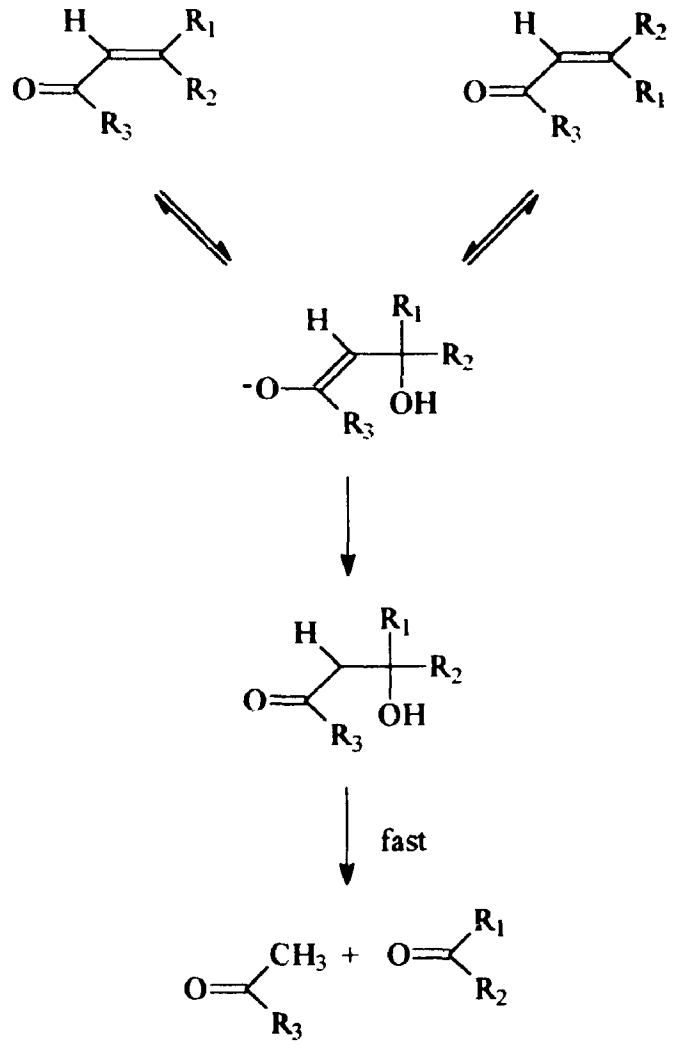

When possible, acid catalyzed equilibration of ketols and enones was used to determine the equilibrium constants for the enone isomerization and hydration processes. Once again the isomerization of the enones was faster than hydration to ketol. Simultaneous fitting of multiple data sets was particularly helpful for acid equilibrations to determine all of the rate constants in a reaction scheme at the same time. The dehydration equilibrium for the trifluoroacetophenone system could not be studied by acid equilibration and was instead determined from the aldol formation reaction.

Hydroxide catalyzed ketol retroaldol was studied either using UV spectrophotometry or HPLC analysis of quenched samples. In no experiment was there an accumulation of dehydration product. The reactions were always pseudo-first order. For the trifluoroacetophenone reaction, the ketol's pKa was within the pH range of interest so the pKa was determined from the pH rate profile for the retroaldol reaction. This had the added benefit that the first order rate constant for the retroaldol cleavage of the ketolate was determined.

HPLC analysis of equilibrated solutions of ketones in aqueous buffer or hydroxide was used to determine the aldol formation equilibrium constants. Except for some acetone self-aldol, the condensation of acetone with trifluoroacetophenone was not complicated by competing aldol reactions because trifluoroacetophenone lacks α-hydrogens. It was complicated by extensive trifluoroacetophenone hydration and pKa's of the trifluoroacetophenone hydrate and product ketol within the pH region of interest. The self-aldol of *p*-nitroacetophenone was straightforward to study because no crossed aldols are possible.

The two crossed aldols involving acetone and *p*-nitroacetophenone necessarily occur at the same time, in addition to the self aldols of both acetone and *p*-nitroacetophenone. In this case, the full complexity of Scheme 15 comes into play. Fortunately the aldol formation rates are appreciably faster than the dehydration steps such that formation could be studied without interference from dehydration products.

The self aldol condensation of acetone has been studied previously[41] and is not examined in this work.

CHAPTER 8: THE ALDOL CONDENSATION OF ACETONE WITH TRIFLUOROACETOPHENONE

8.1 Kinetics of hydroxide catalyzed isomerization and hydration of Z- and E-2-phenyl-1,1,1-trifluoro-2-pentene-4-one (3, 4)

The kinetics of isomerization of the enones 3 and 4 were studied by injecting E-enone into dilute alkaline solution and following the appearance of the Z-enone chromophore by UV spectrophotometry. Experiments starting with Z enone were unsuccessful because the equilibrium strongly favors the Z-enone so the resulting absorbance change was too small. The observed rate constants are then the sum of the forward and reverse rate constants for isomerization and are summarized in Table 22. The isomerization was considerably faster than hydration which was observable as a second kinetic phase at longer times.

The kinetics were also followed in pH 10 borate buffers by HPLC analysis of quenched samples, starting with both Z- and E-isomers. The separation achieved by HPLC allowed isomerization to be followed in both directions. HPLC peak integration-time data were fit simultaneously to the system

$$A \rightleftharpoons B$$

for reaction in both directions allowing determination of both the forward and reverse rate constants and hence the equilibrium constant. The rate and equilibrium constants obtained from these experiments are: $k_{3\text{-}4} = (3.22\pm0.05) \times 10^{-4}\ s^{-1}$, $k_{4\text{-}3} = (8.22\pm0.16) \times 10^{-6}\ s^{-1}$, $K_{3\text{-}4} = (2.55\pm0.07) \times 10^{-2}$. The HPLC data obtained are plotted in Figure 15 with the lines of

best fit determined by the method of least squares. The scale for the experiment starting with Z-enone is expanded to improve readability.

Figure 15. E-Z isomerization of 2-phenyl-1,1,1-trifluoro-2-pentene-4-one in pH 10 borate buffer. Vertical axes are scaled for viewing convenience; For reaction starting with E-enone, full scales are: E-Enone 19.9 mM, Z-Enone 50.3 mM; for reaction starting with Z-enone, full scales are: E-Enone 1.0 mM, Z-Enone 50.3 mM

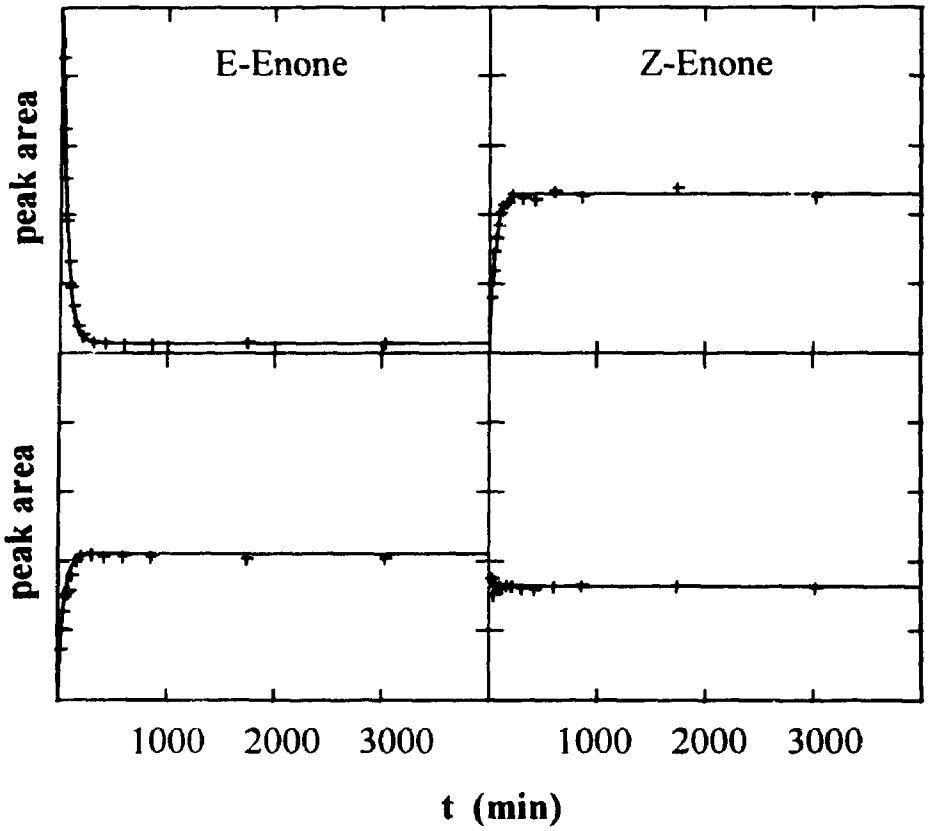

An additional experiment used HPLC analysis of equilibrated solutions of enones to determine the equilibrium constant. The enones were rapidly equilibrated in 0.1 M aqueous sodium hydroxide, quenched, and then analyzed. The results were the same whether starting with the E-enone or Z-enone. The equilibrium constant determined was

$K_{3\text{-}4}$ = (3.08±0.08) × 10^{-2} with negligible hydration to ketol at short times. This equilibrium constant is significantly different than that obtained at pH 10. Because the enone peaks are not completely resolved by HPLC, it was necessary to use PEAKFIT, a mathematical curve fitting program, to fit the peaks to estimate the peak areas. With the Z-enone peak so much larger than the E-enone peak, it is probable that studying only the equilibrated solutions resulted in a systematic error in quantitation. The kinetics study at pH 10 where peaks of varying size are being fit should be less susceptible to this systematic error. For this reason the equilibrium constant determined from the HPLC data at pH 10 is considered the most accurate.

It follows from Table 22 and $K_{3\text{-}4}$ that the second order rate constants for the hydroxide catalyzed isomerization of the enones are: $k_{3\text{-}4}$ = (4.83±0.15) × 10^{-2} M^{-1} s^{-1}, $k_{4\text{-}3}$ = 1.89±0.03 $M^{-1}s^{-1}$.

The kinetics of Z-enone hydration were followed by UV spectrophotometry and were found to be first order in hydroxide concentration. The data are summarized in Table 23. E-enone isomerization experiments, when followed for extended times, showed a second kinetic phase with a rate consistent with enone hydration. Because the hydration is the hydration of a mixture of E- and Z-enones, and because the hydration of both is likely proceed through a common intermediate, the hydration rates of each can be calculated. This is because $k_{obs} = 2\ k_{3\text{-}2} / (1 + K_{3\text{-}4})$ and similarly $k_{obs} = 2\ k_{4\text{-}2} / (1 + K_{4\text{-}3})$. The derivation of these equations has been published.[31]

The second order rate constants for hydroxide catalyzed hydration are then $k_{3\text{-}2}$ = (8.09±0.06) × 10^{-5} M^{-1} s^{-1} and $k_{4\text{-}2}$ = (2.1±0.9) × 10^{-6} M^{-1} s^{-1}.

Table 22. Rate constants for the hydroxide catalyzed isomerization of enone 4.[a]

10^3 [OH^-] (M)	α	β	$10^3\lambda$ (s^{-1})	λ / [OH^-] ($M^{-1}s^{-1}$)
99.6	0.502	1.075	253.2±3.3	2.542±0.033
99.6	0.041	0.165	180.4±4.7	1.811±0.047
99.6	0.580	0.792	18.23±0.01	1.839±0.001
99.6	0.579	0.637	18.01±0.01	1.818±0.001
99.6	0.566	0.777	17.98±0.01	1.815±0.001
9.96	0.408	1.042	18.3±0.1	1.842±0.015
9.96	0.529	0.693	18.23±0.04	1.830±0.004
9.96	0.512	0.671	18.54±0.01	1.861±0.001
9.96	0.495	0.643	17.65±0.03	1.772±0.003
1.17[b]	0.522	0.721	2.503±0.001	2.135±0.001
1.17[b]	0.512	0.712	2.421±0.001	2.066±0.001
1.17[b]	0.520	0.714	2.426±0.001	2.069±0.001
0 1352[b]	0.526	0.744	0.2878±0.0003	2.129±0.002
0.1352[b]	0.510	0.725	0.2893±0.0003	2.140±0.002
			av	1.94±0.04

[a] In aqueous solution at 25.0°C, ionic strength 0.1 (KCl), followed by UV spectrometry at 245 nm. [E-enone], = 91 μM. Data were fitted to: $A = \alpha + \beta \exp(-\lambda t)$. Standard deviations for the parameters are calculated by the least-squares procedure. Average value is weighted mean.

[b] [OH^-] determined by measurement of buffer pH; [OH^-] = $10^{(pH-14)}$

Table 23. Rate constants for the hydroxide catalyzed hydration of Z-2-phenyl-1,1,1-trifluoro-2-pentene-4-one (3).[a]

$[OH^-]^b$ (M)	α	β	$10^5\lambda$ (s^{-1})	$10^4\lambda$ / [OH-] ($M^{-1}s^{-1}$)
0.100	0.152	0.796	1.661±0.001	1.668±0.001
0.100	2.026	0.483	1.739±0.005	1.746±0.005
0.100	2.023	0.477	1.639±0.002	1.646±0.002
0.100 [c]	0.000	0.467	1.614±0.002	1.621±0.002
0.050	0.091	0.798	0.816±0.003	1.638±0.007
0.050	0.104	0.798	0.846±0.004	1.698±0.007
			av	1.658±0.012

[a] In aqueous solution at 25.0°C, ionic strength 0.1 (KCl), followed by UV spectrophotometry at 245 nm. Data were fitted to: $A = \alpha + \beta \exp(-\lambda t)$. Standard deviations for the parameters are calculated by the least-squares procedure. Average value is weighted mean.

[b] Determined by titration against standardized aqueous hydrochloric acid.

[c] hydration phase of E-Z isomerization / hydration starting with E-enone

8.2 Kinetics of hydroxide catalyzed retroaldol of 1,1,1-trifluoro-2-hydroxy-2-phenyl-4-pentanone (2)

The retroaldol cleavage of ketol 2 was studied under pseudo-first order (excess base or buffered) conditions by HPLC analysis of quenched samples . The disappearance of the ketol peak in the HPLC showed first order kinetics and was followed for at least three half lives for pH > 11. At pH 10 and 11, initial rate kinetics were used observing the first 10% of reaction. The rate constants obtained (see Table 24) allow the construction of a pH rate profile (Fig. 16). Dehydration was not detected when starting with ketol, and

retroaldol cleavage was essentially complete and pseudo-first order. Therefore, following from Scheme 17, the reaction can be considered:

$$A \rightleftharpoons B \longrightarrow C$$

where A = ketol, B = ketolate, C = trifluoroacetophenone + acetone

Scheme 17. Aldol condensation of acetone with trifluoroacetophenone; ketone hydration / dissociation and ketol dissociation shown.

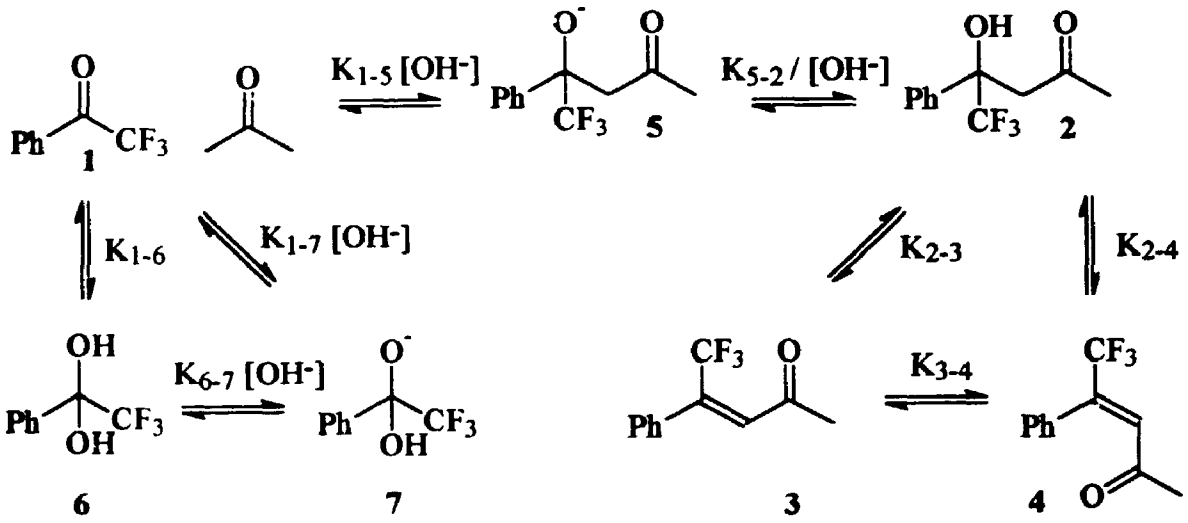

Ketol deprotonation is a rapid equilibrium such that $k_{obs} = k_{5-1} / (1 + K_{5-2} / [OH^-])$. Fitting the data from Table 24 with weighted non-linear least squares to this equation gives $k_{5-1} = (1.50\pm0.09) \times 10^{-5}\ s^{-1}$, $K_{5-2} = K_w / K_a^{ketol} = (1.4\pm0.1) \times 10^{-2}$ M, $K_a^{ketol} = (6.5\pm 0.5) \times 10^{-13}\ M^{-1}$ ($pK_a = 12.19\pm0.04$). Therefore, since $k_{2-1} = k_{5-1} / K_{5-2}$ the second order rate constant for base catalyzed retroaldol of the ketol is $(9.7\pm1.0) \times 10^{-4}\ M^{-1}\ s^{-1}$.

Table 24. Rate constants for the hydroxide catalyzed retroaldol cleavage of 1,1,1-trifluoro-2-hydroxy-2-phenyl-4-pentanone (2).[a]

[OH-][b] (M)	[KETOL][c] (mM)	α	β	$10^6\lambda$ (s^{-1})
0.0983	1.94	-0.00	1.02	12.8 ± 0.2
0.0934	0.986	0.02	1.04	13.0 ± 0.4
0.0483	2.19	0.07	2.42	13.1 ± 0.6
0.0460	0.918	-0.03	1.04	10.8 ± 3.0
0.0244	0.977	0.03	1.05	9.80 ± 0.18
0.0091	2.17	0.00	2.22	5.24 ± 0.41
0.0047	1.28	0.00	1.35	3.37 ± 0.03
0.0024	0.467	0.14	0.41	2.60 ± 0.08
0.0012[d]	1.00	1.44	-1.7E-06	1.16 ± 0.03
0.00020[d]	1.06	1.06	-2.7E-07	0.25 ± 0.01
0.00014[d]	1.00	1.47	-2.7E-07	0.183 ± 0.003

[a] In aqueous solution at 25°C, ionic strength 0.1 (KCl), followed by HPLC analysis on quenched samples; disappearance of the peak due to KETOL was followed. Data were fitted to: $[KETOL] = \alpha + \beta \exp(-\lambda t)$ unless otherwise noted.

[b] $[OH^-]$ determined by titration, or from calculation of dilution with degassed water.

[c] [KETOL] determined from mass of ketol added

[d] $[OH^-]$ determined by measurement of buffer pH; initial rate kinetics fit to $[KETOL] = \alpha + \beta t$; thence $\lambda = -\beta/\alpha$; α in mM

Figure 16. pH dependence of apparent first-order rate constants for retroaldol cleavage of 1,1,1-trifluoro-2-hydroxy-2-phenyl-4-pentanone (2).

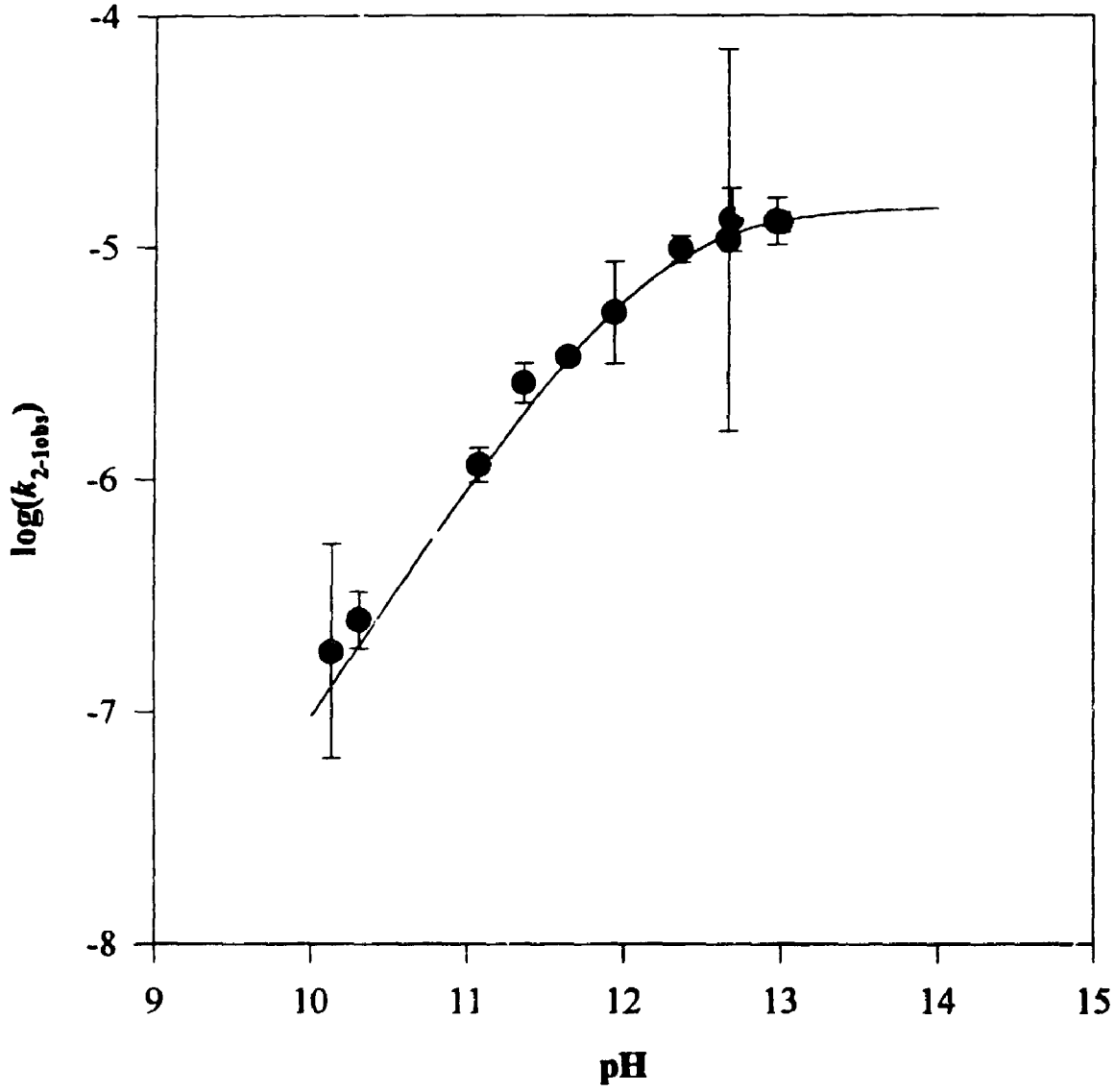

8.3 Aldol formation

Ketol and enone formation were followed in the forward direction by mixing trifluoroacetophenone and acetone in aqueous base or buffer and following the appearance

of products by HPLC. Trifluoroacetophenone was difficult to quantify because of severe peak tailing in the HPLC. This is presumably because of the ketone - hydrate equilibrium, and the best separations are obtained at lower temperatures where this equilibration is slowed. Elevated temperatures (to 40 °C) resulted in more tail than peak while ice temperature gave a tail which did not severely affect the quantitation of the ketol. Early method development using methanol - water eluent with stock solutions of ketone in either water or methanol, showed what appeared to be hemiacetal formation and breakdown on the column. The ratios of peaks and magnitude of absorbance between the peaks were dependent on the composition of both injection solvent and eluent. Acetonitrile - water mixtures showed promise so that the earlier system was abandoned, but its peculiarities support the hydration explanation for tailing.

It seemed imprudent to rely on the integrations or peak heights from trifluoroacetophenone because of peak tailing. The equilibrium concentration of trifluoroacetophenone was taken as its initial concentration, determined by mass used, minus the concentration of ketol present, as determined by HPLC. This undoubtedly introduces error, but that error can be estimated. The trifluoroacetophenone peak was followed and agreed approximately with the calculated concentration.

Trifluoroacetophenone also undergoes slow haloform cleavage with a half-life of 160 hours in 0.1 M hydroxide solution.[54] This effect is ignored in these calculations. Acetone condenses with itself to give diacetone alcohol and mesityl oxide. The HPLC showed the presence of side products including acetone self-condensation products, identified by comparison to authentic samples, which were ignored in the quantitation.

Calculation of the effect of self-aldol on the acetone concentration based on known rates and equilibrium constants[40,41] showed the effect would only be a few percent. This effect is ignored in the calculations.

First order growth of the ketol peak was observed. The reaction was followed for several half-lives and non-linear least-squares was used to determine both the apparent rate constants and the equilibrium concentration of ketol. Only the equilibrium concentration is of interest in this treatment. The apparent equilibrium constant, defined as $K_{app} = [KETOL]_{total} / ([TFA]_{total}[ACETONE])$, is pH dependent because the pK_a's of both the trifluoracetophenone hydrate and the ketol are in the pH range studied. Following Scheme 17, the theoretical pH equilibrium profile should follow:

$$K_{app} = K_{1-2} \times (1 + K_{5-2}[OH^-]) / (1 + K_{1-6} + K_{1-7}[OH^-]) \quad [2]$$

where $K_{1-6} = 77.6$ and $K_{1-7} = 776000\ M^{-1}$ as determined by Stewart,[55,56] and $K_{5-2} = K_w/K_a = (1.4\pm0.1) \times 10^{-2}$ M as determined above. The results of the formation reactions are summarized in Table 25. K_{1-2} was determined for each experiment by correcting K_{app} for hydration and pH effects, and the weighted mean of the individual experiments is $K_{1-2} = (2.657\pm0.003) \times 10^3\ M^{-1}$. K_{app} as a function of pH is shown in Figure 17, along with the theoretical line.

The point at the lowest pH in the aldol formation equilibrium profile shows a very significant deviation from the line. The HPLC data showed a possible decrease in the trifluoroacetophenone concentration which had not occurred in other runs. If the TFA concentration estimated by inspection of the HPLC results is used to calculate the observed equilibrium constant, the point falls much closer to the line. To avoid

inconsistency, this was not done.

Figure 17. Apparent equilibrium constant as a function of pH for the aldol reaction of acetone with trifluoroacetophenone.

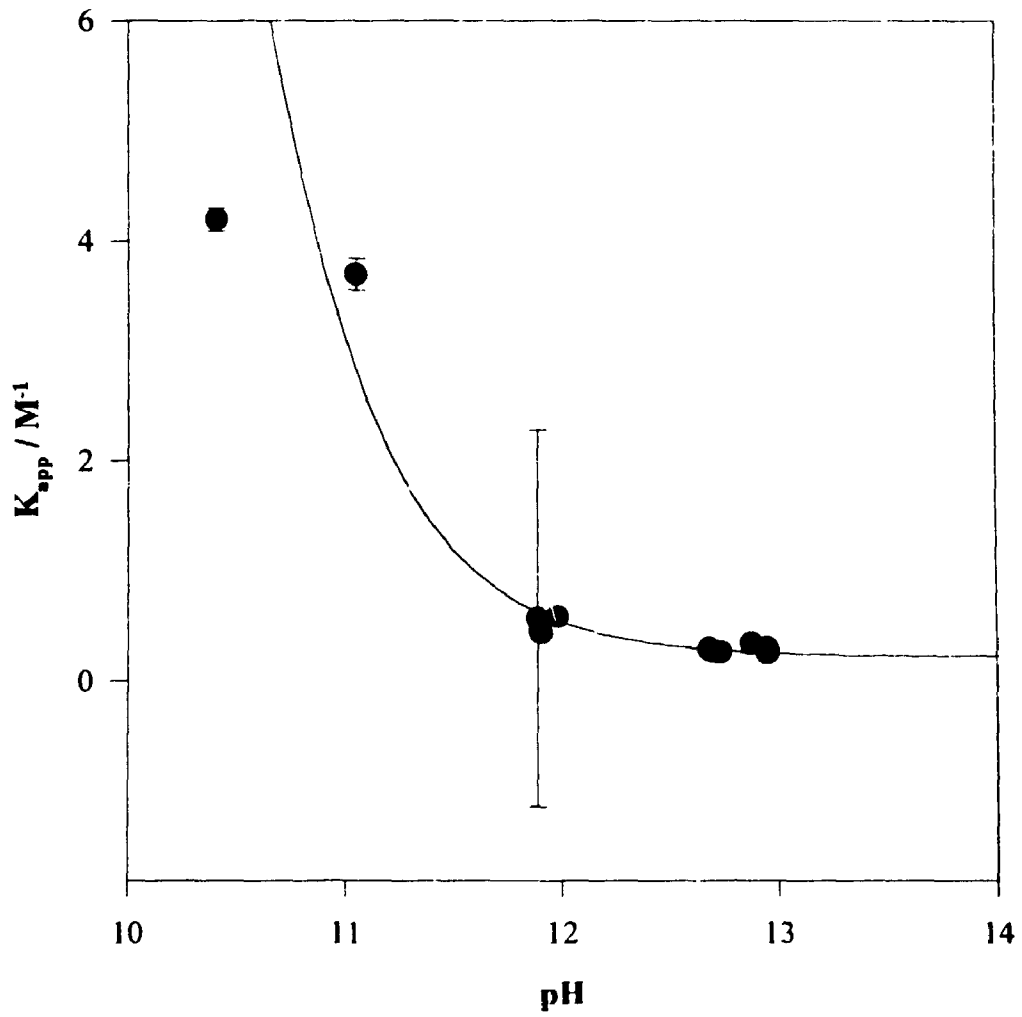

Table 25. Apparent aldol formation constants for the reaction of acetone with trifluoroacetophenone.[a]

10^2 [TFA][b] (M)	[OH^-][b] (M)	[ketol]$_e$[c]	10^2[TFA]$_e$[d] (M)	[acetone]$_e$[d]	pH[e]	K_{app}[f] (M^{-1})	10^{-3} K_{calc}[g] (M^{-1})
2.050±0.002	0.1	5.518±0.039	1.498	1.076	12.87	0.342±0.029	3.46±0.28
1.007±0.002	0.1	2.320±0.016	0.775	0.998	12.94	0.300±0.019	3.06±0.19
1.021±0.002	0.1	0.710±0.009	0.950	0.291	12.95	0.256±0.001	2.62±0.01
1.020±0.002	0.1	0.257±0.009	0.994	0.098	12.95	0.264±0.000	2.698±0.003
1.016±0.002	0.06	2.317±0.024	0.784	0.998	12.68	0.296±0.023	2.69±0.21
0.528±0.002	0.06	0.602±0.007	0.467	0.490	12.73	0.263±0.004	2.45±0.04
1.012±0.002	0.06	0.763±0.011	0.936	0.291	12.69	0.281±0.001	2.56±0.01
1 020±0.002	0.06	0.268±0.004	0.993	0.099	12.70	0.271±0.000	2.481±0.001
1.020±0.002	0.02	3.18±0.01	0.702	0.997	11.90	0.453±0.032	1.88±0.13
1.011±0.002	0.02	3.66±0.69	0.645	0.996	11.89	0.6±1.7	2.32±6.95
1.126±0.002	0.02	1.26±0.05	1.000	0.289	11.91	0.434±0.005	1.81±0.02
1.013±0.002	0.02	0.515±0.003	0.962	0.091	11.98	0.587±0.000	2.728±0.001

0.505±0.002	0.00113	3.36±0.13	0.169	0.538	11.05	3.70±0.14	3.29±0.23
0.510±0.002	0.00026	3.53±0.14	0.157	0.537	10.41	5.47±0.06	1.484±0.016
						av	2.656±0.034

[a] In aqueous hydroxide or buffer solution at 25.0 °C; ionic strength maintained at 0.1 M with KCl; analysis by HPLC

[b] concentration as added to reaction flask

[c] equilibrium concentration of ketol determined by HPLC analysis

[d] concentration corrected for formation of ketol

[e] pH calculated from hydroxide concentration corrected for consumption by TFA hydrate and ketol.

[f] $[ketol]_e / ([TFA]_e[acetone]_e)$

[g] $K_{1\text{-}2}$ calculated from Eqn. 2.

The approach to equilibrium between ketol and enones is expected to be slow except at high pH. At high pH, however, the equilibrium is shifted in favor of the ketol by its conversion to ketolate. As a result, detection of the enones was very difficult, and our estimates of enone concentration at equilibrium are correspondingly imprecise. The best compromise was a hydroxide concentration near 0.05 M HPLC analysis of equilibrated solutions did not separate the two enones so that a hybrid calibration constant calculated using the measured calibration constants for the two enones and the isomerization equilibrium constant was used.

In this way the dehydration equilibrium constants were determined: $K_{2\text{-}3}$ = $(4.3\pm0.4) \times 10^{-3}$ and $K_{2\text{-}4}$ = $(1.1\pm0.1) \times 10^{-4}$. The error estimates are conservative and should be considered the lower limit of uncertainty.

8.4 Summary of results for the aldol condensation of acetone with trifluoroacetophenone.

The rate and equilibrium constants determined for the hydroxide catalyzed reactions in the aldol condensation of acetone with trifluoroacetophenone are summarized in Table 26.

Table 26. Summary of rate and equilibrium constants for the hydroxide catalyzed aldol condensation of acetone with trifluoroacetophenone.

Constant	value	units
$K_{1\text{-}2}$ [a]	$(2.66\pm0.03) \times 10^{3}$	M^{-1}
$k_{1\text{-}2}$ [b]	2.75±0.25	$M^{-2}s^{-1}$
$k_{2\text{-}1}$ [c]	$(1.03\pm0.09) \times 10^{-3}$	$M^{-1}s^{-1}$
$K_{2\text{-}3}$ [d]	$(4.3\pm0.4) \times 10^{-3}$	
$k_{2\text{-}3}$ [e]	$(3.4\pm0.3) \times 10^{-7}$	$M^{-1}s^{-1}$
$k_{3\text{-}2}$ [f]	$(8.08\pm0.06) \times 10^{-5}$	$M^{-1}s^{-1}$
$K_{2\text{-}4}$ [d]	$(1.09\pm0.10) \times 10^{-4}$	
$k_{2\text{-}4}$ [e]	$(0.2\pm9.9) \times 10^{-9}$	$M^{-1}s^{-1}$
$k_{4\text{-}2}$ [f]	$(0.2\pm9.2) \times 10^{-5}$	$M^{-1}s^{-1}$
$K_{3\text{-}4}$ [g]	$(2.55\pm0.07) \times 10^{-2}$	
$k_{3\text{-}4}$ [h]	$(4.83\pm0.15) \times 10^{-2}$	$M^{-1}s^{-1}$
$k_{4\text{-}3}$ [h]	(1.89±0.03)	$M^{-1}s^{-1}$
$K_{5\text{-}2}$ [i]	$(1.44\pm0.11) \times 10^{-2}$	M^{-1}
Other constants:		
K_a^{ketol} [j]	$(6.9\pm0.5) \times 10^{-13}$	M^{-1}
$k_{34}+k_{43}$ [k]	(1.94±0.03)	$M^{-1}s^{-1}$

[a] determined from aldol formation reactions

[b] calculated from $k_{1\text{-}2} = k_{2\text{-}1} \times K_{1\text{-}2}$

[c] determined from hydroxide catalyzed retroaldol

[d] determined by equilibrium concentration in aldol formation

[e] calculated from $k_{2\text{-}3} = k_{3\text{-}2} \times K_{2\text{-}3}$; $k_{2\text{-}4} = k_{4\text{-}2} \times K_{2\text{-}4}$

[f] calculated from observed hydration rate constant using $k_{3\text{-}2} = k_{obs} / (2 (1 + K_{3\text{-}4}))$; $k_{4\text{-}2} = k_{obs} / (2 (1 + K_{4\text{-}3}))$

[g] determined from HPLC analysis of enone equilibration

[h] determined from UV and HPLC studies of isomerization; values calculated by $k_{3\text{-}4} = k_{obs} / (1 + 1 / K_{3\text{-}4})$; $k_{4\text{-}3} = k_{obs} / (1 + K_{3\text{-}4})$;

[i] determined from ketol retroaldol pH rate profile

[j] calculated from $K_a = K_w / K_{5\text{-}2}$

[k] observed second order rate constant from enone isomerizations

CHAPTER 9: THE SELF-ALDOL CONDENSATION OF *p*-NITROACETOPHENONE

Scheme 18. Self-aldol condensation of *p*-nitroacetophenone

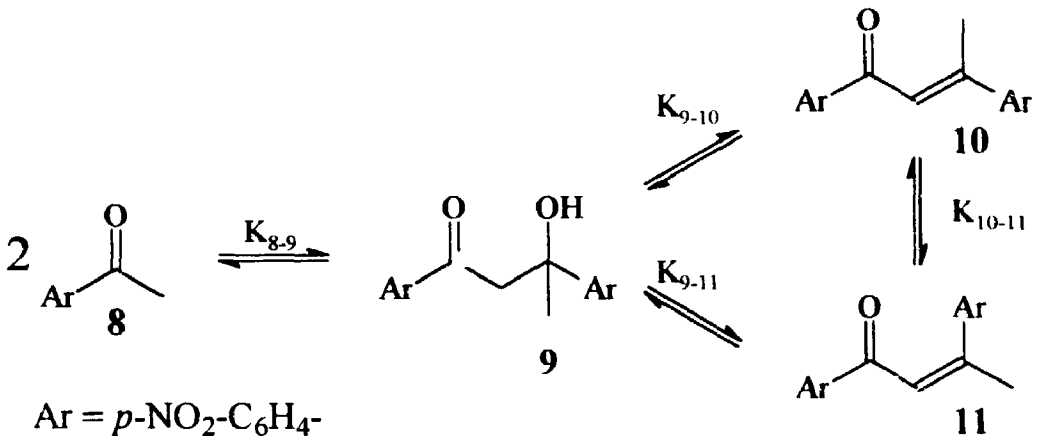

9.1 Kinetics of hydroxide catalyzed retroaldol cleavage of 3-hydroxy-1,3-bis-(4-nitrophenyl)-1-butanone (9)

The retroaldol cleavage of the *p*-nitroacetophenone self-aldol product 9 was studied in aqueous borate buffers between pH 8 and 10 following the appearance of the *p*-nitroacetophenone chromophore by UV spectrophotometry.

The absorbance-time data obtained were analyzed by least squares fitting to a single exponential. The retroaldol cleavage of 9 was first order in hydroxide concentration and followed simple pseudo-first order kinetics. The observed rate constants are reported in Table 27, and the calculated second-order rate constant for hydroxide catalyzed retroaldol cleavage of 9 is $k_{9\text{-}8} = (1.72 \pm 0.04) \times 10^2\ M^{-1}s^{-1}$. No buffer catalysis was observed for the retroaldol reaction.

Table 27. Rate constants for the hydroxide catalyzed retroaldol cleavage of 3-hydroxy-1,3-bis-(4-nitrophenyl)-1-butanone (9). [a]

10^5 [OH^-][b] (M)	α	β	10^3 λ (s^{-1})	10^{-2} λ / [OH^-] ($M^{-1}s^{-1}$)
9.84[c]	0.430	-0.115	19.6±0.1	1.99±0.05
9.84[c]	0.430	-0.100	16.6±0.1	1.68±0.04
9.84[c]	0.442	-0.118	15.7±0.1	1.60±0.04
6.92[d]	0.441	-0.117	12.73±0.04	1.84±0.04
6.92[d]	0.442	-0.117	12.58±0.04	1.82±0.04
6.92[d]	0.430	-0.104	14.36±0.06	2.( ).05
1.00[c]	0.451	-0.119	1.618±0.001	1.61±0.04
1.00[c]	0.443	-0.117	1.540±0.002	1.53±0.04
1.00[c]	0.359	-0.095	1.618±0.002	1.61±0.04
0.86[d]	0.255	-0.067	1.501±0.005	1.75±0.04
0.86[d]	0.310	-0.082	1.429±0.003	1.66±0.04
0.86[d]	0.447	-0.119	1.461±0.004	1.70±0.04
0.089[c]	0.432	-0.103	0.1695±0.0004	1.90±0.04
			av	1.72±0.04

[a] In aqueous borate buffers at 25.0 °C; ionic strength 0.1 M maintained with KCl. Following *p*-nitroacetophenone chromophore at 261 nm by UV spectrophotometry. Absorbance-time data fitted to $A = \alpha + \beta \exp(-\lambda t)$. Cell length 10.000 cm. $[ketol]_i$ = 2.05 μM

[b] [OH^-] taken as $10^{(pH-14)}$ where the pH was measured for the pure buffer.

[c] $[H_3BO_3]_{total}$ = 0.1 M

[d] $[H_3BO_3]_{total}$ = 0.01 M

9.2 Kinetics of hydroxide catalyzed isomerization and hydration of E- and Z-1,3-bis-(4-nitrophenyl)-2-butene-1-one (10, 11)

The kinetics of isomerization and hydration of the enones 10 and 11 were studied in aqueous hydroxide by UV spectrophotometry and HPLC analysis of quenched samples. Rapid retroaldol cleavage of the ketol 9 meant that hydration was a commitment to retroaldol cleavage. The chromophore of the E-enone (10) at 315 nm was used to follow the reactions spectrophotometrically.

Isomerization was faster than hydration, such that two kinetic phases were observed. When starting with Z-enone, the absorbance of the sample solution initially increased as isomerization proceeded, then decreased during hydration of the equilibrium mixture of enones. A sample kinetics plot is shown in Figure 18. When starting with E-enone, the absorbance change due to isomerization was small and poorly defined by the data. The absorbance-time data were fitted by non-linear least squares to a double exponential equation. The isomerization rate constants from the Z-enone experiments were used as constraints on the isomerization rate constant when fitting the E-enone data to allow a better fit of the slower hydration phase. The observed rate constants and derived second-order rate constants are listed in Tables 28 and 29 for reactions starting with E- and Z- enones respectively.

Table 28. Rate constants for the hydroxide catalyzed isomerization and hydration of 10.[a]

[OH⁻] (M)	α	β	$10^5 \lambda_1$[b] (s^{-1})	γ	$10^5 \lambda_2$ (s^{-1})	$10^3 \lambda_1$ / [OH⁻] ($M^{-1}s^{-1}$)	$10^4 \lambda_2$ / [OH⁻] ($M^{-1}s^{-1}$)
0.100[c]	0.063	0.022	93.9±0.3	0.138	4.64±0.03	9.39±0.03	4.64±0.03
0.100[d]	0.031	0.009	94.0±0.1	0.075	5.25±0.02	9.40±0.01	5.25±0.02
0.050[d]	0.028	0.012	47.0±0.1	0.078	2.24±0.01	9.39±0.02	4.48±0.03
0.010[d]	0.030	0.009	9.3012±0.0003	0.074	0.622±0.004	9.3012±0.0003	6.22±0.04
						av 9.301±0.002	5.12±0.31

[a] In aqueous sodium hydroxide solution at 25.0 °C. Ionic strength maintained at 0.1 M with KCl. Following E-enone chromophore at 315 nm by UV spectrophotometry. Cell length 10.000 cm. Absorbance-time data were fitted to $A = \alpha + \beta \exp(-\lambda_1 t) + \gamma \exp(-\lambda_2 t)$. λ_1 and λ_2 correspond to isomerization and hydration phases respectively.

[b] λ_1 constrained to be close to $(9.4 \times 10^{-3}\ M^{-1}s^{-1}) \times [OH^-]$

[c] $[\text{E-enone}]_i = 0.96\ \mu M$

[d] $[\text{E-enone}]_i = 0.48\ \mu M$

Table 29. Rate constants for the hydroxide catalyzed hydration and isomerization of 11.[a]

$[OH^-]$ (M)	α	β	$10^4 \lambda_1$ (s^{-1})	γ	$10^5 \lambda_2$ (s^{-1})	$10^3 \lambda_1 / [OH^-]$ ($M^{-1}s^{-1}$)	$10^4 \lambda_2 / [OH^-]$ ($M^{-1}s^{-1}$)
0.1 [b]	0.046	-0.088	9.67±0.04	0.172	5.717±0.007	9.67±0.04	5.72±0.01
0.1 [c]	0.027	-0.040	9.46±0.05	0.083	6.082±0.015	9.46±0.05	6.08±0.02
0.05 [c]	0.026	-0.041	4.73±0.03	0.086	2.997±0.005	9.45±0.06	5.99±0.01
0.05 [c]	0.024	-0.042	4.69±0.03	0.086	3.027±0.006	9.38±0.06	6.05±0.01
0.01 [c]	0.025	-0.042	0.930±0.005	0.087	0.651±0.004	9.30±0.05	6.51±0.04
						av 9.48±0.07	5.88±0.09

[a] In aqueous sodium hydroxide solution at 25.0 °C. Ionic strength maintained at 0.1 M with KCl. Following E-enone chromophore at 315 nm by UV spectrophotometry. Cell length 10.000 cm. Absorbance-time data were fitted to $A = \alpha + \beta \exp(-\lambda_1 t) + \gamma \exp(-\lambda_2 t)$. λ_1 and λ_2 correspond to isomerization and hydration phases respectively.

[b] $[E\text{-enone}]_i = 0.95\ \mu M$

[c] $[E\text{-enone}]_i = 0.48\ \mu M$

Figure 18. Hydroxide catalyzed isomerization and hydration of 11 followed by UV spectrophotometry. $[11]_i = 0.48\ \mu M$; $\lambda = 315$ nm; $[OH^-] = 0.05$ M

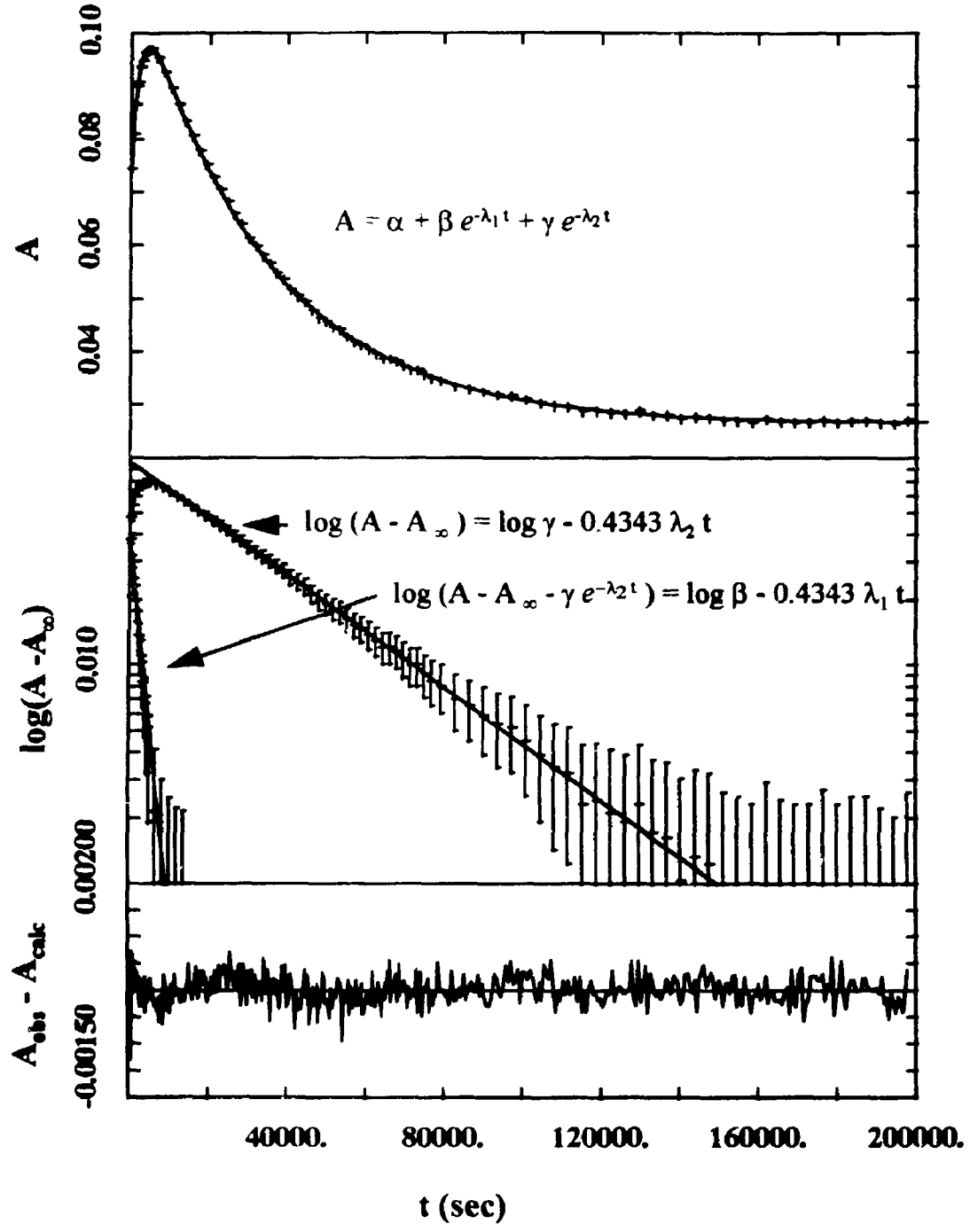

The isomerization and hydration of enones **10** and **11** were also followed by

HPLC analysis of quenched samples to determine the rate and equilibrium constants for E-Z isomerization and the rate constant for hydration. Only the reaction starting with Z-enone was used in the data analysis because of contamination of the E-enone with the Z-isomer. This precluded fitting both data sets simultaneously because the least-squares analysis assumes that only one of the concentrations will be non-zero at time zero. Recrystallization of the E-enone actually increased the Z-enone content because of the dramatic solubility differences between the two enones. The values obtained from the least squares fitting for experiments in 0.1 M and 0.01 M hydroxide solutions are listed in Table 30.

The two hydration rate constants cannot be considered accurate. The data are insufficient to resolve the individual hydration rate constants so that it is better to use the calculated individual rate constants to calculate the observable rate constant for the hydration step, and compare the observable rate constant to the results of the UV experiments. The results are consistent but the observable rate determined from the UV experiments is far more accurate.

Table 30. Results of least squares fitting for the HPLC study of the isomerization and hydration of 11.

[OH⁻] (M)	10^3 k '$_{10\text{-}11}$ / [OH⁻] ($M^{-1}s^{-1}$)	10^3 k '$_{11\text{-}10}$ / [OH⁻] ($M^{-1}s^{-1}$)	10^4 k '$_{10\text{-}9}$ / [OH⁻] [b] ($M^{-1}s^{-1}$)	10^4 k '$_{11\text{-}9}$ / [OH⁻] [b] ($M^{-1}s^{-1}$)	$K_{10\text{-}11}$ [c]
0.100 [d]	4.0±0.6	5.5±0.7	4.6±0.6	5.8±0.6	0.72±0.09
0.010 [e]	4.4±1.3	5.2±1.1	1.1±0.4	4.4±0.2	0.85±0.13
av	1.62±0.02	5.23±0.56	2.65±0.13	2.62±0.04	0.78±0.06

[a] in aqueous sodium hydroxide at 25.0 °C; ionic strength maintained at 0.1 M with KCl; least squares analysis fit peak integrations for both enones and ketol simultaneously for reaction starting with Z-enone; the listed rate constants are designated as k` to distinguish them from the corresponding rate constants derived from these and other experiments.

[b] see notes in the main text about the determination of this rate constant.

[c] $K_{10\text{-}11} = k'_{10\text{-}11} / k'_{11\text{-}10}$

[d] other parameters from least squares fitting: [Z-enone]$_i$ = 1.35±0.06 μM; $\varepsilon_1 = (2.75\pm0.11) \times 10^4$ μM^{-1}; $\varepsilon_2 = (1.85\pm0.17) \times 10^4$ μM^{-1}; $\varepsilon_3 = (2.90\pm0.12) \times 10^4$ μM^{-1}; constraints were [Z-enone]$_i$ = 1.19±0.12 μM; $\varepsilon_1 = (2.56\pm0.06) \times 10^4$ μM^{-1}; $\varepsilon_2 = (2.15\pm0.26) \times 10^4$ μM^{-1}; $\varepsilon_3 = (3.13\pm0.07) \times 10^4$ μM^{-1}

[e] other parameters from least squares fitting: [Z-enone]$_i$ = 1.19±0.09 μM; $\varepsilon_1 = (3.0\pm0.2) \times 10^4$ μM^{-1}; $\varepsilon_2 = (2.1\pm0.3) \times 10^4$ μM^{-1}; $\varepsilon_3 = (2.22\pm0.17) \times 10^4$ μM^{-1}; constraints were [Z-enone]$_i$ = 1.19±0.12 μM; $\varepsilon_1 = (2.56\pm0.06) \times 10^4$ μM^{-1}; $\varepsilon_2 = (2.15\pm0.26) \times 10^4$ μM^{-1}; $\varepsilon_3 = (3.13\pm0.07) \times 10^4$ μM^{-1}

9.3 Isomerization and hydration of E- and Z-1,3-bis-(4-nitrophenyl)-2-butene-1-one (10, 11) in acid

The equilibrium triangle of ketol 9 and enones 10 and 11 was studied starting with each of the two enones in 1 M hydrochloric acid. The appearance or disappearance of each species was followed by HPLC analysis of quenched samples. Sensitivity problems due to low solubility of substrate made the studies sufficiently erratic that a full kinetic analysis was not possible. By inspection, however, it was possible to estimate that isomerization of the two enones had a half life of ca. 25 hrs, and hydration had a half life of ca. 60 hrs. Averaging of the three analyses for the last two points (at 480 and 820 hrs) taken for each solution allowed estimation of the equilibrium composition of the reaction solutions. The results of the analysis of the equilibrated solutions are listed in Table 31. The corresponding equilibrium constants are $K_{9\text{-}10} = 0.77\pm0.13$; $K_{9\text{-}11} = 0.93\pm0.13$; $K_{10\text{-}11}$

Table 31. Isomerization and hydration equilibria determination for 9, 10, and 11. [a]

[9] (μM)	[10] (μM)	[11] (μM)	$K_{9\text{-}10}$	$K_{9\text{-}11}$	$K_{10\text{-}11}$
0.26±0.03 [b]	0.25±0.08	0.24±0.05	0.97±0.34	0.93±0.23	0.96±0.22
0.33±0.02 [c]	0.23±0.07	0.31±0.04	0.69±0.21	0.93±0.14	1.35±0.19
		av	0.77±0.13	0.93±0.13 [d]	1.19±0.19

[a] in 1 M aqueous hydrochloric acid at 25.0 °C; analysis by HPLC;each concentration calculated from three replicates for each of two quenched samples.

[b] starting with 10

[c] starting with 11

[d] error is one-half that calculated for the sum of two values

= 1.19±0.19. The large uncertainties in these values is indicative of the difficulty in obtaining satisfactory kinetics.

9.4 Equilibrium constant determination for the formation of 3-hydroxy-1,3-bis-(4-nitrophenyl)-1-butanone (9) by the hydroxide catalyzed self-aldol reaction of *p*-nitroacetophenone

The hydroxide catalyzed self-aldol reaction of *p*-nitroacetophenone to give ketol 9 was studied in aqueous borate buffer by HPLC analysis of quenched samples. The approach to equilibrium for ketol formation was very fast because the rate constant is dominated by the rapid retroaldol rate. The rate for ketol formation was not studied in the forward direction because the more accurate rate constants can be obtained in the retroaldol sense. The dehydration to give one or the other enone was much slower and it was not followed because significant amounts of undesired and unidentified products formed which made quantitation of the ketol and enones difficult. Because the rate of approach to equilibrium for ketol formation will be approximately the rate of retroaldol cleavage, the reaction reached equilibrium in a few minutes at pH 10 and in a few seconds in 0.1 M NaOH. The determined equilibrium concentrations and equilibrium constants are listed in Table 32.

Table 32. Aldol formation equilibrium constant determination for the self-aldol reaction of *p*-nitroacetophenone.[a]

[PNAC] [b] (mM)	[ketol] [c] μM	10^2 K_{ald} [d] (M^{-1})
2.00	0.072±0.014	1.79±0.39
2.00	0.066±0.013	1.64±0.36
3.20	0.145±0.012	1.42±0.15
4.00	0.229±0.024	1.43±0.17
4.00	0.231±0.023	1.45±0.16
		1.46±0.04

[a] Determined in aqueous pH 10 borate buffer at 0.1 M ionic strength, 25.0 °C, by HPLC analysis for ketol 9.

[b] concentration of *p*-nitroacetophenone was determined from the volume of stock solution injected.

[c] concentration of ketol is the average of 3-6 samples in each experiment; uncertainty was estimated from standard deviation of HPLC determinations and standard deviation of calibration standard determinations.

[d] K_{ald} = [ketol] / [PNAC]^2

9.5 Summary of rate and equilibrium constants for the self-aldol condensation of *p*-nitroacetophenone

The rate and equilibrium constants determined in this work are summarized in Table 33.

Table 33. Summary of rate and equilibrium constants for the self-aldol condensation of *p*-nitroacetophenone. [a]

Constant	value	units
$K_{8\text{-}9}$ [b]	$(1.46\pm0.04) \times 10^{-2}$	M^{-1}
$k_{8\text{-}9}$ [c]	2.52 ± 0.10	$M^{-2}s^{-1}$
$k_{9\text{-}8}$ [d]	$(1.72\pm0.04) \times 10^{2}$	$M^{-1}s^{-1}$
$K_{9\text{-}10}$ [e]	(0.72 ± 0.17)	
$k_{9\text{-}10}$ [f]	$(3.7\pm0.9) \times 10^{-4}$	$M^{-1}s^{-1}$
$k_{10\text{-}9}$ [g]	$(5.2\pm0.2) \times 10^{-4}$	$M^{-1}s^{-1}$
$K_{9\text{-}11}$ [h]	0.93 ± 0.13	
$k_{9\text{-}11}$ [i]	$(6.2\pm1.0) \times 10^{-4}$	$M^{-1}s^{-1}$
$k_{11\text{-}9}$ [j]	$(6.7\pm0.4) \times 10^{-4}$	$M^{-1}s^{-1}$
$K_{10\text{-}11}$ [k]	0.78 ± 0.06	
$k_{10\text{-}11}$ [l]	$(4.15\pm0.19) \times 10^{-3}$	$M^{-1}s^{-1}$
$k_{11\text{-}10}$ [l]	$(5.34\pm0.19) \times 10^{-3}$	$M^{-1}s^{-1}$

[a] subscripts on all constants refer to Scheme 18

[b] determined from base catalyzed aldol formation

[c] calculated from $k_{8\text{-}9} = k_{9\text{-}8} \times K_{8\text{-}9}$

[d] determined from base catalyzed retroaldol cleavage

[e] calculated from $K_{9\text{-}10} = K_{9\text{-}11} / K_{10\text{-}11}$

[f] calculated from $k_{9\text{-}10} = k_{10\text{-}9} \times K_{9\text{-}10}$

[g] determined from the observable rate constant for hydration of enones followed by UV spectrophotometry by $k_{10\text{-}9} = k_{obs} /(2\ (1 + K_{10\text{-}11}))$

[h] determined from acid catalyzed equilibration of ketol 9 and enones 10 and 11

[i] calculated from $k_{11\text{-}9} \times K_{9\text{-}11}$

[j] determined from the observable rate constant for hydration of enones followed by UV spectrophotometry by $k_{11\text{-}9} = k_{obs} /(2\ (1 + 1 / K_{10\text{-}11}))$

[k] from HPLC study of base catalyzed isomerization and hydration of **11**

[l] from UV study of base catalyzed isomerization and hydration experiments; values calculated by $k_{10\text{-}11} = k_{obs} / (1 + 1 / K_{10\text{-}11})$; $k_{11\text{-}10} = k_{obs} / (1 + K_{10\text{-}11})$

CHAPTER 10: THE ALDOL CONDENSATION OF ACETONE WITH *p*-NITROACETOPHENONE

Scheme 19. Aldol condensation of acetone with *p*-nitroacetophenone

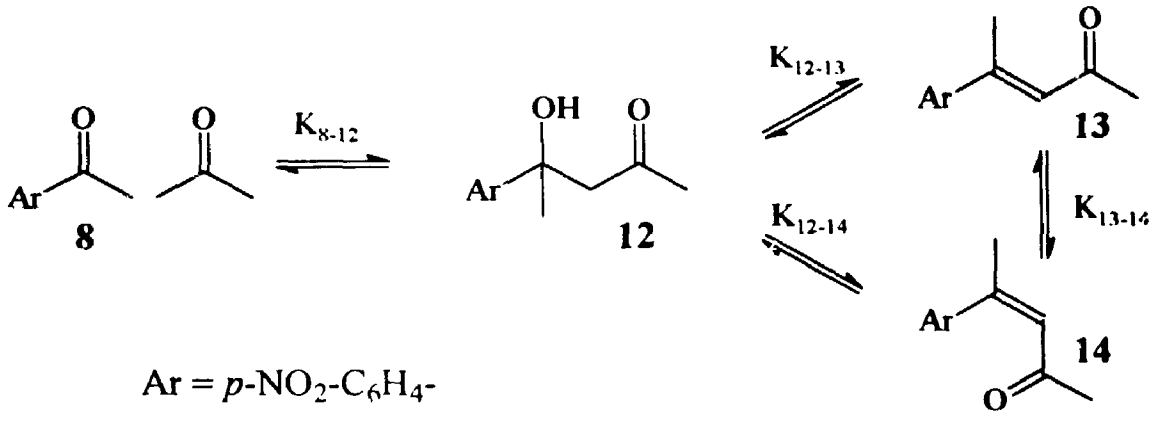

Ar = *p*-NO_2-C_6H_4-

10.1 Kinetics of the hydroxide catalyzed retroaldol cleavage of 4-hydroxy-4-(4-nitrophenyl)-2-pentanone (12)

The hydroxide catalyzed retroaldol cleavage of ketol **12**, the aldol product of acetone enolate with *p*-nitroacetophenone, was studied in dilute aqueous hydroxide by UV spectrophotometry, following the appearance of the *p*-nitroacetophenone chromophore. The change in the chromophore was substantial because of the creation of a carbonyl in conjugation with the aromatic ring. The absorbance-time data were fitted to a single exponential equation and the observed rate constants are listed in Table 34. The kinetics were pseudo-first order and showed a first order hydroxide concentration dependence. The calculated second order rate constant for hydroxide catalyzed retroaldol cleavage of ketol **12** is $k_{12\text{-}8} = 0.301 \pm 0.009\ M^{-1}s^{-1}$.

Table 34. Rate constants for the hydroxide catalyzed retroaldol cleavage of 12.[a]

10^3 [OH^-] (M)	α	β	10^3 λ (s^{-1})	λ / [OH^-] ($M^{-1}s^{-1}$)
99.1	0.704	-0.465	33.2±0.4	0.335±0.005
99.1	0.709	-0.397	30.1±0.3	0.304±0.004
99.1	0.696	-0.329	27.49±0.04	0.277±0.003
9.91	0.761	-0.359	2.843±0.002	0.287±0.014
9.91	0.694	-0.326	2.858±0.001	0.288±0.014
9.91	0.705	-0.330	2.805±0.001	0.283±0.014
0.800[b]	0.699	-0.328	0.276±0.000	0.345±0.008
0.800[b]	0.707	-0.334	0.2613±0.0001	0.327±0.008
0.741[b]	0.695	-0.326	0.2420±0.0001	0.326±0.008
			av	0.301±0.009

[a] In aqueous sodium hydroxide at 25.0 °C; ionic strength 0.1 M maintained with KCl. Following appearance of the *p*-nitroacetophenone chromophore at 261 nm by UV spectrophotometry. Absorbance-time data fitted to $A = \alpha + \beta \exp(-\lambda t)$. Cell length 10.000 cm. [ketol]$_t$ = 5.51 μM

[b] [OH^-] taken as $10^{(pH-14)}$ where the pH was measured for the reaction solution following the run

10.2 Kinetics of the hydroxide catalyzed isomerization and hydration of E- and Z-4-(4-nitrophenyl)-3-pentene-2-one (13, 14)

The hydroxide catalyzed isomerization and hydration of enones **13** and **14** were studied in dilute alkaline solution by both UV spectrophotometry and HPLC analysis of quenched samples. Isomerization was fast relative to hydration and ketol formation was a commitment to retroaldol cleavage. Both isomerization and hydration kinetics were first-

order in hydroxide concentration.

UV spectrophotometry was used to follow the isomerization and hydration of the enones by following the change in absorbance at the wavelength of the E-enone chromophore. Starting with Z-enone there was an initial increase in absorbance as E-enone was formed, followed by a slower decrease in absorbance as the equilibrium mixture of enones underwent hydration. Starting with E-enone there was a two-phase decrease in absorbance. The absorbance-time data were fitted to a double exponential equation by non-linear least squares. The observed rate constants and pre-exponential terms are listed in Table 35.

HPLC analysis of quenched samples gave concentrations of each of the species present as a function of time. Experiments were run starting with both E- and Z-enones. Both sets of peak integration-time data were analyzed together by non-linear least squares fitting to the chemical equation:

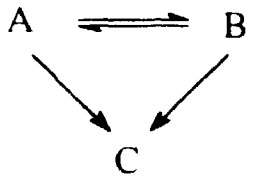

where A = E-enone, B = Z-enone, C = ketol, allowing determination of the individual rate constants. The results of least squares fitting are listed in Table 36. A plot of the data with the lines of best fit is shown in Figure 19.

Table 35. Rate constants for the hydroxide catalyzed isomerization and hydration of enones 13 and 14 followed by UV spectrophotometry.[a]

α	β	$10^4 \lambda_1$ (s^{-1})	γ	$10^6 \lambda_2$ (s^{-1})		$10^3 \lambda_1$ / [OH⁻] ($M^{-1}s^{-1}$)	$10^5 \lambda_2$ / [OH⁻] ($M^{-1}s^{-1}$)
0.079[b]	0.023	1.233±0.031	.204	2.969±0.009		1.244±0.031	2 ·95±0.009
0.078[c]	-0.162	0.741±0.002	0.298	2.718±0.006		0.741±0.002	2.718±0.006
					av	0.743±0.026	2.80±0.12

[a] Reactions carried out in 0.0991 M sodium hydroxide at 25.0 °C; followed by UV spectrophotometry at 305 nm; absorbance-time data were fitted to $A = \alpha + \beta \exp(-\lambda_1 t) + \gamma \exp(-\lambda_2 t)$

[b] starting with E-enone $[E\text{-enone}]_i = 1.89\ \mu M$

[c] starting with Z-enone $[Z\text{-enone}]_i = 2.44\ \mu M$

Table 36. Results of least squares fitting for the HPLC study of the hydroxide catalyzed isomerization and hydration of enones 13 and 14. [a]

[OH⁻] (M)	10^4 k'$_{13\text{-}14}$ / [OH⁻] ($M^{-1}s^{-1}$)	10^4 k'$_{14\text{-}13}$ / [OH⁻] ($M^{-1}s^{-1}$)	10^5 k'$_{13\text{-}12}$ / [OH⁻] [b] ($M^{-1}s^{-1}$)	10^5 k'$_{14\text{-}12}$ / [OH⁻] [b] ($M^{-1}s^{-1}$)	$K_{13\text{-}14}$ [c]
0.100 [d]	1.65±0.06	4.89±0.12	2.73±0.09	2.60±0.24	0.338±0.017
0.050 [e]	1.60±0.05	6.14±0.20	2.44±0.15	2.72±0.58	0.261±0.013
Av	1.62±0.02	5.23±0.56	2.65±0.13	2.62±0.04	0.29±0.04

[a] in aqueous sodium hydroxide at 25.0 °C; ionic strength maintained at 0.1 M with KCl; least squares analysis fit peak integrations for both enones and *p*-nitroacetophenone simultaneously for reaction starting with both Z- and E-enones; the listed rate constants are designated as k' to distinguish them from the corresponding rate constants derived from these and other experiments.

[b] see notes in the main text about the determination of this rate constant.

[c] $K_{13\text{-}14} = k'_{13\text{-}14} / k'_{14\text{-}13}$

[d] other parameters from least squares fitting: [Z-enone]$_i$ = 9±3 μM; [E-enone]$_i$ = 3±1 μM; $\varepsilon_1 = (1.6\pm0.5) \times 10^4$ μM^{-1}; $\varepsilon_2 = (1.7\pm0.6) \times 10^4$ μM^{-1}; $\varepsilon_3 = (1.4\pm0.5) \times 10^4$ μM^{-1}; constraints were [Z-enone]$_i$ = 9.76±0.97 μM; $\varepsilon_1 = (1.55\pm0.15) \times 10^4$ μM^{-1}; $\varepsilon_2 = (1.64\pm0.16) \times 10^4$ μM^{-1}; $\varepsilon_1 = (1.56\pm0.16) \times 10^4$ μM^{-1}

[e] other parameters from least squares fitting: [Z-enone]$_i$ = 9±3 μM; [E-enone]$_i$ = 3±1 μM; $\varepsilon_1 = (1.7\pm0.5) \times 10^4$ μM^{-1}; $\varepsilon_2 = (1.5\pm0.6) \times 10^4$ μM^{-1}; $\varepsilon_3 = (1.4\pm0.5) \times 10^4$ μM^{-1}; constraints were $\varepsilon_1 = (1.55\pm0.15) \times 10^4$ μM^{-1}; $\varepsilon_2 = (1.64\pm0.16) \times 10^4$ μM^{-1}; $\varepsilon_1 = (1.56\pm0.16) \times 10^4$ μM^{-1}

It is important to recognize that the two rate constants $k'_{13\text{-}12}$ and $k'_{14\text{-}12}$ had a strong covariance and that the data did not support an accurate determination of the individual rate constants. The observable rate constant for the slower kinetic phase can be calculated as a function of the four microscopic rate constants. The second order rate constants so obtained are $(2.70\pm0.13) \times 10^{-5}$ and $(2.50\pm0.27) \times 10^{-5}$ $M^{-1}s^{-1}$ for reaction in 0.10 M and 0.05 M sodium hydroxide respectively.

Figure 19. Results of HPLC kinetics for the isomerization and hydration of E- and Z-4-(4-nitrophenyl)-3-pentene-2-one (13, 14) in 0.1 M sodium hydroxide. Full scale in each plot represents 100% of starting material present in that form.

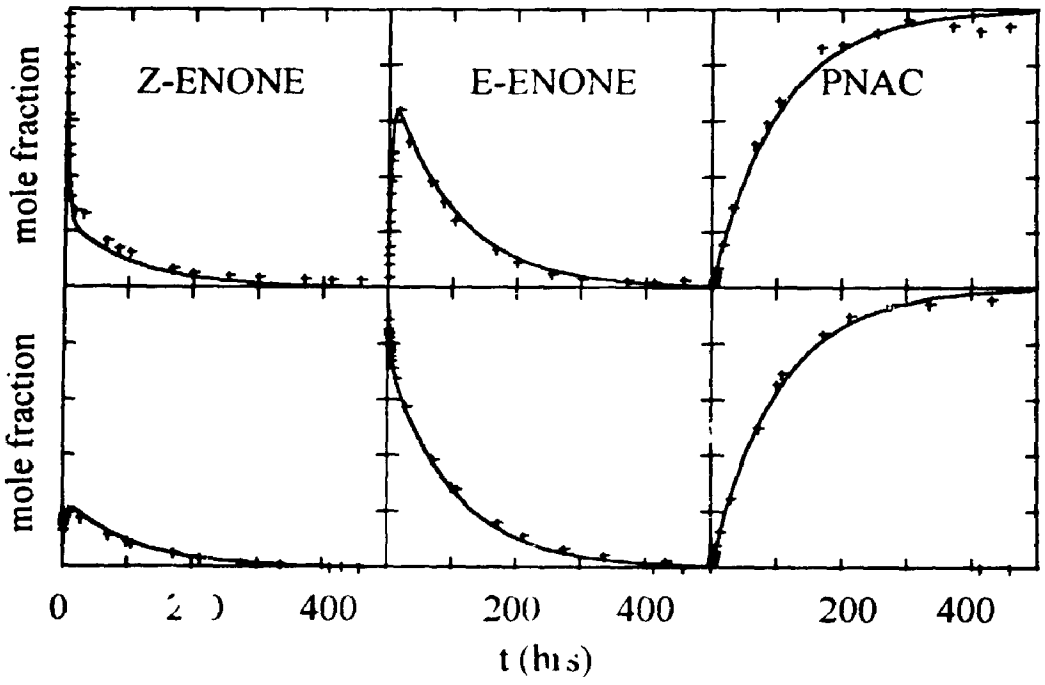

The individual hydration rate constants can now be determined in the same way for both the HPLC and UV experiments. They are calculated by: $k_{13\text{-}14} = k_{obs} / (2 (1 + 1 / K_{13\text{-}14}))$; $k_{14\text{-}13} = k_{obs} / (2 (1 + K_{13\text{-}14}))$. The derivation of these equations has been published previously.[31] The results of these calculations are listed in the summary table at the end of this chapter.

10.3 Kinetics of isomerization and hydration of E- and Z-4-(4-nitrophenyl)-3-pentene-2-one (13, 14) in acid

The kinetics of isomerization and hydration of enones **13** and **14** and dehydration of ketol **12** were studied by HPLC analysis of quenched samples.

The amounts of both enones and the ketol were followed by HPLC analysis in three experiments starting with each of the three compounds. Peak integrations for the three compounds in the three experiments were fit simultaneously to the cyclic equilibrium:

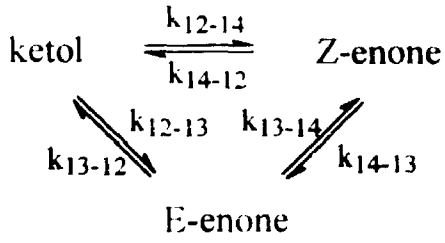

This allowed determination of all six rate constants of which only five are independent. The other is determined by the microscopic reversibility constraint. The results of least squares analysis are listed in Table 37. The lines of best fit to the three experiments are shown in Figure 20.

Table 37. Results of least squares analysis for the HPLC study of the equilibration in acid of ketol 12 and enones 13 and 14. [a, b]

Parameter	Value
$k_{12\text{-}13}$	$(2.02\pm0.07) \times 10^{-6}$
$k_{12\text{-}14}$	$(8.3\pm0.3) \times 10^{-7}$
$k_{14\text{-}12}$	$(5.04\pm0.14) \times 10^{-6}$
$k_{13\text{-}14}$	$(6.97\pm0.16) \times 10^{-6}$
$k_{14\text{-}13}$	$(2.64\pm0.05) \times 10^{-5}$
[ketol]$_1$	31.9±0.8
[Z-enone]$_1$	13.4±0.3
[E-Enone]$_1$	21.6±0.5
ε_{12}	$(1.89\pm0.05) \times 10^{4}$
ε_{14}	$(2.23\pm0.05) \times 10^{4}$
ε_{13}	$(2.35\pm0.05) \times 10^{4}$
Derived constants:	
$k_{13\text{-}12}$	$(3.23\pm0.11) \times 10^{-7}$
$K_{12\text{-}13}$	0.624±0.011
$K_{12\text{-}14}$	0.165±0.004
$K_{13\text{-}14}$	0.264±0.005

[a] rate constants in s^{-1} are pseudo-first order for reaction in 1 M hydrochloric acid; equilibrium constants are unitless; [compound]$_1$ is the starting concentration of enone or ketol in each of the three experiments. ε parameters are the HPLC calibration constants in μM^{-1} to convert peak area to concentration.

[b] constraints place on fitting were. [Z-enone]$_1$ = 15.12±1.5 μM, $\varepsilon_{12} = (1.42\pm0.05) \times 10^4\ \mu M^{-1}$, $\varepsilon_{14} = (1.64\pm0.05) \times 10^4\ \mu M^{-1}$

Figure 20. HPLC results for the equilibration in acid of ketol 12 and enones 13 and 14. Plots are, from the top, starting with ketol, Z-enone, and E-enone. Vertical scale in each plot is the fraction of starting material present in each of the three forms. Full scale is 100% in each case.

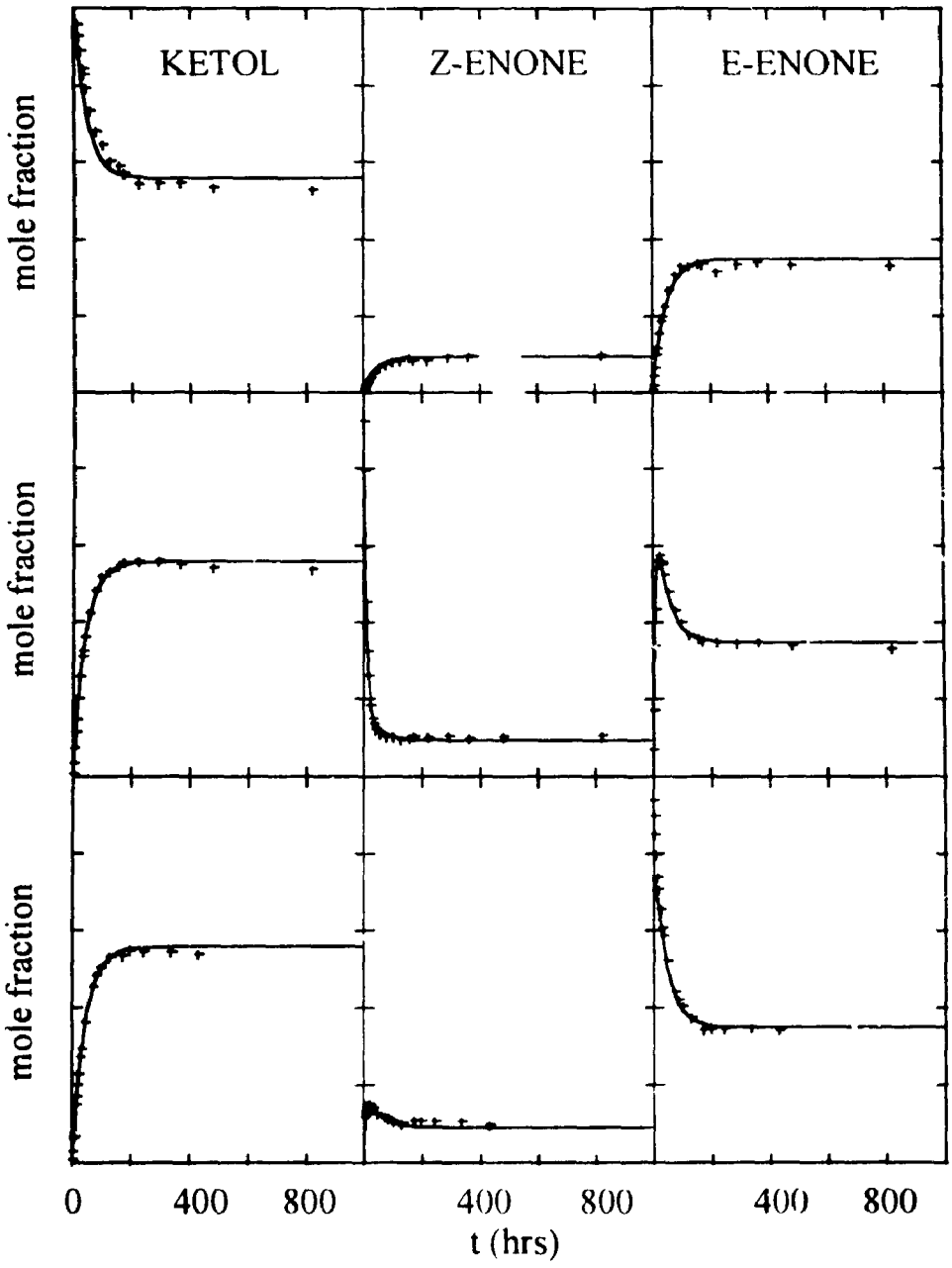

10.4 Determination of the equilibrium constant for the hydroxide catalyzed aldol formation of 4-hydroxy-4-(4-nitrophenyl)-2-pentanone (12)

The equilibrium constant for the aldol reaction of acetone with *p*-nitroacetophenone to give the ketol 4-hydroxy-4-(4-nitrophenyl)-2-pentanone (12) was measured by equilibrating solutions of the two ketones in aqueous base or buffer and determining the concentration of ketol present at equilibrium by HPLC analysis of quenched samples. Equilibration is rapid because the rate of approach to equilibrium is dominated by the rapid retroaldol rate. Because the dehydration to enones is much slower than the aldol formation, it was possible to determine the ketol concentration without interference from enones or subsequent condensation products.

The results of the equilibration experiments are listed in Table 38 along with the calculated equilibrium constants. The acetone concentration was varied to confirm that the peak being followed was indeed the ketol, and that the equilibrium behaved as expected. The consistency of results between experiments with different concentrations validates the method used.

Table 38. Aldol formation equilibrium constant determination for the reaction of acetone with *p*-nitroacetophenone.[a]

[PNAC] [b] (mM)	[acetone] [b] (M)	[ketol] [c] (μM)		10^2 K_{ald} [d] (M^{-1})
2.00 [e]	1.10	26.13±0.13		1.19±0.02
2.00 [e]	1.10	26.17±0.13		1.19±0.02
2.00 [e]	1.10	28.66±0.14		1.30±0.02
2.00 [f]	1.10	24.02±0.12		1.09±0.02
2.00 [f]	1.10	23.72±0.12		1.08±0.02
2.00 [e]	0.11	2.79±0.01		1.27±0.02
			av	1.17±0.04

[a] determined in aqueous solution at 0.1 M ionic strength at 25.0 °C;
[b] determined by amount added to reaction flask
[c] determined by HPLC analysis; errors are estimated from calibration standard error
[d] K_{ald} = [ketol] / ([acetone] [PNAC])
[e] in 0.1 M NaOH
[f] in pH 10 borate buffer, ionic strength maintained with KCl

10.5 Summary of rate and equilibrium constants for the aldol condensation of acetone with *p*-nitroacetophenone.

The rate and equilibrium constants determined in the acid and base catalyzed aldol reactions of acetone with *p*-nitroacetophenone are summarized in Table 39.

Table 39. Summary of rate and equilibrium constants for the aldol condensation of acetone with *p*-nitroacetophenone. [a]

Constant	value	units
$K_{8\text{-}12}$ [b]	$(1.17\pm0.04) \times 10^{-2}$	M^{-1}
$k_{8\text{-}12}$ [c]	$(3.53\pm0.15) \times 10^{-3}$	$M^{-2}s^{-1}$
$k_{12\text{-}8}$ [d]	0.301 ± 0.009	$M^{-1}s^{-1}$
$K_{12\text{-}13}$ [e]	0.624 ± 0.011	
$k_{12\text{-}13}$ [f]	$(1.08\pm0.03) \times 10^{-5}$	$M^{-1}s^{-1}$
$k_{13\text{-}12}$ [g]	$(1.73\pm0.04) \times 10^{-5}$	$M^{-1}s^{-1}$
$K_{12\text{-}14}$ [e]	0.165 ± 0.004	
$k_{12\text{-}14}$ [h]	$(1.06\pm0.03) \times 10^{-5}$	$M^{-1}s^{-1}$
$k_{14\text{-}12}$ [i]	$(6.41\pm0.15) \times 10^{-5}$	$M^{-1}s^{-1}$
$K_{13\text{-}14}$ [j]	0.270 ± 0.014	
$k_{13\text{-}14}$ [k]	$(1.61\pm0.04) \times 10^{-4}$	$M^{-1}s^{-1}$
$k_{14\text{-}13}$ [k]	$(5.4\pm0.4) \times 10^{-4}$	$M^{-1}s^{-1}$
Acid catalyzed rate constants		
$k^{H+}_{12\text{-}13}$ [l]	$(2.02\pm0.07) \times 10^{-6}$	s^{-1}
$k^{H+}_{13\text{-}12}$ [l]	$(3.23\pm0.11) \times 10^{-6}$	s^{-1}
$k^{H+}_{12\text{-}14}$ [l]	$(8.3\pm0.3) \times 10^{-7}$	s^{-1}
$k^{H+}_{14\text{-}12}$ [l]	$(5.04\pm0.14) \times 10^{-6}$	s^{-1}
$k^{H+}_{13\text{-}14}$ [l]	$(6.97\pm0.16) \times 10^{-6}$	s^{-1}
$k^{H+}_{14\text{-}13}$ [l]	$(2.64\pm0.05) \times 10^{-5}$	s^{-1}

[a] subscripts on all constants refer Scheme 19

[b] determined from base catalyzed aldol formation

[c] calculated from $k_{8\text{-}12} = k_{12\text{-}8} \times K_{8\text{-}12}$

[d] determined from base catalyzed retroaldol cleavage

[e] determined from acid catalyzed equilibration of ketol **12** and enones **13** and **14**

[f] calculated from $k_{13\text{-}12} \times K_{12\text{-}13}$

[g] weighted average of values determined from UV and HPLC experiments; individual rate constants were determined from the observable rate constant by $k_{13\text{-}12} = k_{obs} / (2\ (1 + K_{13\text{-}14}))$

[h] calculated from $k_{14\text{-}12} \times K_{12\text{-}14}$

[i] weighted average of values determined from UV and HPLC experiments; $k_{obs} = 2\ k_{14\text{-}12}\ (1 + 1 / K_{13\text{-}14})$

[j] weighted average of values obtained from acid catalyzed equilibration of ketol and enones, and base catalyzed isomerization and hydration of enones

[k] weighted average of values obtained from UV and HPLC base catalyzed isomerization and hydration experiments; values for UV experiments calculated from $k_{13\text{-}14} = k_{obs} / (1 + 1 / K_{13\text{-}14})$; $k_{14\text{-}13} = k_{obs} / (1 + K_{13\text{-}14})$

[l] determined from the acid catalyzed equilibration of ketol **12** and enones **13** and **14**

CHAPTER 11: THE ALDOL REACTION OF *p*-NITROACETOPHENONE WITH ACETONE

Scheme 20. Aldol condensation of *p*-nitroacetophenone with acetone

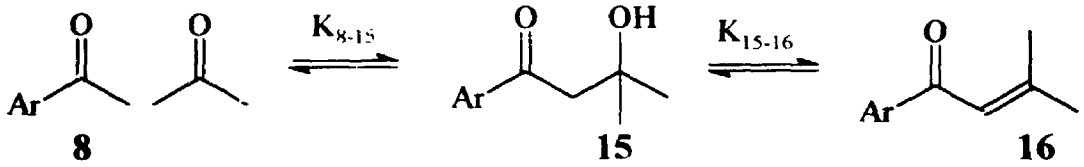

8 **15** **16**

11.1 Kinetics of hydroxide catalyzed retroaldol cleavage of 3-hydroxy-3-methyl-1-(4-nitrophenyl)-1-butanone (15)

The retroaldol cleavage of **15**, the aldol product of *p*-nitroacetophenone enolate with acetone, was studied in dilute aqueous base by following the disappearance of the ketol chromophore by UV spectrophotometry. The change in chromophore is small because there is no change in the conjugation of the system. The chromophore of the ketol is essentially the same as that of *p*-nitroacetophenone; there are only small changes in the chromophore induced by the additional groups of the ketol. This placed two constraints on the experimental conditions. The time for reaction had to be short enough that instrumental drift or similar effects would be negligible and the reaction had to be slow enough that enough points could be collected with an adequate period (filter or smoothing factor) to see a smooth change in absorbance.

The absorbance-time data were fitted to a single exponential equation and the observed rate constants are listed in Table 40. The kinetics were pseudo-first order and showed a first order dependence on hydroxide concentration. The calculated second order

rate constant for hydroxide catalyzed retroaldol of 3-hydroxy-3-methyl-1-(4-nitrophenyl)-1-butanone (**15**) is $k_{15\text{-}8}$ = 1.01±0.05 $M^{-1}s^{-1}$.

Table 40. Rate constants for the hydroxide catalyzed retroaldol cleavage of 15[a]

10^4 [OH^-][b] (M)	α	β	10^4 λ (s^{-1})	λ / [OH^-] ($M^{-1}s^{-1}$)
0.991[c]	0.982	0.038	0.892±0.006	0.90±0.01
0.991[c]	0.977	0.043	0.821±0.006	0.83±0.01
0.991[c]	0.964	0.043	0.817±0.014	0.82±0.01
13.0[d]	0.978	0.033	14.60±0.09	1.12±0.01
13.0[d]	0.983	0.034	15.19±0.09	1.17±0.01
13.0[d]	1.944	0.066	14.33±0.09	1.10±0.01
13.0[d]	0.388	0.013	12.27±0.09	0.94±0.01
13.0[d]	0.977	0.033	14.66±0.08	1.13±0.01
			av	1.01±0.05

[a] In aqueous borate or carbonate buffer at 25.0 °C; ionic strength 0.1 M maintained with KCl. Following ketol chromophore at 268.4 nm by UV spectrophotometry. Absorbance-time data fitted to $A = \alpha + \beta \exp(-\lambda t)$. Cell length 2.000 cm. [ketol]$_i$ = 7.36 μM

[b] [OH^-] taken as $10^{(pH-14)}$ where the pH was measured for the pure buffer

[c] borate buffer: $[H_3BO_3]_{total}$ = 0.05 M

[d] carbonate buffer: $[NaHCO_3]$ = 0.0018 M, $[Na_2CO_3]$ = 0.03232 M

A single experiment followed by HPLC analysis of quenched samples verified that the rate of change in absorbance of the UV kinetics was the rate of retroaldol of the ketol. Given the small change in absorbance and the problems in purification, this check was necessary. The HPLC kinetics showed a smooth first order decrease in the amount of

ketol and a corresponding increase in the concentration of *p*-nitroacetophenone.

11.2 Kinetics of hydroxide catalyzed hydration of 3-methyl-1-(4-nitrophenyl)-2-butene-1-one (16)

The hydroxide catalyzed hydration of the enone **16** was studied by UV spectrophotometry and by HPLC analysis of quenched samples. With only one geometrical isomer, there was no isomerization to observe and the hydration kinetics were simple pseudo-first order with a first order dependence on hydroxide concentration. Hydration to give ketol **15** was a commitment to retroaldol cleavage so that the observed

Table 41. Rate constants for the hydroxide catalyzed hydration of (16).[a]

[OH⁻] (M)	α	β	$10^4 \lambda$ (s^{-1})	$10^3 \lambda$ / [OH⁻] ($M^{-1}s^{-1}$)
0.100[b]	0.566	0.398	3.01±0.01	3.01±0.03
0.100[c]	0.227	0.157	2.589±0.003	2.59±0.03
0.050[b]	0.550	0.402	1.595±0.009	3.19±0.07
0.099[c]	0.232	0.161	2.620±0.008	2.64±0.05
0.099[c]	0.237	0.160	2.916±0.006	2.94±0.06
0.010[c]	0.226	0.156	0.2856±0.0005	2.88±0.14
0.010[c]	0.229	0.159	0.2598±0.0005	2.62±0.13
			av	2.79±0.09

[a] In aqueous sodium hydroxide at 25.0 °C; ionic strength 0.1 M maintained with KCl. Following the disappearance of the enone chromophore at 277.5 nm by UV spectrophotometry. Absorbance-time data fitted to $A = \alpha + \beta \exp(-\lambda t)$. Cell length 10.000 cm.

[b] [enone]$_t$ = 4.94 μM

[c] [enone]$_t$ = 1.98 M

rate constant was simply that for hydration. The results of the least squares analysis of the UV experiments are listed in Table 41. The resulting second-order rate constant for hydroxide catalyzed hydration is $k_{16\text{-}15} = (2.79 \pm 0.09) \times 10^{-3}\ M^{-1}s^{-1}$.

11.3 Kinetics of acid catalyzed hydration of 3-methyl-1-(4-nitrophenyl)-2-butene-1-one (16)

The hydration kinetics of the enone **16** were studied in 1 M hydrochloric acid by HPLC analysis of quenched samples and by UV spectrophotometry.

The equilibrium is a largely a simple A = B isomerization but significant retroaldol was observed by HPLC analysis. The data were fitted to the system in equation 1

$$A \rightleftharpoons B \longrightarrow C \qquad [1]$$

where A = enone, B = ketol, C = PNAC. The peak integration-time data for each of the three compounds from the HPLC analyses was fitted by non-linear least squares. The results of the fitting are listed in Table 42.

Table 42. Results of the least squares fitting for the acid catalyzed hydration of 1-(4-nitrophenyl)-2-butene-1-one (16) followed by HPLC.[a,b]

Parameter	Value
$k_{16\text{-}15}$	$(7.65\pm0.13) \times 10^{-6}$
$k_{15\text{-}16}$	$(1.25\pm0.03) \times 10^{-6}$
$k_{15\text{-}8}$	$(1.45\pm0.06) \times 10^{-7}$
$[enone]_i$	(37.9 ± 3.0)
ε_{16}	$(3.15\pm0.25) \times 10^{4}$
ε_{15}	$(1.73\pm0.14) \times 10^{4}$
ε_{8}	$(1.65\pm0.15) \times 10^{4}$

[a] rate constants are in s^{-1} and are pseudo-first order for reaction in 1 M hydrochloric acid; $[enone]_i$ is the stating concentration of enone. ε parameters are the HPLC calibration constants in μM^{-1} to convert area to concentration.

[b] constraints placed on least squares parameters were: $[enone]_i = 37.9\pm3.0$ μM, $\varepsilon_{16} = (3.18\pm0.03) \times 10^{4}$ μM^{-1}, $\varepsilon_{8} = (1.56\pm0.04) \times 10^{4}$ μM^{-1}

Figure 21. HPLC results of the acid catalyzed equilibration of enone 16 with ketol 15. Plot scaling is in area units and was chosen for convenience. Full scale values for enone, ketol, and PNAC are, respectively, 48 μM, 58 μM, and 15 μM .

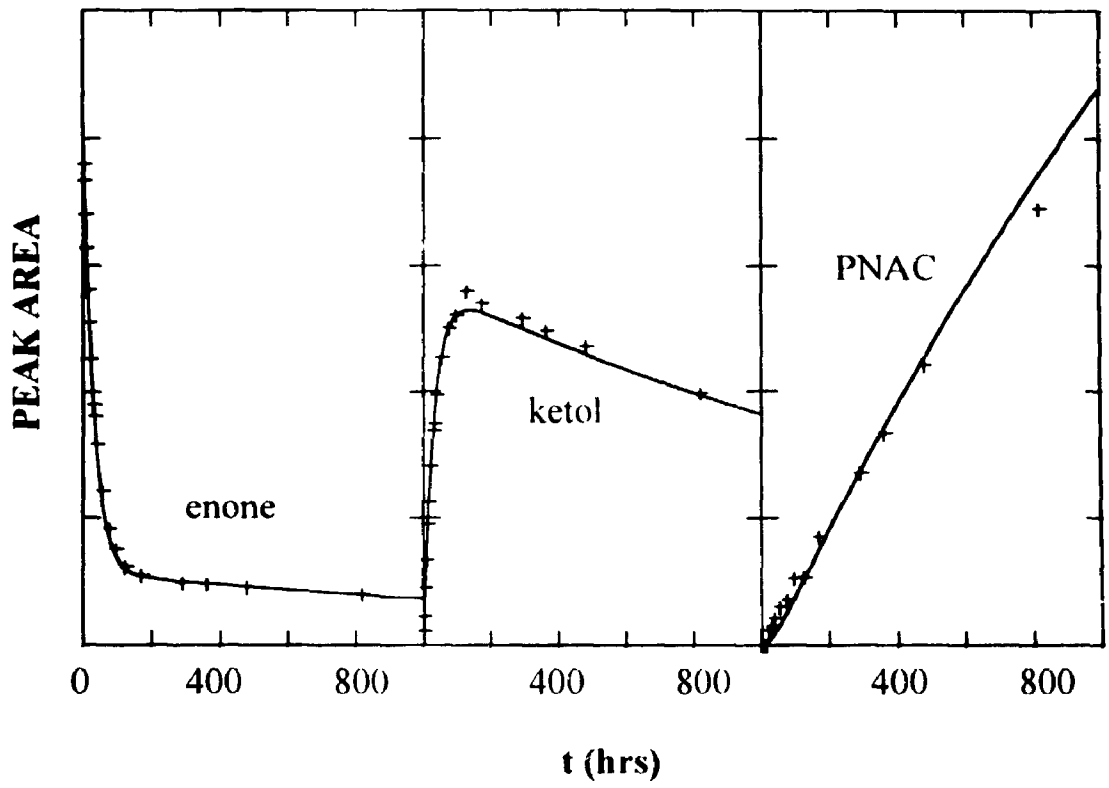

The hydration of the enone was also followed in 0.1 M sodium hydroxide solution by UV spectrophotometry following the disappearance of the enone chromophore. The observed rate constant was (8.83±0.01) × 10^{-6} s^{-1}. Because the observed rate constant is the sum of the forward and reverse rate constants for the reaction, we can compare this value to the $k^{H+}_{15\text{-}16} + k^{H+}_{16\text{-}15}$ (8.90±0.14) × 10^{-6} s^{-1} from Table 42 and find they agree very well.

11.4 Determination of the equilibrium constant for the hydroxide catalyzed aldol reaction of *p*-nitroacetophenone with acetone

The hydroxide catalyzed aldol reaction of *p*-nitroacetophenone with acetone was studied concurrently with the reaction of acetone with *p*-nitroacetophenone in 0.1 M sodium hydroxide and in pH 10 borate buffer and the data obtained are listed in Table 43.

The equilibrium constant obtained for this reaction is $(1.98\pm0.03) \times 10^{-3}$ M^{-1}.

Table 43. Determination of the aldol formation equilibrium constant for the reaction of *p*-nitroacetophenone with acetone.[a]

[PNAC][b] (mM)	[acetone][b] (M)	[ketol][c] (μM)	10^3 K_{ald}[d] (M^{-1})
2.00[e]	1.10	4.49±0.22	2.04±0.11
2.00[e]	1.10	4.60±0.23	2.09±0.11
2.00[e]	1.10	4.10±0.21	1.86±0.10
2.00[f]	1.10	4.28±0.21	1.94±0.10
2.00[f]	1.10	4.41±0.22	2.01±0.10
2.00[e]	0.11	0.43±0.02	1.94±0.10
		av	1.98±0.03

[a] determined in aqueous solution at 0.1 M ionic strength at 25.0 °C;
[b] determined by amount added to reaction flask
[c] determined by HPLC analysis; errors are estimated from calibration standard error
[d] K_{ald} = [ketol] / ([acetone] [PNAC])
[e] in 0.1 M NaOH
[f] in pH 10 borate buffer, ionic strength maintained at 0.1 M with KCl.

11.5 Summary of rate and equilibrium constants for the aldol condensation of *p*-nitroacetophenone with acetone

The rate and equilibrium constants determined in this work are summarized in Table 44.

Table 44. Summary of rate and equilibrium constants for the aldol condensation of *p*-nitroacetophenone with acetone.[a]

Constant	value	units
$K_{8\text{-}15}$[b]	$(1.98\pm0.03)\times10^{-3}$	M^{-1}
$k_{8\text{-}15}$[c]	$(2.00\pm0.10)\times10^{-3}$	$M^{-2}s^{-1}$
$k_{15\text{-}8}$[d]	1.01 ± 0.05	$M^{-1}s^{-1}$
$K_{15\text{-}16}$[e]	0.163 ± 0.004	
$k_{15\text{-}16}$[f]	$(4.56\pm0.19)\times10^{-4}$	$M^{-1}s^{-1}$
$k_{16\text{-}15}$[g]	$(2.79\pm0.09)\times10^{-3}$	$M^{-1}s^{-1}$
Acid catalyzed rate constants		
$k^{H+}_{15\text{-}16}$[h]	$(1.25\pm0.03)\times10^{-6}$	$M^{-1}s^{-1}$
$k^{H+}_{16\text{-}15}$[h]	$(7.65\pm0.13)\times10^{-6}$	$M^{-1}s^{-1}$

[a] all rate and equilibrium constants are for reaction at 25.0 °C in aqueous solution; base catalyzed reactions are at 0.1 M ionic strength; acid catalyzed reactions were at 1.0 M ionic strength

[b] from aldol formation in aqueous base

[c] calculated from $K_{8\text{-}15} \times k_{15\text{-}8}$

[d] from base catalyzed retroaldol

[e] from acid catalyzed hydration equilibrium

[f] calculated from $K_{15\text{-}16} \times k_{16\text{-}15}$

[g] from base catalyzed hydration

[h] from acid catalyzed hydration equilibrium

CHAPTER 12: DISCUSSION AND CONCLUSIONS FOR THE ALDOL CONDENSATIONS

12.1 Discussion

With the four aldol condensations of interest fully characterized, substituent effects in the aldol reaction and the ability of Marcus Theory to predict aldol reaction rates can be assessed.

Table 45 summarizes the predicted and observed equilibrium and rate constants for the four aldol reactions studied, as well as adjusted predicted rate constants. These were calculated in the same way as the predicted rate constants but using the experimentally determined instead of estimated equilibrium constants.

Table 45. Comparison of predicted and measured equilibrium and hydroxide catalyzed rate constants for the aldol reactions. [a]

		$\log(K_{ald} / M^{-1})$ [a]		$\log(k+ / M^{-2}s^{-1})$ [b]			$\log(k- / M^{-1}s^{-1})$ [b]		
Nuc.	Elec.	Pred.	Meas.	Pred.	Adj. [c]	Meas.	Pred.	Adj. [c]	Meas.
acetone	TFA	2.47	3.42	0.67	0.87	0.44	-1.80	-2.55	-2.99
PNAC	PNAC	-2.41	-1.84	-0.80	-0.53	0.40	1.61	1.30	2.24
acetone	PNAC	-2.30	-1.93	-2.37	-2.21	-2.45	-0.07	-0.28	-0.52
PNAC	acetone	-1.26	-2.70	-1.05	-1.76	-2.70	0.21	0.95	0.00

[a] equilibrium constant for the formation of neutral ketol from neutral ketone plus netral ketone

[b] observable macroscopic rate constant

[c] adjusted predicted values are estimated rate constants based on the aldol formation constants determined in this work

From the predictions for the aldol reaction of acetone with trifluoroacetophenone, the estimated K_{ald} and keto! pKa were both significantly different than those determined in this study. Using the experimentally determined values, the Marcus Theory prediction is significantly closer to the observed rate constants: within 0.44 log units for the retroaldol rate. There is another significant source of uncertainty in these calculations. The calculated K_{ald} is very sensitive to the hydration equilibrium constant for TFA and the pKa of the hydrate. Changing the values of either of these constants results in significant changes in the calculated K_{ald}. Therefore the uncertainty in K_{ald} for this reaction is more realistically about 0.5 log units. In spite of these uncertainties, both the revised and original estimates give predictions within approximately an order of magnitude.

The reaction of acetone with PNAC shows very good agreement among the predicted, revised, and actual rate and equilibrium constants.

The reactions of PNAC with both acetone and PNAC do not show as good an agreement. The estimated and observed equilibrium constants are quite different especially for PNAC plus acetone. Although the predicted and revised rate constants for retroaldol do agree within an order of magnitude with the observed rate constants, they just barely do so.

Figure 22 shows the relationship of the aldol formation equilibrium constants (K_{ald}) with the hydration equilibrium constant (K_{H2O}) for the electrophile ketone. The values used are listed in Table 46 and are all reactions with a methyl ketone as the nucleophile.

Table 46. Aldol formation and electrophile hydration equilibrium constants for a series of aldol condensations with methyl ketones and aldehydes as nucleophiles.

Nucleophile	Electrophile	log (K_{hyd} / M^{-1}) [a]	log (K_{ald} / M^{-1})
Me_2CO	$PhCOCH_3$	-6.92 [b]	-2.72 [h]
Me_2CO	PNAC	-6.11 [c]	-1.93 [i]
PNAC	PNAC	-6.11 [c]	-1.84 [i]
PNAC	Me_2CO	-4.60 [d]	-2.70 [i]
Me_2CO	Me_2CO	-4.60 [d]	-1.45 [j]
$PhCOCH_3$	Me_2CO	-4.60 [d]	-2.60 [k]
MeCHO	Me_2CO	-4.60 [d]	-0.40 [b]
$PhCOCH_3$	PhCHO	-2.83 [e]	0.63 [l]
Me_2CO	PhCHO	-2.83 [e]	1.07 [m]
MeCHO	PhCHO	-2.83 [e]	0.59 [n]
Me_2CO	MeCHO	-1.72 [f]	1.59 [b]
$PhCOCH_3$	MeCHO	-1.72 [f]	0.65 [b]
MeCHO	MeCHO	-1.72 [f]	2.60 [o]
Me_2CO	$PhCOCF_3$	1.40 [g]	3.42 [i]
MeCHO	CH_2O	1.60 [e]	7.78 [o]
Me_2CO	CH_2O	1.60 [e]	6.67 [b]
$PhCOCH_3$	CH_2O	1.60 [e]	5.74 [b]

[a] K_{hyd} is the hydration equilibrium constant for the electrophile

[b] Ref. 35

[c] calculated from dimethyl acetal formation equilibrium[57] by the method described in Ref. 58

[d] Ref. 59, 60

[e] Ref. 46
[f] Ref. 61
[g] Ref. 56
[h] Ref. 31
[i] this work
[j] Ref. 41
[k] Ref. 31
[l] Ref. 38
[m] Ref. 62
[n] Ref. 39
[o] Ref. 37

Figure 22. Relationship of aldol formation and electrophile hydration equilibrium constants for a series of aldol reactions with methyl ketones and aldehydes as nucleophiles. Squares represent data determined in this work.

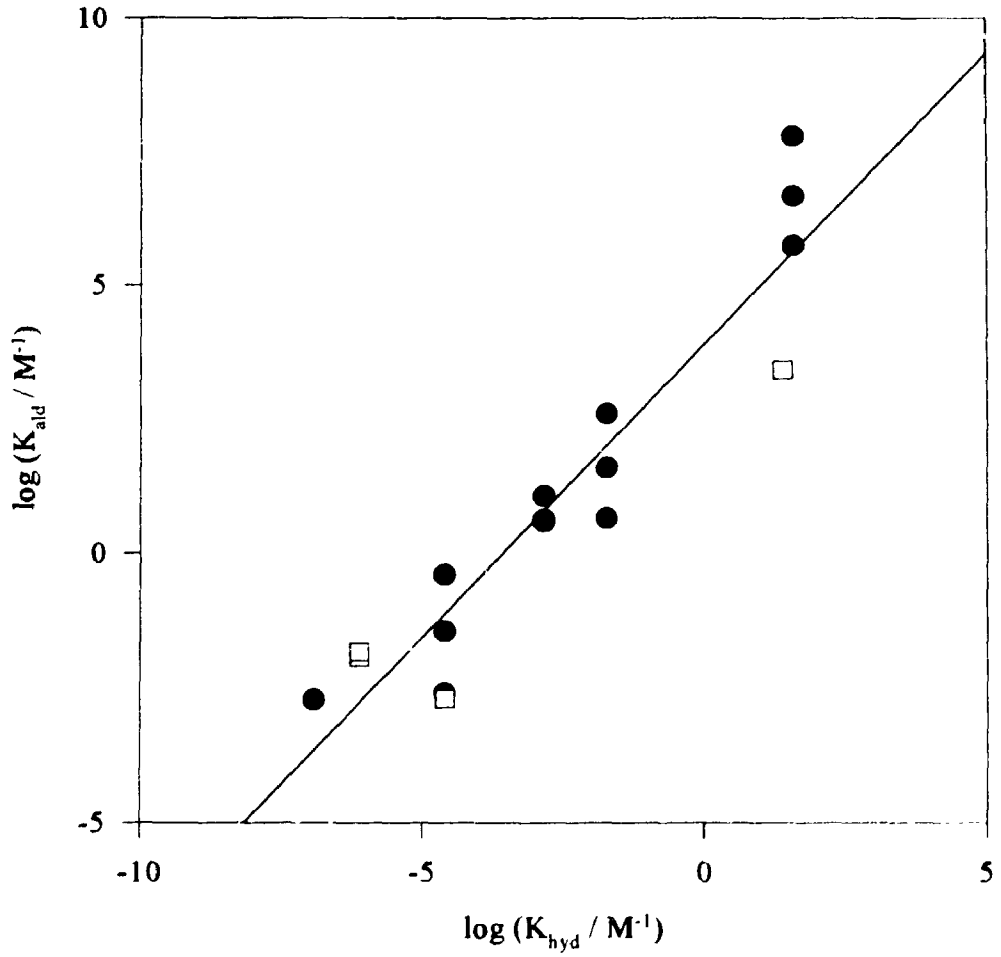

All of the points would appear to fit a common line. The absence of clear multiple lines indicates the lack of sensitivity of K_{ald} to the substituents on the nucleophile methyl ketone. The line of best fit to all of the data is: log K_{ald} = (3.89±1.15) + (1.09±0.10) × log K_{H2O}. This suggests it may often be satisfactory to estimate K_{ald} for reactions with methyl ketones as nucleophile directly from K_{H2O} for the electrophile ketone. This would be easier than using the γ and Δ of Sander and Jencks, though not as accurate where there is a significant amount of information available to determine Δ and γ values.

In general, the reactions with aromatic ketones as nucleophile are below the line of best fit to all of the data. This shows that the nucleophile does affect the observed equilibrium constant so that the Sander and Jencks method should be used where possible.

A comparison of some of the data in Table 46 shows further trends. With acetone as electrophile, the change in log K_{ald} is only 0.1 units on going from acetophenone to *p*-nitroacetophenone as nucleophile. This demonstrates that if one wishes to increase the aldol formation equilibrium constant in a reaction with an aromatic ketone as nucleophile, there will be very little effect from changing the substitution on the nucleophile ring. Likewise, even changing from PNAC to acetone as nucleophile only results in a 1.25 unit change in log K_{ald}.

K_{ald} is far more sensitive to substitution on the electrophile. With acetone as nucleophile, an equilibrium enhancement of 6.14 log units can be achieved by changing from acetophenone to trifluoroacetophenone as electrophile. Changing the electrophile from acetophenone to PNAC increases the equilibrium constant by 0.79 log units, recalling that the same change in nucleophile caused only a 0.1 unit change in log K_{ald}.

Figure 23 shows how the data determined in this study compare with those obtained previously. The rate and equilibrium constants are for reaction within the encounter complex, and the line corresponds to the previously published[20] intrinsic barrier upon which the predictions for these experiments were based. The good agreement of the new points with the theoretical line is further evidence that Marcus theory holds for these aldol reactions.

Figure 23. Marcus plot for the aldol addition step. Filled squares are points determined in this work; all other data were previously published.[20] The line calculated from the published intrinsic barrier, 10.17 in units of log k

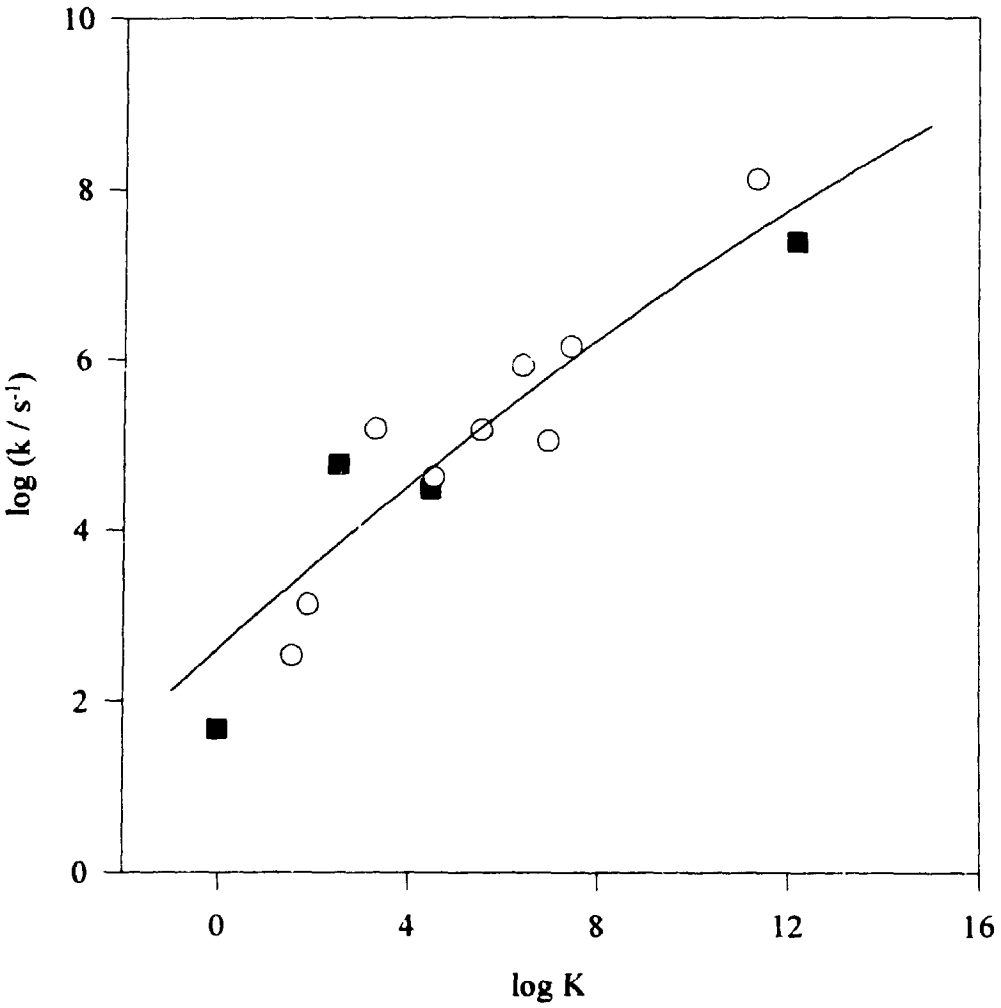

12.2 Conclusions

The equilibrium and hydroxide catalyzed rate constants have been determined for

four previously unstudied aldol condensations. In addition to adding to the list of fully characterized aldol condensations, this has allowed the evaluation of the use of Marcus Theory in the prediction of the rates of aldol reactions.

The best method for enhancing the reactivity of an aldol reaction is to use electron-withdrawing substituents on the electrophile ketone (or aldehyde). This will achieve a much greater enhancement of reactivity than a comparable change of the nucleophile. In particular, reactivity was greatly enhanced for trifluoroacetophenone compared to the other ketone electrophiles.

Marcus Theory has worked well in the prediction of the rates of the reactions studied. Errors and uncertainties in the estimations of equilibrium constants and ketol pKa's are the greatest source of trouble because the accuracy of the predictions depend heavily on the accuracy of these estimations. When one must use estimated formation equilibrium constants and ketol pKa's, Marcus Theory can be expected to give predicted rate constants within approximately an order of magnitude of the actual value.

Where the data exist for good estimates, or where there are experimental values for formation equilibrium constants and ketol pKa's, the agreement of experiment with Marcus Theory predictions is expected to be better. As a larger body of rate and equilibrium data is accumulated, a more complete analysis may make it possible to estimate adjustments to the intrinsic barrier. These adjustments could be used to account for variation in steric hindrance of either the nucleophile or the electrophile, and improve the accuracy of predictions. This would obviously increase the utility of Marcus Theory in this type of prediction.

Marcus Theory has been applied to acetal and orthoester hydrolysis, aldol condensations, simple proton transfers,[17] E2 eliminations,[24] and other reactions.[59,63]

The use of Marcus theory to describe more than simple atom transfers has been criticized by Ritchie.[64] The theoretical justification for the use of the theory for more complicated reactions has lagged behind the application of the theory to such problems. It has been found, however, that Marcus theory works empirically for reactions for which it was not designed. Although Marcus theory may not be an accurate model for such reactions, it is often more important that the theory provide useful predicitions and this it does in a broad array of applications.

As more and more sophisticated computational packages become available and computer power increases, the importance of such a simple method as Marcus Theory may decline. Marcus Theory's ability to make useful predictions about useful reactions can be exploited today with comparative ease. This is its greatest strength.

CHAPTER 13: EXPERIMENTAL

13.1 Synthesis of ketols and enones

13.1.1 Materials and equipment

Solvents and salts were BDH reagent grade unless otherwise noted. All other chemicals were from Aldrich.

THF was dried by refluxing over sodium, and distilling. Methylene chloride was dried by passage over Activity I basic alumina. DMF was dried by fractional distillation at reduced pressure from calcium hydride. Diisoproplyamine and triethylamine were dried and purified by fractional distillation from phenyl isocyanate,[65] and stored under nitrogen. Acetone was spectrophotometric grade and was used without further purification. *p*-Nitroacetophenone was recrystallized first from methanol and then from petroleum ether - acetone. Trimethylsilyl chloride was distilled prior to use and stored under nitrogen. The sodium bicarbonate solution was saturated and ice cold. The aqueous hydrochloric acid was 1.5 M and ice cold.

Syringes were stored in a 100 °C oven and then flushed with nitrogen and allowed to cool before use. All other glassware was flame dried with alternating evacuation and nitrogen flushing.

13.1.2 Preparation of 1,1,1-trifluoro-2-hydroxy-2-phenyl-4-pentanone (2)

n-Butyllithium (8.7 mL × 2.3 M, 20 mmol) in hexane was added via syringe to 50 mL dry THF in a 250 mL round-bottomed flask under nitrogen in a dry ice - acetone bath.

Dry diisopropylamine (2.80 mL, 20 mmol) in 20 mL dry THF was added via syringe to the flask and stirred for 15 min. Acetone (1.48 mL, 20 mmol) in 20 mL dry THF was added via syringe over 15 min and stirred for 30 min. Trifluoroacetophenone (2.67 mL, 19 mmol) in 20 mL dry THF was added via syringe over 15 min and stirred for 1 h. Acetic acid (2.34 mL, 40 mmol) in 10 mL water was then added dropwise via syringe over 5 min and the mixture was allowed to warm to room temperature with continued stirring. The mixture was poured into 100 g ice water and the phases were separated. The aqueous phase was extracted with 4 × 50 mL-portions of ethyl acetate. The combined organic extracts were dried first with 2 × 50 mL saturated aqueous sodium chloride and then over anhydrous magnesium sulphate. Rotary evaporation at reduced pressure gave an oil (3.71 g, 80%) which solidified on standing. This was recrystallized twice from 20% diethyl ether in *n*-hexane to give white crystals (mp 57.0 - 57.5 °C) identified by NMR, IR, and MS to be the desired ketol. Subsequently, a synthesis by a different method appeared.[52] The physical and spectroscopic properties were in agreement.

UV (CH_3CN): λ_{max} : 211.9 nm, ε_{max}: 3011, $\varepsilon_{256.7}$: 230, $\varepsilon_{261.2}$: 221. ^1H NMR ($CDCl_3$, 300 MHz) δ 2.18 (s, 3H), 3.19 (d, 1H, J = 17.2 Hz), 3.35 (d, 1H, J = 17.2 Hz), 5.44 (s, 1H), 7.37 (m, 3H), 7.55 (m, 2H); ^{13}C NMR ($CDCl_3$, 75.46 MHz) δ: 32.05, 45.05, 75.97 (q, J = 29.2 Hz) 124.44 (q, J = 284.9 Hz) , 126.1, 128.44, 128.79, 137.39, 208.97. IR (KBr) cm^{-1}: 3468, 3069, 2918, 1716, 1406, 1168, 759, 738, 712. MS *m/z* (M^+) calcd for $C_{11}H_{11}F_3O_2$ 232.07112, found 232.07116.

Lit.[52] mp. 56 °C. ^1H NMR ($CDCl_3$, 100 MHz) δ 2.09 (s, 3H), 3.23 (dd, 2H), 5.50 (s,

1H). IR cm^{-1}: 1705, 3460

13.1.3 Preparation of E-2-phenyl-1,1,1-trifluoro-2-pentene-4-one (4)

The E-enone **4** was prepared by photoisomerization of the Z-enone **3** which had been prepared by the literature method.[66] 1.0 g of Z-2-phenyl-1,1,1-trifluoro-2-pentene-4-one (1.0 g) in 10 mL chloroform was irradiated with a Pyrex filtered medium pressure mercury lamp for 20 h. ^1H NMR analysis showed a 1:1 mixture of E- and Z-isomers with no apparent side products. The solution was evaporated to give a yellow liquid which was chromatographed by Low Pressure Column Chromatography using a linear gradient of 0-20% ethyl acetate in hexanes on 60 g of silica gel (Merck 60 PF 254). Fractions were pooled according to TLC analysis and evaporated separately to give yellow liquids shown to be E- and Z-enones respectively by ^1H NMR analysis. Each of the enones was micro-distilled at reduced pressure and characterized by UV, IR, ^1H and ^{13}C NMR, and MS.

Z-Isomer (3): UV (CH_3CN): λ_{max} : 205 nm, ε_{max}: 12583, ε_{247}: 3387. ^1H NMR ($CDCl_3$, 300 MHz) δ 1.88 (s, 3H), 6.69 (q, 1H, J = 1.39 Hz), 7.26-7.30 and 7.38-7.48 (m, 5H); ^{13}C NMR ($CDCl_3$, 75.46 MHz) δ 30.42, 122.78 (q, J = 275 Hz) 128.73, 129.03, 129.86, 130.84, 132.78 (q, J = 4.9 Hz), 138.99 (q, J = 31 Hz), 199.24 IR (neat) cm^{-1}: 1711, 1686, 1282, 1241, 1175, 1139, 707; MS *m/z* (M^+) calcd for $C_{11}H_9F_3O$ 214.0605, found 214.0600.

E-Isomer (4): UV (CH_3CN): λ_{max} : 242 nm, ε_{max}: 8873; ε_{208}: 8167; ^1H NMR ($CDCl_3$, 300 MHz): δ 2.40 (s, 3H), 6.43 (s, 1H), 7.38-7.41 (m, 5H); ^{13}C NMR ($CDCl_3$, 75.46 MHz): δ 30.5, 122.5 (q, J = 276 Hz), 127.7, 128.7, 129.4, 133.3, 134.4 (q, J = 31.5 Hz), 136.2 (q, J = 3.3 Hz), 200.5; IR (neat) cm^{-1}: 3468, 3069, 2918, 1716, 1406, 1168, 769, 712; MS

m/z (M^+) calcd for $C_{11}H_9F_3O$ 214.0605, found 214.0602.

13.1.4 Preparation of 4-hydroxy-4-(4-nitrophenyl)-2-pentanone (12)

n-Butyllithium (13.6 mL × 2.2 M, 30 mmoles) was added via syringe with stirring under a nitrogen blanket to 50 mL of THF in a 250 mL round-bottomed flask in a dry ice - acetone bath. Diisopropylamine (4.25 mL, 29.5 mmoles) in 25 mL of THF was added via syringe to the reaction flask over 5 minutes. Residual diisopropylamine solution was rinsed into the flask with 2 × 2 mL THF portions. The mixture was stirred for 20 min at which time the reaction temperature was -75 °C. Acetone (2.17 mL, 29.5 mmoles) in 25 mL THF was added via dropping funnnel over 20 min followed by 2 × 2mL THF rinses. The reaction temperature was maintained at or below -72 °C during the addition. After stirring for 40 min, *p*-nitroacetophenone (6.6 g, 40 mmoles) in 25 mL THF was added dropwise over 40 min, with the temperature maintained at or below -72 °C. The red-brown solution was stirred for 45 min. Acetic acid (6.86 mL, 60 mmoles) in 20 mL water was added dropwise via dropping funnel over 15 min and then the cooling bath was removed and the mixture was brought to room temperature. The entire mixture was poured into 100 mL of an ice slush and the flask was rinsed with small portions of THF and water. The layers were separated and the aqueous phase was extracted with 3 × 100 mL portions of ethyl acetate. The combined organic extracts were dried with saturated aqueous sodium chloride and then over anhydrous magnesium sulfate. Evaporation at reduced pressure gave a red oil (8.2 g) which solidified on long standing. ^{1}H NMR analysis of the solid showed the desired ketol and *p*-nitroacetophenone in a 7.8:1 ratio in addition to some residual solvent

Crude ketol (2.0 g) was dissolved in hot diethyl ether and then the flask was cooled in dry ice. The flask was slowly warmed and continuous scratching with a glass rod induced rapid crystallization. The flask was again heated on a steam bath and then cooled to room temperature and then to 0 °C. Crystals formed with scratching, were collected (0.58 g, 29%) and recrystallized a second time (0.38 g, 66%) giving a pale yellow powder (mp 53-4 °C). The combined mother liquors, still mainly ketol, were retained for later recovery.

UV (CH_3CN): λ_{max} : 271 nm, ε_{max}: 9220, ε_{214}: 5860; ^1H NMR ($CDCl_3$, 300 MHz) δ 1.50 (s, 3H), 2.11 (s, 3H), 2.92 (d, 1H, J = 17 Hz), 3.18 (d, 1H, J = 17 Hz), 4.64 (s, 1H), 7.58 (d, 2H, J = 9 Hz), 8.17 (d, 2H, J = 9 Hz); ^{13}C NMR ($CDCl_3$, 75.46 MHz) δ 30.47, 31.69, 53.49, 73.23, 123.67, 125.48, 146.87, 154.82, 210.04; MS *m/z* (M^+) calcd for $C_{11}H_{13}NO_4$ 223.0845, found 223.0849; Anal. for $C_{11}H_{13}NO_4$ calcd C 59.19%, H 5.87% found C 59.23%, H 5.99%.

13.1.5 Preparation of E-4-(4-nitrophenyl)-3-pentene-2-one (13)

4-Hydroxy-4-(4-nitrophenyl)-2-pentanone (0.14 g) was mixed with 2 g silica gel, a few millilitres of methanol and twelve drops of concentrated hydrochloric acid in an evaporating dish. The mixture was heated on a steam bath for 1 h and the product was extracted by washing the silica with ethyl acetate in a sintered glass funnel. Evaporation of the extract gave yellow crystals (0.12 g, 93%, 5.5:1 E:Z) which were recrystallized from methanol giving a 36 mg first crop (E > 98% by NMR analysis) which was used for characterization.

UV (CH_3CN): λ_{max} : 302 nm, ε_{max}: 1 400. ^1H NMR ($CDCl_3$, 300 MHz) δ 2.31 (s, 3H),

2.52 (d, 3H, J = 1.3 Hz), 6.51 (d, 1H, J = 1.3 Hz), 7.60 (d, 2H, J = 9.0 Hz), 8.22 (d, 2H, J = 9.0 Hz); ^{13}C NMR ($CDCl_3$, 75.46 MHz) δ 18.3, 32.3, 123.9, 126.9, 127.4, 148.0, 149.0, 151.0, 198.5; MS m/z (M^+) calcd for $C_{11}H_{11}NO_3$ 205.0739, found 205.0734.

13.1.6 Preparation of Z-4-(4-nitrophenyl)-3-pentene-2-one (14)

E-4-(4-nitrophenyl)-3-pentene-2-one (0.45 g), prepared by the method above but without recrystallization, was dissolved in 15 mL spectroscopic grade chloroform in a screw capped test tube. The sample was irradiated for 5 h with a Pyrex filtered medium pressure mercury lamp, when ^{1}H NMR analysis showed the isomers present in the ratio 1.4:1 Z:E. The chloroform solution was mixed with 2 g silica gel and evaporated to dryness in vacuo.

The isomer mixture, adsorbed on silica, was loaded on a column of 60 g silica gel (60 PF 254) and eluted under low pressure with a 0-50% linear gradient of ethyl acetate in hexanes. Fractions were pooled according to TLC analysis and evaporated to dryness giving purified E isomer (0.139 g, 31%) and Z-isomer (0.172 g, 38%). The E-isomer solidified immediately as a pale yellow solid, and the Z-isomer remained an oil. Some strongly adsorbed material remained at the head of the column and was not isolated.

The Z-isomer was dissolved in 2 mL diethyl ether and the flask was chilled in dry ice. Crystals formed but did not persist on warming to room temperature or water ice temperature. The flask was again chilled in dry ice and the supernatant removed by Pasteur pipette. The flask was warmed to room temperature and 5 mL diethyl ether was added. The resulting solution was filtered through a Gelman 1 µm glass fibre syringe filter to remove suspended impurites and then the solvent was removed under reduced pressure.

Fresh diethyl ether (1.5 mL) was added under dry nitrogen and the flask was chilled in dry ice. When the crystals had formed, the ether was removed by vacuum with the flask kept chilled. The crystals remained solid in the absence of solvent on warming to room temperature. The solid (0.134 g, 78%) was collected and charcterized. mp: 43.5-44.5 °C. UV (CH_3CH): λ_{max} : 216 nm, ε_{max}: 12700, ε_{281}: 10900 ^{1}H NMR ($CDCl_3$, 300 MHz) δ 2.01 (s, 3H), 2.16 (d, 3H, J = 1.5 Hz), 6.27 (d, 1H, J = 1.5 Hz), 7.31 (d, 2H, J = 9.8 Hz), 8.20 (d, 2H, J = 9.8 Hz); ^{13}C NMR ($CDCl_3$, 75.46 MHz) δ 27.0, 31.1, 123.7, 127.8, 128.0, 147.4, 148.1, 150.6, 197.7; ^{13}C/^{1}H HETCOR: correlation between C(123.7) and H(8.20), C(127.8) and H(6.27), C(128.0) and H(7.31). MS *m/z* (M^+) calcd for $C_{11}H_{11}NO_3$ 205.0739, found 205.0738

13.1.7 Preparation of 1-(4-nitrophenyl)-1-trimethylsilyloxy-ethene

The trimethylsilyl enol ether of *p*-nitroacetophenone has previously been synthesized[67] by a literature method,[68] but its spectroscopic properties and detailed synthesis have not been published. The generosity of Dr. Tidwell for providing the experimental details for its preparation[69] is greatly appreciated.

p-Nitroacetophenone (10.0 g, 60.6 mmoles) was dissolved in 50 mL dry DMF in a 250 mL three-neck round-bottomed flask. Triethylamine (20.2 mL, 0.147 mol) was added via syringe to the flask. Trimethylsilyl chloride (8.4 mL, 90 mmoles) was added via syringe and the mixture was refluxed for 3 h during which a white precipitate formed. The mixture was allowed to cool to room temperature for 2 h and was then chilled in ice.

The mixture was transferred to a 1 L separatory funnel and 200 mL of cold petroleum ether was added, extracting the DMF into the aqueous layer and the colored

product into the organic layer. The aqueous layer was drained off and the organic layer was twice extracted with 200 mL bicarbonate solution. The combined aqueous washes were back-extracted with 100 mL petroleum ether. The combined organic extracts were extracted sequentially with 100 mL bicarbonate, 100 mL hydrochloric acid, and 100 mL bicarbonate. The red-brown organic layer was dried over calcium chloride and then evaporated to give a reddish liquid (12.13 g, 84%) which showed 0.5% *p*-nitro-acetophenone by ^{1}H NMR analysis. The product was distilled at 1.15 mm Hg and 117°C to give 11.2 g of a clear orange-yellow liquid. The boiling point and NMR agreed with that of Tidwell.[69]

Unlike the preparations of House[68] and Tidwell,[67,69] no immediate solid formation was observed. An earlier attempt which yielded only 10% showed considerable precipitate formation when using older and less scrupulously dry DMF. It is likely that immediate precipitate formation is the result of rapid hydrolysis of the trimethylsilyl chloride by residual water while the slower formation results from the desired reaction.

13.1.8 Preparation of 3-hydroxy-1,3-bis-(4-nitrophenyl)-1-butanone (9)

p-Nitroacetophenone (1.652 g, 10 mmol) was dissolved with stirring in 80 mL of methylene chloride in a 250 mL round-bottomed flask. The flask was chilled in an ice bath and titanium tetrachloride (1.10 mL, 10 mmol) was added via syringe. 1-(4-nitrophenyl)-1-trimethylsiloxy-ethene (2.37 g, 10 mmol) in 40 mL methylene chloride was added with stirring via addition funnel over 20 min. After 1 h, the flask was warmed to room temperature and stirred for 45 h.

The reaction mixture was poured into 150 mL water and 150 mL of diethyl ether

was added. The layers were separated and the aqueous phase was extracted with 2 × 100 mL portions of ether. The combined organic extracts were dried with 2 × 100 mL portions of saturated sodium chloride and then over anhydrous sodium sulfate. Rotary evaporation at reduced pressure gave 3.56 g (126%) of a reddish-brown solid.

A 1.5 g portion of the crude product was purified by Low Pressure Column Chromatography on 175 g silica gel (60 PF 254) in a 2.5 × 60 cm column, eluting with a 0 - 100% linear gradient of ethyl acetate - hexanes (1.5 L total volume). Fractions were pooled according to TLC analysis and the ketol fraction was evaporated to give 0.49 g (33%) of an orange-brown solid which was recrystallized from acetone - petroleum ether. The identity was confirmed to be 9 by ^{1}H and ^{13}C NMR and MS.

UV (CH_3CN): λ_{max} : 268 nm, ε_{max}: 20000. ^{1}H NMR ($CDCl_3$, 300 MHz) δ 3.46 (d, 1H, J = 17.8 Hz), 3.82 (d, 1H, J = 17.8 Hz), 4.45 (s, 1H), 7.63 (d, 2H, J = 8.6 Hz), 8.04 (d, 2H, J = 8.6 Hz), 8.17 (d, 2H, J = 8.6 Hz), 8.30 (d, 2H, J = 8.6 Hz); ^{13}C NMR ($CDCl_3$, 75.46 MHz) δ 30.7, 49.5, 73.5, 123.8, 124.1, 125.5, 129.2, 140.7, 147.0, 150.8, 154.6, 198.9; COSY: correlation between doublets at 7.63 and 8.17 ppm and between 8.04 and 8.30 ppm. $^{13}C/^{1}H$ HETCOR: correlation between C(123.8) and H(8.17), C(124.1) and H(8.30), C(125.5) and H(7.63) , C(129.2) and H(8.04). MS m/z (M^+) calcd for $C_{16}H_{14}N_2O_6$ 330.0852, found 330.0849.

13.1.9 Preparation of 3-hydroxy-3-methyl-1-(4-nitrophenyl)-1-butanone (15)

Acetone (0.739 mL, 10.0 mmol) was added via syringe to 80 mL methylene chloride under nitrogen in a 250 mL three-neck round-bottomed flask chilled in an ice bath. Titanium tetrachloride (1.10 mL, 10.0 mmol) was added via syringe and the

mixture was stirred for 20 min.

1-(4-nitrophenyl)-1-trimethylsiloxy-ethene (2.37 g, 10.0 mmol) in 40 mL methylene chloride was added dropwise from an addition funnel over 1 h. The reaction was stirred at ice temperature for an additional 2 h after which TLC analysis showed no further reaction. The reaction was quenched by pouring into 200 mL cold water. This was transferred to a 1 L separatory funnel with 200 mL cold ether. The layers were separated and the aqueous layer extracted with 2 × 150 mL portions of ether. The combined organic extracts were dried with saturated aqueous NaCl and then over anhydrous sodium sulfate. Evaporation gave a thick reddish-yellow oil (2.11 g, 95%) which ^{1}H NMR indicated was mainly the desired ketol. Attempts to obtain crystals failed.

The ketol was purified by Low Pressure Column Chromatography on silica gel (Merck 60 PF 254) eluting with a linear gradient of 0-50% ethyl acetate in hexanes. Fractions were pooled according to TLC analysis and evaporated to give a viscous oil. Attempts to obtain crystals failed. No purified yield was obtained. The ketol's identity was confirmed by ^{1}H and ^{13}C NMR and MS.

UV (CH_3CN): λ_{max} : 267.8 nm, ε_{max}: 13500. ^{1}H NMR ($CDCl_3$, 300 MHz) δ 1.34 (s, 6H), 3.17 (s, 2H), 3.6 (br s, 1H), 8.09 (d, 2H, J = 9.1 Hz), 8.29 (d, 2H, J = 9.1 Hz); ^{13}C NMR ($CDCl_3$, 75.46 MHz) δ 29.5, 49.5, 69.9, 123.8, 129.1, 129.2, 141.6, 150.4, 199.6;. MS *m/z* (M^++1) calcd for $C_{11}H_{14}NO_4$ 224.0923, found 224.0927.

13.2 UV Kinetics

Kinetics followed by UV spectrophotometry were carried out using a Cary 210 UV/Visible spectrophotometer with a thermostatted (water jacket) cell holder and thermal

isolator plates. A Neslab Exacal EX-300 circulating bath at 24.8 °C maintained the cell temperature at 25.0±0.1 °C as monitored by a thermistor in the cell holder. Cells were Far-UV Spectrosil in 1, 2, 5, and 10 cm lengths.

Reactions were initiated by injection of a stock solution of substrate from a microsyringe into the cell containing all other reactants, which had been in the thermostatted cell holder for at least 15 min. The volume and concentration of stock solutions were adjusted to give suitable injection volumes, reactant concentrations, and absorbance ranges. Mixing was accomplished for most reactions by repeated rapid inversion of the cell. Very rapid reactions which could be carried out in 1-2 cm cells were started by dispensing the injection solution from the syringe onto the flattened end of a glass rod, which was rapidly plunged into the cell to effect mixing.

Digital absorbance data were taken from the Digital Interface Port of the Cary 210 and stored by one of two methods. Initially a Dynabyte BC_2 controller board stored absorbance-time data until the completion of a run when the data were transferred to an IBM-compatible microcomputer for permanent storage and processing. Later, a London Research and Development Corp. 24 bit I/O board coupled with a custom adapter board, permitted direct capture and storage with an IBM compatible microcomputer. A Best Power Technologies 1.3 kVA Fortress Uninterruptible Power Supply provided backup for both the Cary spectrophotometer and data capture computer.

All reactions were carried out under pseudo-first order conditions and data were collected for ten half lives unless slow reaction rates made this prohibitive.

Data were fitted to the appropriate equation using computer programs employing

weighted least squares. Direct, semi-log, and residual plots of the experimental data and calculated lines were made as appropriate.

13.3 HPLC Kinetics

13.3.1 Samples

Reactions followed by HPLC analysis were carried out in suitable reaction vessels which were kept at 25.0±0.1 °C in a Neslab Exacal EX-300 thermostatted water bath. Samples were withdrawn at intervals and quenched with an appropriate quench solution.

13.3.2 Quench solutions and procedures

Quench solutions for reactions in base were aqueous potassium dihydrogen orthophosphate, citric acid, or phosphoric acid. Quench solutions for reactions in acid were aqueous disodium hydrogen orthophosphate, trisodium citrate, or sodium hydroxide and trisodium citrate. Concentrations of quench solutions were chosen so that equal volumes of sample and quench solutions would give buffered quenched solutions.

The buffer pH was chosen to minimize reaction after quenching. Rapid retroaldol in reactions involving the ketols 3-hydroxy-3-methyl-1-(4-nitrophenyl)-1-butanone (**15**) or 3-hydroxy-1,3-bis-(4-nitrophenyl)-1-butanone (**9**) required a quenched solution to be below pH 5 which was the reason for the use of citrate buffers.

Reactions run in hydroxide solution or basic buffer had 0.5 mL aliquots of reaction solution injected via Hamilton syringe into 2 mL serum capped autosampler vials which contained 0.5 mL of the appropriate quench solution. The quench solutions were dispensed either by a Gilson 231-401 autosampling injector operating as a dispensor or by

a 500 μL Hamilton syringe.

Reactions run in acid had 0.5 mL aliquots transferred via Hamilton syringe to empty 2 mL autosampler vials which were chilled in ice. Quench solution (0.5 mL) was then injected into the vials via syringe. The quench solution for the reactions run in 1 M hydrochloric acid was 0.9 M sodium hydroxide and 0.067 M trisodium citrate and would have caused significant retroaldol in the reactions studied if the quench order was reversed.

13.3.3 Analysis procedures

Quenched samples were usually refrigerated for analysis in groups. Analyses used external standards and were performed in triplicate to allow calculation of sample standard deviations. Eluents were different mixtures of aqueous acetonitrile or aqueous methanol. Analyses involving trifluoroacetophenone were carried out at 0 °C in an ice bath to reduce peak tailing.

The elution conditions for the various experiments, along with the retention times for the various compounds, are listed in Table 47.

Table 47. Eluent composition and compound retention times for HPLC analysis.[a]

Compound	t_R(min)	Eluent
1	2.7	45:55 ACN:H_2O
	1.9	60:40 ACN:H_2O
2	5.2	45:55 ACN:H_2O
	2.7	60:40 ACN:H_2O

3	4.2	60:40 ACN:H_2O
	6.9	60:40 MeOH:H_2O
4	4.2	60:40 ACN:H_2O
	6.4	60:40 MeOH:H_2O
[illegible]	2.6	55:45 ACN:H_2O
	2.2	60:40 ACN:H_2O
	15.9	10-70% MeOH:H2O
9	2.6	55:45 ACN:H_2O
	3.0	60:40 ACN:H_2O
	21.3	10-70% MeOH:H2O
10	7.1	60:40 ACN:H_2O
11	4.7	60:40 ACN:H_2O
12	2.2	55:45 ACN:H_2O
	14.9	10-70% MeOH:H2O
13	3.8	55:45 ACN:H_2O
14	3.1	55:45 ACN:H_2O
15	2.1	55:45 ACN:H_2O
	17.6	10-70% MeOH:H2O
16	5.6	55:45 ACN:H_2O

a separations carried out using a Merck Lichrospher C18 column (4 x 150 mm); separations involving trifluoroacetophenone using 45:55 ACN:H_2O were carried out at water ice temperature; gradient separation using methanol / water was a linear gradient over 20 minutes - the water contained 0.001 M H_3PO_4

13.4 Preparation of Stock Solutions, Buffer Solutions, Aqueous Sodium Hydroxide and Hydrochloride Solutions

13.4.1 Substrate stock solutions

Stock solutions were prepared in spectrophotometric grade methanol or acetonitrile by weighing purified compounds into volumetric flasks and diluting to the mark. These solutions were stored in the refrigerator.

13.4.2 Buffers

Aqueous borate buffers were prepared by addition of aqueous hydroxide to a stock solution of boric acid and potassium chloride, and diluting to the desired volume with 0.1 M potassium chloride solution. The ionic strength was maintained at 0.1 M.

Aqueous carbonate buffers were prepared by mixing appropriate volumes of stock solutions of aqueous sodium carbonate and aqueous sodium hydrogen carbonate, and diluting to the desired volume. The ionic strength was maintained at 0.1 M.

13.4.3 Aqueous sodium hydroxide and hydrochloride solutions

Hydrochloric acid solution was prepared by dilution of concentrated hydrochloric acid (BDH) in nitrogen degassed doubly distilled water. The concentration was determined by triplicate titrations against Trizma base (trishydroxymethylaminomethane) to a Methyl Red endpoint.

Sodium hydroxide solution was prepared by dissolving sodium hydroxide (BDH, reagent grade) in nitrogen degassed doubly distilled water. The concentration was determined by titration with standardized hydrochloride solution to phenolphthalein and

Methyl Red endpoints, and then correcting for carbonate.

13.5 General Methods and Equipment

13.5.1 HPLC

Analysis was carried out on an HPLC system composed of two Waters 510 pumps, a Waters 490 Programmable Multiwavelength Detector, a Waters 680 Automatic Gradient Controller, a Gilson 231-401 Autosampling Injector, Gilson 506C interface and analog-digital converter, with data acquisition and system control from Gilson 715 HPLC Software running on a DataTrain 486SX microcomputer. The column used was a reversed phase Merck LiChrospher 100 RP-18 (5μm). Solvents were vacuum filtered through a 0.22 μM membrane filter prior to use.

13.5.2 Preparative Chromatography

Terochem 1918 silica gel (20-45 μm) was used for gravity column chromatography. Samples were pre-adsorbed on silica and, following evaporation of solvent, were loaded dry on the top of the column.

Low Pressure Column Chromatography was carried out on Merck Art. 7747 60 PF 254 silica gel in 1.5 and 2.5 cm diameter Spectrum columns. A teflon diaphragm pump with an overpressure relief valve, coupled to a variable speed drive unit was used for pumping. An Isco automatic fraction collector was also used to collect fractions of 5-15 mL

13.5.3 NMR Spectroscopy

NMR spectra were taken on Varian XL-200, Gemini 200 or Gemini 300 NMR spectrometers. Chemical shifts were recorded in parts per million (ppm) relative to residual $CHCl_3$ (7.24 ppm) in $CDCl_3$. Common abbreviations were used for the nmr data: s: singlet, d: doublet, t: triplet, q: quartet, dd: doublet of doublets, m: multiplet.

13.5.4 IR Spectroscopy

Infrared spectra were recorded with Perkin-Elmer System 2000 FT-IR or Bruker IFS-32 spectrometers.

13.5.5 UV Spectroscopy

UV spectra were obtained on the Cary 210 already described and on a Shimadzu UV-160 UV-Visible spectrophotometer.

13.5.6 Melting points

Melting points are uncorrected and were determined with a Thomas Hoover capillary melting point apparatus.

13.5.7 Mass spectrometry

Mass spectrometry was carried out on a Finnigan MAT 8250.

13.5.8 Elemental analysis

Elemental analysis was p .formed by Galbraith Laboratories, Inc.

13.5.9 Least squares analysis

Least squares analysis was carried out using FORTRAN programs developed in this lab using the methods of Bevington[70] and Deming.[71] Linear fits used weighted values for both independent and dependent variables. Non-linear fitting assumed that the independent variable was free from error, but used weighted dependent variables.

Extensive modifications were made to the non-linear least squares programs in the course of this work. Provision was made for the imposition of constraints on any parameter(s). This allowed parameters not well defined by the data to be constrained to be close to independently determined values so that a better fit to the other parameters could be obtained. The method used is described by Deming.[71]

The program used to simultaneously fit multiple species in multiple experiments uses functions of the individual rate constants to determine observable rate constants and pre-exponential terms for the change in concentration / integration of each species. This allows the determination of both rate constants in an equilibrium, for example, where otherwise three separate calculations would be required: calculation of the observed rate constant, calculation of the equilibrium constant, and the determination of the individual rate constants from the observed rate and equilibrium constant. Simultaneous fitting is a particular advantage when considering a cyclic equilibrium where the observable pre-exponentials and rate constants are complicated functions of the individual rate constants. Simultaneous fitting also allows each set of data to act as a constraint on the others, which results in much better fits when some of the data are of poor quality.

APPENDICES

APPENDIX I: DETAILS OF MARCUS THEORY ANALYSIS OF DMOP AND TMOA HYDROLYSES

Table 48. pKa values used in Marcus Theory analysis. [a]

Compound	pKa
H_3O^+	-1.74 [b]
H_2O	15.74 [b]
MeOH	16.04 [b]
PhOH	10.00 [b]
CF_3CH_2OH (TFE)	12.40 [b]
Me2C(OMe)(O+(H)Me)	-5.86 [c]
$Me_2C(OMe)(OH)$	14.64 [d]
$(CH_3)_2C(OMe)(O^+H)$	40.00 [e]
$(CH_3)_2C(OMe)_2$	40.00 [e]
MeC(OMe)(OMe)(O+(H)Me)	-9.12 [c]
$CH_3C(OMe)_3$	38.00 [e]

[a] pKa's not determined by others were calculated from linear free energy realtionships; the group contributions (σ^*) are: CH_3- 0.00; CH_3O- 1.81; HO- 1.34; and CH3(H)O+- 5 55. [45,72] ρ^* values are -1.32 for alcohols,[73] -1.8 for protonated alcohols / ethers taken to be the same as ammonium ions,[74] and -1.32 for C-H bonds[24]

[b] Ref. 75

[c] calculated from the pKa of protonated methyl ethyl ether[76] correcting for substituent effects

[d] Calculated from equation for tertiary carbinols[44,45]

[e] Calculated from equation for C-H ionization[24]

Table 49. Equilibrium constants used in the Marcus Theory analysis.

Equilibrium	log K	ΔG
$Me_2C(OMe)_2 + H^+ ==== Me_2C^+OMe + HOMe$	-2.64	3.61 [a]
$Me_2C(OMe)_2 ==== Me_2C^+OMe + {}^-OMe$	-18.18	24.82 [b]
$MeC(OMe)_3 + H^+ ==== MeC^+(OMe)_2 + HOMe$	-0.92	1.26 [c]
$MeC(OMe)_3 ==== MeC^+(OMe)_2 + {}^-OMe$	-16.46	22.48 [d]
$Me_2(OMe)(OH) + MeOH ==== Me_2C(OMe)_2 + H_2O$	-1.42	1.94 [e]
$Me_2(OMe)_2 ==== MeC(OMe)=CH_2 + MeOH$	-2.79	3.81 [f]
$Me_2(OMe)(OH) ==== Me_2C(OMe)=CH_2 + H_2O$	-4.21	5.75 [g]
$MeC(OCH3)_3 ==== CH_2=C(OMe)_2 + MeOH$		11.88 [h]
$MeCOCH_3 ==== MeC(OH)=CH_2$	-8.33	11.37 [i]

[a] determined from k_{H+} / k_{MeOH} where k_{h+} is the specific acid catalyzed rate constant for hydrolysis determined in this work and k_{MeOH} is the rate of trapping of the cation by methanol[77]

[b] calculated from the above equilibrium and the pKa of methanol

[c] determined from incorporation of labelled methanol into trimethylorthobenzoate (TMOB)[78] to determine ratio of k_{H2O} to k_{MeOH} for trapping of cation; k_{H2O} is similar for TMOA[79] and TMOB[80] so k_{MeOH} is assumed to be the same for both. This allows calculation of k_{H2O} for trapping of the cation from TMOA.

[d] calculated from the above equilibrium and the pKa of methanol

[e] calculated from dimethyl acetal formation[58] and methanol addition to acetone[60]

[f] Ref. 81

[g] calculated from acetal-hemicaetal equilibrium and equilibrium above

[h] calculated from free energies of formation of the individual species[82]

[i] Ref. 83

Table 50. Calculation of corner energies for use in Marcus Theory analysis of DMOP and TMOA hydrolyses. Energy in kcal.

		ΔG_{rel} [a]	ΔpKa [b]	ΔG_{pKa} [c]	hydrogen bond [d]			ΔG_{IP} [e]	ΔG_{enc} [f]	ΔG_{Cplx} [g]	ΔG_{desol} [h]	ΔG_{corner} [i]	ΔG_{zeroed} [j]
					pK HA [k]	pK HB [l]	log K [m]	ΔG_{hb} [n]						
Reaction square for acid catalyzed hydrolysis of DMOP - Step 1													
$Me_2C(OMe)(OMe,H_3O^+)$	00				-1 26	-5 86	-3 07	1 78		1 35	3 13		3 13	0 00
$Me_2C(OMe)(O^+(H)Me)$	10		5.56	7 59									7 59	4 46
$Me_2C^+(OMe),OMe,H_3O^+$	01	3 61	15.54	21.23	-1.26	15 54	1 74	-4 79	-2 97	3 94	-3 82	6 13	27 14	24 01
$Me_2C^+(OMe),HOMe$	11	3 61								2.42	2 42		6 02	2 89
Reaction square for uncatalyzed hydrolysis of DMOP - Step 1														
$Me_2C(OMe)(OMe),H_2O$	00												0 00	0 00
$Me_2C(OMe)(O^+(H)Me),OH$	10		19 56	26.71	-5 86	16.04	2.88	-6 36	-2 32	2.83	-5 85		20.86	20 86
$Me_2C(O^+Me),MeO^-,H_2O$	01	3 61	15.54	21 23					-1 64	1.76	0.12	6 13	31.09	31 09
$Me_2C(O^+Me),MeOH,OH$	11	3 61	14 00	19.12	15 54	16.04	-1 93	0 21	-0 98	4 83	4 06		26 79	26 79

		ΔG_{rel} [a]	ΔpKa [b]	ΔG_{pKa} [c]	hydrogen bond [d]			ΔG_{IP} [e]	ΔG_{enc} [f]	ΔG_{Cplx} [g]	ΔG_{desol} [h]	ΔG_{corner}	ΔG_{zeroed} [j]
					pK HA [k]	pK HB [l]	log K [m] ΔG_{hb} [n]						
Reaction square for hydroxide catalyzed hydrolysis of DMOP via E2 elimination - Step 1													
$MeC(OMe)_2(CH_3,OH^-)$	00			0.00					1 76	1 76	7.10	8.86	0 00
$MeC(OMe)_2(CH_2^-,H_2O)$	10		26 00	35 52						0 00		35.52	26 65
$MeC^+(OMe)(CH_3,OH^-),MeO^-$	01	24 82		0 00				-1 26	3.94	2 68	6 13	33 63	24.77
$MeC(OMe)=CH_2,MeO^-,H_2O$	11	3 81	1 54	2 10					1.76	1 76	6 13	13 81	4 94
Reaction square for hydroxide catalyzed hydrolysis of DMOP via E2 elimination - Step 2													
$MeC(OMe)=CH_2,OH^-,H_2O$	00								2 42	2 42	7 10	9 52	0 00
$MeC^+(OMe)(CH_3,OH^-),OH^-$	10	18 92						-1 26	4 59	3 33	6 13	28 38	18 86
$MeC(OH)(OMe)(CH_2^-,H_2O),H_2O$	01	-5 75	26 00	35 52								29 77	20 25
$MeC(OH)(OMe)(CH_3,OH^-)$	11	-5 75							1 76	1 76	7 10	3 11	-6 40
Reaction square for phenol catalyzed hydrolysis of DMOP - Step 1													
$Me_2C(OMe)(OMe\ HOPh)$	00				10 00	-5 86	-2 40	0 86		2 01	2 86		2 86	0 00
$Me_2C(OMe)O^+(H)Me,^-OPh)$	10		15 56	21 25	-5 86	10 00	1 17	-4 01	-2 32	2 42	-3 92		17 34	14 47

		ΔG_{rel} [a]	ΔpKa [b]	ΔG_{pKa} [c]	hydrogen bond [d]				ΔG_{IP} [e]	ΔG_{enc} [f]	ΔG_{Cplx} [g]	ΔG_{desol} [h]	ΔG_{corner} [i]	ΔG_{zeroed} [j]
					pK HA [k]	pK HB [l]	log K [m]	ΔG_{hb} [n]						
$Me_2C^+(OMe)$,(OMe,HOPh)	01	24 82			10 00	15 54	-0 72	-1 44	-1.64	4 18	1 11	6 13	32 06	29 19
$Me_2C^+(OMe)$,HOMe,OPh	11	3 61	10 00	13 66	15 54	10 00	-1 97	0 27	-0.98	4 42	3 70		20 97	18 10
Reaction square for trifluoroethanol catalyzed hydrolysis of DMOF - Step 1														
$Me_2C(OMe)$(OMe HOR)	00				12 40	-5 86	-2 26	0 66		2 01	2 67		2 67	0 00
$Me_2C(OMe)(O^+(H)Me,OR)$	10		17 96	24 53	-5 86	12 40	1 85	-4 95	-2 32	2 42	-4 85		19 68	17 01
$Me_2C^+(OMe)$,(OMe,HOR)	01	24 82			12.40	15 54	-1 25	-0 72	-1 64	4 18	1 82	6 13	32 77	30.11
$Me_2C^+(OMe)$,HOMe,OR	11	3 61	12 40	16 94	15.54	12 40	-1 95	0 25	-0 98	4.83	4 09		24 64	21 97
Reaction square for acid catalyzed hydrolysis of TMOA - Step 1														
$MeC(OMe)_2$(OMe H_3O^+)	00				-1 26	-9 12	-3 81	2 78		1 11	3 89		3 89	0 00
$MeC(OMe)_2(O^+(H)Me)$	10		8 64	11 80							0 00		11 80	7 91
$MeC^+(OMe)_2$,(OMe,H_3O^+)	01	1 26	15 54	21.23	-1 26	15 54	1 74	-4 79	-1.57	3.53	-2 84	6 13	25 78	21 89
$MeC^+(OMe)_2$,HOMe	11	1 26								2 01	2 01		3 27	-0 63

		ΔG_{rel} [a]	ΔpKa [b]	ΔG_{pKa} [c]	hydrogen bond [d]			ΔG_{IP} [e]	ΔG_{enc} [f]	ΔG_{Cplx} [g]	ΔG_{desol} [h]	ΔG_{corner}	$\Delta G_{revised}$ [j]
					pK HA [k]	pK HB [l]	log K [m]	ΔG_{bb} [n]						
Reaction square for uncatalyzed hyrolysis of TMOA - Step 1													
$MeC(OMe)_2(OMe),H_2O$	00											0.00	0 00
$MeC(OMe)_2(O^+HMe),^-OH$	10		22 64	30 92	-9 12	16 04	3 62	-7 36	-2 32	2 83	-6.85	24 07	24 07
$MeC^+(OMe)_2,MeO^-,H_2O$	01	-0 62	15 54	21 23					-2 32	1.76	-0.56	6.13	26 18	26 18
$MeC(OMe)(O^+Me),MeOH,^-OH$	11	-0 62	14 00	19 12	15 54	16 04	-1 93	0 21	-1 42	4 83	3 63	22 13	22 13	
Reaction square for hydroxide catalyzed hydrolysis of TMOA via E2 elimination- Step 1													
$(MeO)_2C(OMe)(CH_3,OH^-)$	00									1 52	1 52	7 10	8 62	0 00
$(MeO)_2C(OMe)(CH_2^-,H_2O)$	10		24 00	32 78							0 00		32 78	24 16
$(MeO)_2C^+(CH_3,OH^-),MeO^-$	01	22 48	0 00	0.00					-1 69	3 94	. 25	6 13	30 86	22 23
$(MeO)_2C=CH_2,MeO^-,H_2O$	11	11 88	1 54	2 10						1 76	1 76	6 13	21 88	13 25
Reaction square for phenol catalyzed hydrolysis of TMOA - Step 1													
$MeC(OMe)_2(OMe\ HOPh)$	0 0				10 00	-8 64	-2 62	1 16		1 76	2 92		2 92	0 00
$MeC(OMe)_2(O^+(H)Me,^-OPh)$	10		18 64	25 46	-9 12	10 00	1 64	-4 66	-2 32	2 42	-4 57		20 89	17 97

		ΔG_{rel} [a]	ΔpKa [b]	ΔG_{pKa} [c]	hydrogen bond [d]				ΔG_{IP} [e]	ΔG_{enc} [f]	ΔG_{Cplx} [g]	ΔG_{donel} [h]	ΔG_{corner} [i]	ΔG_{screed} [j]
					pK HA [k]	pK HB [l]	log K [m]	ΔG_{bb} [n]						
$MeC^+(OMe)_2$,(OMe,HOPh)	01	22 48			10 00	15 54	-3 72	-1.44	-1 64	4.59	1 52	6 13	30.13	27 20
$MeC^+(OMe)_2$,HOMe,OPh	11	1.26	10 00	13 66	15.54	10 00	-1.97	0.27	-1.41	4.42	3.28		18.20	15.28
Reaction square for TFE catalyzed hydrolysis of TMOA - Step 1														
$MeC(OMe)_2$(OMe.HOR)	00				12.40	-8 64	-2.39	0.84		1.76	2.61		2.61	0.00
$MeC(OMe)_2(O^+(H)Me,OR)$	10		21.04	28.74	-9.12	12.40	2.43	-5.74	-2 32	2.83	-5.23		23.51	20.90
$MeC^+(OMe)_2$,(OMe,HOR)	01	22.48			12 40	15 54	-1.25	-0.72	-1.64	4.59	2.23	6.13	30.84	28.23
$MeC^+(OMe)_2$,HOMe,OR	11	1 26	12.40	16.94	15 54	12.40	-1.95	0.25	-1.41	4.83	3.67		21.87	19.26

[a] free energy change from point "00"

[b] changes in protonation not included in ΔG_{rel}

[c] calculated from ΔpKa

[d] hydrogen bonding to species other than solvent

[e] calculated as $\Delta G_{IP} = 2.32 \times \Sigma ((q1\ q2) / r)$, where q1 and q2 are the charges being brought together, r is the distance between the charges in the encounter complex, and 2.32 is the energy term for one repulsive interaction at a distance of r, according to Ref. 84 The sum is taken over all of the charge-charge interactions. This is described in the Marcus theory results section.

[f] symmetry corrected encounter complex for ation calculated from

$$\Delta G_{enc} = \sum_i (-0.593 \times \ln\left(\frac{\prod n_R \sigma_R}{\prod n_P \sigma_P} \times 2^{p-q} \times 0.0085\right))$$

where σ is the external symmetry number, n is the internal symmetry number and R = reactants, P = products, p is the number of racemic products and q is the numb:r of racemic reactants. This follows from Hine[59,85]

[g] $\Delta G_{Cmplx} = \Delta G_{HB} + \Delta G_{IP} + \Delta G_{enc}$

h correction for removal of water from hydration shell of an anion to form encounter complex, Refs 20,84

i $\Delta G_{corner} = \Delta G_{rel} + \Delta G_{pKa} - \Delta G_{Cmplx} + \Delta G_{desolv}$

j $\Delta G_{rezeroed} = \Delta G_{corner} - \Delta G_{corner,\ 00}$

k pKa of proton donor in hydrogen bond, symmetry corrected

l pKa of proton acceptor in hydrogen bond, symmetry corrected

m equilibrium constant for hydrogen bond formation, by the method of Stahl and Jencks[86]

n free energy for hydrogen bond formation, calculated from the equilibrium constanrt for bond formation, corrected to exclude the encounter complex formation component of the equilibrium

APPENDIX II: MARCUS THEORY CALCULATIONS FOR THE ALDOL REACTIONS

The first requirement for the application of Marcus Theory to the aldol reaction is the determination or estimation of the overall equilibrium constant for the reaction of interest. One method for estimating the equilibrium constants is to use the Linear Free Energy Relationship $\log K_e = \Delta\gamma + A$ of Sander and Jencks[46] for additions to carbonyls. Δ measures the sensitivity of a carbonyl to the affinity of a nucleophile and γ measures the affinity of a given nucleophile. Of the two nucleophiles of interest, only acetone has a γ value available[20] ($\gamma = 0.5$). The γ value for *p*-nitroacetophenone will be taken as 0.05, the same as that for acetophenone.[20] A Δ value of 0.92 is likewise known for acetone.[35] A reasonable estimate of the Δ value for *p*-nitroacetophenone can be made from the two equilibrium constants for addition which are known. The water addition was estimated from the dimethyl acetal formation constant.[57]

Determination of Δ value for PNAC:

For additon to *p*-nitroacetophenone:

$\log K_{HSO3-}$	1.64 [87]
$\log K_{H2O}$	-6.11
$\log K_{HSO3-} - \log K_{H2O}$	7.76
γ_{H2O}	-3.58 [46]
γ_{HSO3-}	4.02 [46]
$\gamma_{HSO3-} - \gamma_{H2O}$	7.60

Therefore $\Delta = \delta \log K / \delta \gamma$ 1.02

Now the aldol equilibrium constants are calculated by:

$$\log K_{ald} = \Delta (\gamma_{Nu} - \gamma_{H2O}) + \log K_{H2O}$$

This results in the equilibrium constants reported in Table 51. The equilibrium constant for formation of the acetone-trifluoroacetophenone aldol is taken from Guthrie's work[20] which uses the equation for the line of best fit to all of the addition data for the ketone.

The pKa's of the ketols are estimated using the equation for tertiary alcohols.[44,45]

$$pKa = 17.03 - 1.32 \Sigma\sigma^* \quad [3]$$

Estimations of this type are described in detail elsewhere.[72] The σ^* values used are listed below. All come from Perrin.[72]

group	σ^*
p-NO_2-C_6H_4-	1.26
CH_3-CO-CH_2-	0.62
C_6H_5-	0.75
C_6H_5CO-	2.2
p-NO_2-C_6H_4-CH_2-	0.45
C_6H_5-CH_2-CH_2-	-0.06
CH_3-CH_2-CH_2-	-0.12
CF_3-	2.61

The details for each of the ketols are summarized below. Two methods were used to estimate the pKa's for estimation for **9** and **15** because it was not clear which of the two

methods of estimating the effect of a *p*-nitrophenacyl substituent would be the most accurate. The average value of the two methods should be a reasonable estimate.

pKa estimation for 1,1,1-trifluoro-2-hydroxy-2-phenyl-4-pentanone (2)

	σ*
C_6H_5-	0.75
CF_3-	2.61
CH_3COCH_2-	0.62
Σσ*	**3.98**
pKa	**11.78**

pKa estimation for 3-hydroxy-1,3-bis-(4-nitrophenyl)-1-butanone (9)

Method 1

$C_6H_5COCH_2$-	0.88	taken as 0.4 × C_6H_5CO-
(-)C_6H_5-CH_2-CH_2-	0.06	minus $PhCH_2CH_2$ to give C=O
p-NO_2-C_6H_4-CH_2-CH_2-	0.18	taken as 0.4 × *p*-NO_2-C_6H_4-CH_2-
p-NO_2-C_6H_4-	1.26	
Σσ*	**2.38**	
pKa	**13.89**	

Method 2

p-NO_2-C_6H_4-CH_2-CH_2-	0.18	taken as 0.4 × *p*-NO_2-C_6H_4-CH_2-
(-)CH_3-CH_2-CH_2-	0.12	minus propyl gives distant *p*-NO_2-C_6H_4-
CH_3-CO-CH_2-	0.62	
p-NO_2-C_6H_4-	1.26	
Σσ*	**2.18**	
pKa	**14.15**	

pKa estimation for 4-hydroxy-4-(4-nitrophenyl)-2-pentanone (12)

p-NO_2-C_6H_4-	1.26	
CH_3-CO-CH_2-	0.62	
Σσ*	**1.88**	
pKa	**14.55**	

pKa estimation for 3-hydroxy-3-methyl-1-(4-nitrophenyl)-1-butanone (15)

Method 1

$C_6H_5COCH_2$-	0.88	taken as 0.4 × C_6H_5CO-
(-)C_6H_5-CH_2-CH_2-	0.06	minus Ph-CH_2-CH_2 gives C=O contribution
p-NO_2-C_6H_4-CH_2-CH_2-	0.18	taken as 0.4 × *p*-NO_2-C_6H_4-CH_2-
Σσ*	**1.12**	
pKa	**15.55**	

Method 2

p-NO_2-C_6H_4-CH_2-CH_2-	0.18	taken as 0.4 × *p*-NO_2-C_6H_4-CH_2-
(-)CH_3-CH_2-CH_2-	0.12	minus propyl group gives distant *p*-NO_2-C_6H_4-
CH_3-CO-CH_2-	0.62	
Σσ*	**0.92**	
pKa	**15.82**	

Table 51. Detailed Marcus Theory calculations of rate constants for the aldol reactions.[a]

Nucleophile	Electrophile	pKa^{Nu}	pKa^{ketol}	$\log K_{ald}$ [b]	$\log K_{mic}$ [c]	$\log K_2$ [d]	ΔG [e]	$\Delta G^{\ddagger}$ [f]	$\log k_{2+}$ [g]	$\log k_{mic}$ [h]	$\log k_+$ [i]	$\log k_-$ [j]
Acetone	TFA	19.16 [k]	11.78	2.47	9.85	11.62	-15.85	7.09	7.60	5.83	0.67	-1.80
PNAC	PNAC	16.60 [l]	14.02	-2.41	0.17	1.94	-2.65	12.60	3.57	1.80	-0.80	1.61
Acetone	PNAC	19.16 [k]	14.55	-2.30	2.32	4.09	-5.57	11.24	4.56	2.79	-2.37	-0.07
PNAC	Acetone	16.60 [l]	15.68	-1.26	-0.35	1.42	-1.94	12.94	3.32	1.55	-1.05	0.21

[a] following the literature method[20]

[b] estimated above

[c] K_{mic} is microscopic equilibrium constant shown in Scheme 8 $\log K_{mic} = \log K_{ald} + pKa^{Nu} - pKa^{ketol}$

[d] $\log K_2 = \log K_{mic} - \log K_{enc}$ where K_{enc} is the equilibrium constant for encounter complex formation; $\log K_{enc} = -1.77$

[e] ΔG is the free energy change in $kcal.mol^{-1}$ corresponding to the equilibrium K_2

[f] $\Delta G^{\ddagger}$ is the free energy of activation calculated from Marcus Theory using $\Delta G^{\ddagger} = \Delta \tilde{G}(1 + \Delta G / (4\Delta \tilde{G}))^2$ where $\Delta \tilde{G} = 13.8$ $kcal.mol^{-1}$.[20]

[g] k_{2+} is the rate constant calculated from $\Delta G^{\ddagger}$

[h] k_{mic} is the microscopic rate constant calculated from $k_{2+} \times K_{enc}$

[i] k_+ (in $M^{-2}s^{-1}$) is the macroscopic forward rate constant for aldol formation: $\log k_+ = \log k_{mic} - pKa^{Nu} + 14$

[j] k_- (in $M^{-1}s^{-1}$) is the macroscopic retroaldol rate constant calculated from $\log K_{ald}$ and $\log k_+$

[k] Ref. 42

[l] Ref. 43 using values obtained from ref. 47 and corrected using ref. 48

REFERENCES

(1) Kosaric, N.; Duvnjak, Z.; Farkas, A.; Sahm, H.; Bringer-Meyer, S.; Goebel, O.; Mayer, D. In *Ullmann's Encyclopedia of Industrial Chemistry*; 5 ed.VCH Verlasgesellschaft: Weinheim, 1987; Vol. A 9; pp 587.

(2) Bronsted, J. N.; Wynne-Jones, W. F. K. *Transactions of the Faraday Society* **1929**, *25*, 59.

(3) Lahti, M.; Kauppi, K. *Acta Chemica Scandinavica* **1986**, *A 40*, 533.

(4) Lahti, M.; Kovero, E. *Acta Chemica Scandinavica* **1988**, *A 42*, 124.

(5) Fife, T. H.; Jao, L. K. *Journal of the American Chemical Society* **1968**, *90*, 4081.

(6) Fife, T. H.; Brod, L. H. *Journal of the American Chemical Society* **1970**, *92*, 1681.

(7) Anderson, E.; Fife, T. H. *Journal of the American Chemical Society* **1969**, *91*, 7163.

(8) De Wolfe, R. H.; Ivanetich, K. M.; Perry, N. F. *Journal of Organic Chemistry* **1969**, *34*, 848.

(9) Fife, T., F.; Natarajan, R. *Journal of the American Chemical Society* **1986**, *108*, 2425.

(10) Capon, B.; Nimmo, K. *Journal of the Chemical Society, Perkin Transactions II* **1975**, 1113.

(11) Jensen, J. L.; Herold, L. R.; Lenz, P. A.; Trusty, S.; Sergi, V.; Bell, K.; Rogers, P. *Journal of the American Chemical Society* **1979**, *101*, 4672.

(12) Anderson, E.; Fife, T. H. *Journal of the American Chemical Society* **1971**, *93*, 1701.

(13) Guthrie, J. P. *Journal of the American Chemical Society* **1980**, *102*, 5286.

(14) Capon, B. *Pure and Applied Chemistry* **1977**, *49*, 1001.

(15) Fife, T. H. *Accounts of Chemical Research* **1971**, *5*, 264.

(16) Marcus, R. A. *Annual Reviews of Physical Chemistry* **1964**, 155.

(17) Cohen, A. O.; Marcus, R. A. *Journal of Physical Chemistry* **1968**, *72*, 4249.

(18) Marcus, R. A. *Journal of the American Chemical Society* **1969**, *91*, 7224.

(19) Marcus, R. A. *Journal of Physical Chemistry* **1968**, *72*, 891.

(20) Guthrie, J. P. *Journal of the American Chemical Society* **1991**, *113*, 7249.

(21) Fairclough, R. A.; Hinshelwood, C. N. *Journal of the Chemical Society* **1937**, 538.

(22) Barker, J. Chemistry 490 Thesis, University of Western Ontario, 1988.

(23) LeBlanc, C. Chemistry 490 Thesis, University of Western Ontario, 1985.

(24) Guthrie, J. P. *Canadian Journal of Chemistry* **1990**, *68*, 1643.

(25) Augustine, R. L. *Catalytic hydrogenation; techniques and applications in organic synthesis*; M. Dekker: New York, 1965, pp 188.

(26) Neilsen, A. T.; Houlihan, W. J. *Organic Reactions*; John Wiley and Sons. New York, 1968; Vol. 16.

(27) references to reviews are available in general reference texts such as March, J. *Advanced Organic Chemistry*, 4th ed ; John Wiley and Sons Inc.: New York, 1992.

(28) Jensen, J. L.; Carre, D. J. *Journal of Organic Chemistry* **1974**, *39*, 2103.

(29) Noyce, D. S., Reed, W. L. *Journal of the American Chemical Soc. ty* **1959**, *81*, 624.

(30) Kim, Y. K.; Hatfield, J. D. *Journal of Chemical and Engineering Data* **1985**, *30*, 149.

(31) Guthrie, J. P.; Wang, X.-P. *Canadian Journal of Chemistry* **1992**, *70*, 10.

(32) Noyce, D. S.; Pryor, W. A.; Bottini, A. H. *Journal of the American Chemical Society* **1955**, *77*, 1402.

(33) Guthrie, J. P.; Wang, X.-P. *Canadian Journal of Chemistry* **1991**, *69*, 33.

(34) Guthrie, J. P. *Canadian Journal of Chemistry* **1974**, *52*, 2037.

(35) Guthrie, J. P. *Canadian Journal of Chemistry* **1978**, *56*, 962.

(36) Guthrie, J. P. *Canadian Journal of Chemistry* **1981**, *59*, 45.

(37) Guthrie, J. P.; Dawson, B. A. *Canadian Journal of Chemistry* **1983**, *61*, 171.

(38) Guthrie, J. P.; Cossar, J.; Cullimore, P. A.; Kamkar, N. M.; Taylor, K. F. *Canadian Journal of Chemistry* **1983**, *61*, 2621.

(39) Guthrie, J. P.; Cooper, K. J.; Cossar, J.; Dawson, B. A. *Canadian Journal of Chemistry* **1984**, *62*, 1441.

(40) French, C. C. *Journal of the American Chemical Society* **1929**, *51*, 3215.

(41) Koelichen, K. *Zeitschrift fur physikalen chemie* **1900**, *33*, 129.

(42) Chiang, Y.; Kresge, A. J.; Tang, Y. S.; Wirz, J. *Journal of the American Chemical Society* **1984**, *106*, 460.

(43) Keeffe, J. R.; Kresge, A. J. In *The chemistry of enols*; Z. Rappoport, Ed.; John Wiley and Sons: Chichester, 1990; pp 399.

(44) Takahashi, S.; Cohen, L. A.; Miller, H. K.; Peake, E. *Journal of Organic Chemistry* **1971**, *36*, 1205.

(45) Guthrie, J. P. *Journal of the American Chemical Society* **1978**, *100*, 5892.

(46) Sander, E. G.; Jencks, W. P. *Journal of the American Chemical Society* **1968**, *90*, 6154.

(47) Guthrie, J. P.; Cossar, J.; Klym, A. *Canadian Journal of Chemistry* **1987**, *65*, 2154.

(48) Keeffe, J. R.; Kresge, A. J.; Toullec, J. *Canadian Journal of Chemistry* **1986**, *64*, 1224.

(49) Dull, D. L.; Baxter, I.; Mosher, H. S. *Journal of the Chemical Society* **1967**, *32*, 1622.

(50) Mazza, L. J.; Guarna, A. *Synthesis* **1980**, 41.

(51) Russell, G. A.; Ros, F. *Journal of the American Chemical Society* **1985**, *107*, 2506.

(52) Sosnovskikh, V. Y.; Ovsyannikov, I. S.; Aleksandrova, I. A. *Zhurnal Organicheskoi Khimii* **1992**, *28*, 518.

(53) Mukaiyama, T.; Banno, K.; Narasaka, K. *Journal of the American Chemical Society* **1974**, *96*, 7503.

(54) Guthrie, J. P.; Cossar, J. *Canadian Journal of Chemistry* **1990**, *68*, 1640.

(55) Stewart, R.; Van der Linden, R. *Canadian Journal of Chemistry* **1960**, *38*, 399.

(56) Stewart, R.; Van Dyke, J. D. *Canadian Journal of Chemistry* **1970**, *48*, 3961.

(57) Toullec, J.; El-Alaoui, M.; Kleffert, P. *Journal of Organic Chemistry* **1983**, *48*, 4808.

(58) Guthrie, J. P. *Canadian Journal of Chemistry* **1975**, *53*, 898.

(59) Hine, J. *Journal of the American Chemical Society* **1971**, *93*, 3701.

(60) Hine, J.; Redding, R. W. *Journal of Organic Chemistry* **1970**, *35*, 2769.

(61) Kurz, J. L. *Journal of the American Chemical Society* **1967**, *89*, 3524.

(62) Guthrie, J. P.; Cossar, J.; Taylor, K. F. *Canadian Journal of Chemistry* **1984**, *62*, 1958.

(63) Albery, W. J. *Annual Reviews of Physical Chemistry* **1980**, *31*, 227.

(64) Ritchie, C. D.; Kubisty, C.; Ting, G. Y. *Journal of the American Chemical Society* **1983**, *105*, 279.

(65) Fieser, L. F.; Fieser, M. *Reagents for organic synthesis*; John Wiley and Sons, Inc.: New York, 1967; Vol. 1.

(66) Ramirez, F.; Dershowitz, S. *Journal of Organic Chemistry* **1957**, *22*, 41.

(67) Novice, M. H.; Seikaly, H. R.; Seiz, A. D.; Tidwell, T. T. *Journal of the American Chemical Society* **1980**, *102*, 5835.

(68) House, H. O.; Czuba, L. J.; Gall, M.; Olmstead, H. D. *Journal of Organic Chemistry* **1969**, *34*, 2324.

(69) Tidwell, T. J., personal communication.

(70) Bevington, P. R. *Data reduction and error analysis for the physical sciences*; McGraw-Hill: New York, 1969, pp 336.

(71) Deming, W. E. *Statistical adjustment of data*; Dover Publications Inc.: New York, 1964, pp 261.

(72) Perrin, D. D.; Dempsey, B.; Serjeant, E. P. *pKa prediction for organic acids and bases*; Chapman and Hall: London, 1981, pp 146.

(73) Fox, J. P.; Jencks, W. P. *Journal of the American Chemical Society* **1974**, *96*, 1436.

(74) Guthrie, J. P. *Journal of the American Chemical Society* **1974**, *96*, 3608.

(75) Jencks, W. P.; Regenstein, J. In *Handbook of biochemistry and molecular biology*; 3 ed.; G. D. Fasman, Ed.; CRC Press Inc.: Cleveland, 1976; Vol. I; pp 305.

(76) Bonvicini, P.; Levi, A.; Lucchini, V.; Modena, G.; Scorrano, G. *Journal of the American Chemical Society* **1973**, *95*, 5960.

(77) Amyes, T. L.; Jencks, W. P. *Journal of the American Chemical Society* **1989**, *111*, 7888.

(78) Wenthe, A. M.; Cordes, E. H. *Journal of the American Chemical Society* **1965**, *87*, 3173.

(79) McClelland, R. A.; Steenken, S. *Journal of the American Chemical Society* **1988**, *110*, 5860.

(80) McClelland, R. A.; Ahmad, M. *Journal of the American Chemical Society* **1978**, *100*, 7031.

(81) Liu, Z.; Guthrie, J. P. *Canadian Journal of Chemistry*, submitted for publication.

(82) Guthrie, J. P. *Canadian Journal of Chemistry* **1992**, *70*, 1042.

(83) Keefe, J. R.; Kresge, A. J. In *The chemistry of enols*; Z. Rappoport, Ed.; John Wiley and Sons: New York, 1990; pp 399.

(84) Guthrie, J. P. *Journal of the American Chemical Society* **1991**, *113*, 3941.

(85) Hine, J. *Structural effects on equilibria in organic chemistry*; John Wiley and Sons: New York, 1975, pp 347.

(86) Stahl, N.; Jencks, W. P. *Journal of the American Chemical Society* **1986**, *108*, 4196.

(87) Young, P. R.; Jencks, W. P. *Journal of the American Chemical Society* **1979**, *101*, 3288.